



UCGE Reports
Number 20263

Department of Geomatics Engineering

**Precise Relative Navigation for Satellite Formation
Flying Using GPS**

(URL: <http://www.geomatics.ucalgary.ca/research/publications/GradTheses.html>)

By

Qais Marji

January 2008



THE UNIVERSITY OF CALGARY

Precise Relative Navigation for Satellite Formation Flying Using GPS

by

Qais Marji

A THESIS

SUBMITTED TO THE FACULTY OF GRADUATE STUDIES
IN PARTIAL FULFILMENT OF THE REQUIREMENTS FOR THE
DEGREE OF MASTER OF SCIENCE

DEPARTMENT OF GEOMATICS ENGINEERING

CALGARY, ALBERTA

JANUARY, 2008

© QAIS MARJI 2008

ABSTRACT

Formation flying is a key technology for both deep-space and orbital applications that involves the use and control of multiple spacecraft in an autonomous configuration. Thus, the fundamental issue is to determine the relative state between the spacecraft within the desired accuracy. The Canadian Advanced Nanospace eXperiment (CanX) program of the Space Flight Laboratory at the University of Toronto Institute for Aerospace Studies (UTIAS/SFL) has allowed Canadian engineering researchers to test nano-scale satellites in space. In this work, the use of carrier phase differential GPS (CDGPS) technique is demonstrated to estimate the relative position and velocity between nano-satellites. The objective is to achieve centimetre-level relative position accuracy for a simulated mission. Hardware-in-the-loop (HWIL) demonstrations were performed using NovAtel's GPS RF signal simulator along with the use of two OEM4-G2L GPS receivers. To achieve the highest positioning accuracy possible, estimation of the double difference (DD) L1 carrier phase ambiguities was conducted within a Kalman filter using the Least-squares AMBiguity Decorrelation Adjustment (LAMBDA) approach. Simulation test scenarios indicate relative position and velocity accuracies of 4 mm and less than 3 cm/s can be achieved over a 1 km baseline, and 2-3 mm and less than 2.5 cm/s for a 100 m baseline using a data rate of 1 second. These results demonstrate that the navigation performance achieved is within the CanX-4 and 5 mission requirements.

ACKNOWLEDGEMENTS

I wish to thank my adviser, Professor Elizabeth Cannon, for her tenacious dedication and support offered during my graduate studies, research, and dissertation work. Her unflagging enthusiasm and encouragement propelled my work while her intellectual vigour greatly inspired the methodology, approaches, and critical notions adopted in my research.

My parents and family always gave me boundless love and encouragement to follow whatever path I chose. Their continual support gave me the strength, motivation, and willingness to continue my research. My gratitude is beyond words.

Professor Gerard Lachapelle is also acknowledged for his encouragement throughout the course of my program.

I appreciate the help I received from my colleagues in the geomatics department. My special gratitude goes to my friends Raymond Tsoi, Richard Ong and Lance De Groot for their kind encouragement and support during my work.

The author gratefully acknowledges Michelle Martin and Behtash Charkhand from NovAtel Inc. for their help and cooperation.

DEDICATION

Dedicated to my beloved parents Kamal and Sahar Marji who instilled the value of education in me, and for their belief that I can make it.

Also dedicated to my beloved fiancée Maisa for her love and encouragement during my study

Also dedicated to my brothers Mamoon, and Majd Marji for their words of wisdom and encouragement.

TABLE OF CONTENTS

APPROVAL PAGE	ii
ABSTRACT	ii
ACKNOWLEDGEMENTS	iii
DEDICATION	iv
TABLE OF CONTENTS	v
LIST OF TABLES	ix
LIST OF FIGURES	xi
LIST OF SYMBOLS	xv
LIST OF ABBREVIATIONS	xvi
CHAPTER 1	19
INTRODUCTION	19
1.1 Formation Flying Using GPS	20
1.2 CanX Program Overview	21
1.3 Research Objectives and Motivation	22
1.4 Thesis Outline	25
CHAPTER 2	27
GPS OBSERVATIONS AND ERROR SOURCES	27
2.1 Observation Types	27
2.1.1 Pseudorange Measurements	28
2.1.2 Carrier Phase Measurements	30
2.1.3 Doppler Measurements	31
2.2 Relative Positioning Models and Orbit Configuration	32
2.2.1 Single Difference Model	32
2.2.2 Double Difference Model	33
2.2.3 Orbit Configuration	34
2.3 GPS Error Sources	36
2.3.1 Orbital Error	37

2.3.2	Clock Error	38
2.3.3	Ionospheric Delay	38
2.3.4	Multipath.....	40
2.3.5	Receiver Noise.....	42
2.4	Coordinate Systems	43
2.4.1	Inertial Coordinate System	43
2.4.2	Orbital Coordinate System	44
2.4.3	Orbiting Coordinate System (Hill Frame).....	44
2.4.4	Geodetic Coordinate System	45
2.4.5	Local Geodetic Coordinate System	46
2.4.6	Coordinate Transformation.....	46
CHAPTER 3.....		50
RELATIVE SPACECRAFT POSITIONING		50
3.1	Measurement Model	51
3.2	Extended Kalman Filter	52
3.2.1	EKF Dynamic Model.....	53
3.2.2	EKF Measurement Model.....	53
3.3	Integer Ambiguity Resolution.....	54
3.3.1	Integer Ambiguity Estimation	55
3.4	Availability of Chief and Deputy Positions and Velocities.....	56
3.4.1	Case I (Ideal): Chief and Deputy Each Track ≥ 4 SVs and the Data Link is Available.....	57
3.4.2	Case II: Chief and Deputy Each Track ≥ 4 SVs and the Data Link is not Available.....	58
3.4.3	Case III: Chief Tracks ≥ 4 SVs, Deputy Tracks < 4 SVs and the Data Link is Available	58
3.4.4	Case IV: Chief Tracks < 4 SVs, Deputy Tracks ≥ 4 SVs and the Data Link is Available	59
3.5	Summary.....	61

CHAPTER 4.....	62
HARDWARE-IN-THE-LOOP DEMONSTRATION.....	62
4.1 OEM4-G2L Receiver Overview.....	62
4.2 NOVATEL FFTB Environment.....	63
4.3 NOVATEL FFTB Setup.....	67
4.4 Formations.....	69
4.5 Summary.....	70
CHAPTER 5.....	71
TEST SCENARIOS AND AVAILABILITY TEST RESULTS.....	71
5.1 Analysis of GPS Satellites in View versus GPS Antenna Boresight Angle from Zenith.....	71
5.1.1 Test Concept.....	71
5.1.2 Simulation Scenario.....	72
5.1.3 Satellite Availability.....	72
5.2 Test Results and Analysis.....	75
5.2.1 Test Results for Zero Degree Elevation.....	75
5.2.2 Test Results for 45 Degree Elevation.....	78
5.2.3 Test Results for 90 Degree Elevation.....	81
5.2.4 Test Results for 180 and 225 Degree Elevation.....	84
5.2.5 Test Results for 270 Degree Elevation.....	86
5.2.6 Analysis.....	88
5.3 Summary.....	93
CHAPTER 6.....	94
RELATIVE NAVIGATION TESTS AND RESULTS.....	94
6.1 Test Scenarios.....	94
6.1.1 HWIL Demonstration.....	94
6.1.2 GPS Errors.....	95
6.1.3 Processing Procedure.....	97
6.2 Modifications.....	98

6.3	Results and Analysis	99
6.3.1	Test Results Using SimGEN Trajectory	99
6.3.2	Test Results Using OEM4-G2L Trajectory	116
6.3.3	Signal Outages Tests and Results	122
6.4	Summary	127
CHAPTER 7	128
CONCLUSIONS AND RECOMMENDATIONS		128
7.1	Conclusions	128
7.2	Recommendations	130
REFERENCES		132
APPENDIX A.....		141
Software Development.....		141

LIST OF TABLES

Table 1-1: Performance Requirements for CanX-4 and -5 (3σ Error) (Caillibot et al., 2005).....	21
Table 2-1: Main Characteristics of Pseudorange and Carrier Phase Data (Hofmann Wellenhof et al., 1997)	28
Table 2-2: Receiver Noise for Different Observations (Hofmann Wellenhof et al., 1997)	42
Table 2-3: GPS Error Sources and their Magnitudes. (Lachapelle, 2005)	42
Table 3-1: Scenarios Description Summary of Available Information at the Deputy.....	60
Table 4-1: GPS Receiver Performance (OEM4-G2L, 2003).....	63
Table 4-2: Hardware Configuration Used in These Tests	65
Table 4-3: CanX-4 and -5 Orbital Parameters (Caillibot et al., 2005).....	70
Table 5-1: Satellites in View versus Antenna Boresight Angle	88
Table 5-2: Percentage of Satellites in View versus Antenna Boresight Angle.....	90
Table 6-1: RMS Level of GPS Errors.....	96
Table 6-2: Statistics for Relative Position Errors	101
Table 6-3: Statistics for Relative Velocity Errors.....	102
Table 6-4: Statistics for Relative Position Errors	106
Table 6-5: Statistics for Relative Velocity Errors.....	107
Table 6-6: Statistics for Relative Position Errors	108
Table 6-7: Statistics for Relative Velocity Errors	109
Table 6-8: Statistics for Relative Position Errors	111
Table 6-9: Statistics for Relative Velocity Errors	113

Table 6-10: Statistics for Relative Position Errors	118
Table 6-11: Statistics for Relative Velocity Errors	119
Table 6-12: Statistics for Relative Position Errors	120
Table 6-13: Statistics for Relative Velocity Error	121
Table A-1: Extracted Data from Range Message	143
Table A-2: Quality Flags to Check (NovAtel Inc., 2002).....	144
Table A-3: Number of Bytes as a Function of Satellites Tracked	144
Table A-4: BESTXYZ (Message 241) Structure (NovAtel Inc., 2002)	145
Table A-5: Extracted Data From BestXYZ Log reference.....	146
Table A-6: Total Extracted Data to be Transmitted.....	147
Table A-7: Number of Bytes as a Function of Satellites Tracked	147

LIST OF FIGURES

Figure 2-1: Overall Viewing Geometry for Relative Spacecraft Positioning Using Differenced GPS Observations (Kroes, 2006)	33
Figure 2-2: Keplerian Orbital Parameters (Busse, 2003).....	36
Figure 2-3: Direct and Multipath Signal.....	41
Figure 2-4: Representation of Orbital, Inertial and Hill Coordinate Systems (Schwarz, 1999).....	45
Figure 2-5: Representation of the Global and Local Geodetic Coordinate Systems (Moritz, 1980).....	46
Figure 3-1: Integer Ambiguity Estimation Procedure (Teunissen, 1999).....	56
Figure 4-1: NovAtel OEM4-G2L Dual-Frequency GPS Receiver (125X85 mm) (OEM4- G2L, 2003)	63
Figure 4-2: FFTB Setup	64
Figure 5-1: Theoretical Number of GPS Satellites Simulated by SimGEN	74
Figure 5-2: Sky Plot (Spirent, 2005).....	74
Figure 5-3: Number of Satellites Tracked for a Zero Degree Angle	76
Figure 5-4: Number of Satellites Used in Solution for a Zero Degree Boresight Angle..	77
Figure 5-5: Position and Geometric Dilution of Precision for a Zero Degree Boresight Angle	77
Figure 5-6: Horizontal and Vertical Dilution of Precision for a Zero Degree Boresight Angle	78
Figure 5-7: Number of Satellites Tracked for a 45 Degree Boresight Angle	79

Figure 5-8: Number of Satellites Used in Solution for a 45 Degree Angle for 45 Degree Boresight Angle.....	80
Figure 5-9: Position and Geometric Dilution of Precision for a 45 Degree Boresight Angle	80
Figure 5-10: Horizontal and Vertical Dilution of Precision for a 45 Degree Boresight Angle	81
Figure 5-11: Number of Satellites Tracked for a 90 Degree Boresight Angle	82
Figure 5-12: Number of Satellites Used in Solution for a 90 Degree Boresight Angle ...	83
Figure 5-13: Position and Geometric Dilution of Precision for a 90 Degree Boresight Angle	83
Figure 5-14: Horizontal and Vertical Dilution of Precision for a 90 Degree Boresight Angle	84
Figure 5-15: Number of Satellites Tracked for a 180 Degree Boresight Angle	85
Figure 5-16: Number of Satellites Tracked for a 225 Degree Boresight Angle	85
Figure 5-17: Number of Satellites Tracked for a 270 Degree Boresight Angle	86
Figure 5-18: Number of Satellites Used in Solution for a 270 Degree Boresight Angle .	87
Figure 5-19: Position and Geometric Dilution of Precision for a 270 Degree Boresight Angle	87
Figure 5-20: Horizontal and Vertical Dilution of Precision for a 270 Degree Boresight Angle	88
Figure 5-21: Satellites in View versus Antenna Boresight Angle	89
Figure 5-22: Analysis of DOP for Zero deg Elevation.....	91
Figure 5-23: Analysis of DOP for 45 deg Elevation.....	91

Figure 5-24: Analysis of DOP for 90 deg Elevation.....	92
Figure 5-25: Analysis of DOP for 270 deg Elevation.....	92
Figure 6-1: GPS Satellite Availability and GDOP for LEO Spacecraft.....	97
Figure 6-2: Test 1 Relative Position Errors (100m Baseline).....	100
Figure 6-3: Test 1 Relative Velocity Errors (100m Baseline).....	102
Figure 6-4: L1 Phase Residuals Error for Satellites 1-8	103
Figure 6-5: L1 Phase Residuals Error for Satellites 9-16	104
Figure 6-6: L1 Doppler Residuals Error for Satellites 1-8	104
Figure 6-7: L1 Doppler Residuals Error for Satellites 9-16	105
Figure 6-8: Test 1 Relative Position Errors (1 km Baseline).....	106
Figure 6-9: Test 1 Relative Velocity Errors (1km Baseline).....	107
Figure 6-10: Test 1 Relative Position Errors (5km Baseline).....	108
Figure 6-11: Test 1 Relative Velocity Errors (5km Baseline).....	109
Figure 6-12a: Test 1 Relative Position Errors (Multipath).....	111
Figure 6-13: Test 1 Relative Velocity Errors (Multipath).....	113
Figure 6-14: L1 Phase Residuals Error for Satellites 9-16	114
Figure 6-15: L1 Phase Residuals Error for Satellites 17-24	115
Figure 6-16: L1 Doppler Residuals Error for Satellites 9-16	115
Figure 6-17: L1 Doppler Residuals Error for Satellites 16 -24	116
Figure 6-18: Test 2 Relative Position Errors (100 m Baseline).....	118
Figure 6-19: Test 2 Relative Velocity Errors (100 m Baseline).....	119
Figure 6-20: Test 2 Relative Position Errors (1 km Baseline).....	120
Figure 6-21: Test 2 Relative Velocity Errors (1km Baseline).....	121

Figure 6-22: Relative Position Error During Signal Outages (5 sec)	122
Figure 6-23: Relative Velocity Error During Signal Outages (5 sec).....	123
Figure 6-24: Relative Position Error During Signal Outages (30 sec)	124
Figure 6-25: Relative Velocity Error During Signal Outages (30 sec).....	125
Figure 6-26: Relative Position Error During Signal Outages (60 sec)	126
Figure 6-27: Relative Velocity Error During Signal Outages (60 sec).....	126
Figure A-1: Bytes Comparison Between New and NovAtel Format	148
Figure A-2: Data Extraction Flowchart	149

LIST OF SYMBOLS

c	Speed of Light
h	Ellipsoidal Height (m)
\dot{h}	Vertical Velocity (m/sec)
I	Ionospheric Delay (m)
$L1$	GPS Signal at Frequency of 1575.42 MHz
$L2$	GPS signal at Frequency of 1226.70 MHz
N	Phase Ambiguity
P	Pseudorange Observable (m)
T	Tropospheric Delay (m)
λ	GPS carrier Wavelength (m)
$\nabla\Delta$	Double Difference Operator
φ	Latitude (rad)
λ	Longitude (rad)
$\dot{\varphi}$	Latitude Rate (rad/sec)
$\dot{\lambda}$	Longitude Rate (rad/sec)

LIST OF ABBREVIATIONS

2D	Two Dimensional
3D	Three Dimensional
C/A	Coarse Acquisition
CANX	Canadian Advanced Nanospace eXperiment
CDGPS	Carrier phase Differential GPS
CRC	Cyclic Redundancy Check
DD	Double Difference
DOP	Dilution Of Precision
ECEF	Earth Centered Earth Fixed
EKF	Extended Kalman Filter
FF	Formation Flying
FFTB	Formation Flying Test Bed
GRACE	Gravity Recovery and Climate Experiment
GNSS	Global Navigation Satellite System
GPS	Global Positioning System

GSFC	Goddard Space Flight Center
HWIL	Hardware-in-the-loop
LAMBDA	Least-squares AMBiguity Decorrelation Adjustment
LEO	Low Earth Orbit
MBS	Moving Base Station
NCP	North Celestial Pole
P-Code	Precise Code
PPM	Part Per Million
PRN	PseudoRandom Noise
RAAN	Right Ascension of Ascending Node
RMS	Root Mean Square
RTK	Real Time Kinematic
SD	Single Difference
STD	Standard Deviation
TEC	Total Electron Content
UTIAS/SFL	University of Toronto Institute for Aerospace Studies/ Space Flight Laboratory

WGS₈₄ World Geodetic System of 1984

CHAPTER 1

INTRODUCTION

Formation flying is a key technology for both deep-space and orbital applications that involves the use and control of multiple spacecraft in an autonomous configuration. Thus, the fundamental issue is to determine the relative state between the spacecraft within the desired accuracy. Currently, the Space Flight Laboratory (SFL) at the University of Toronto's Institute for Aerospace Studies (UTIAS) is leading the Canadian Advanced Nanospace eXperiment (CanX) program which provides a structure for the rapid development of nanosatellite technologies. Within this program is a precise formation flying mission using two identical nanosatellites (CanX-4&5). For the formation flying experiment, only one of the satellites (Deputy) is required to be controlled relative to the master/reference satellite (Chief) (Caillibot et al., 2005). The goal of this mission is to verify technologies like centimetre-level accuracy GPS-based position determination that can be implemented on nano- or micro-satellites developed at low cost and over a short time period (Sarda et al., 2006). The control accuracy is one of the challenges that can be faced during the formation flying mission, as it has a significant impact on the fuel consumption needed to maintain the satellites in a specific configuration. Nanosatellites are considered as low Earth orbiting satellites (LEOs), which are often distributed in satellite constellations, because the coverage area provided by a single LEO satellite is relatively small, and the satellite travels at a high speed (e.g. 7 km/s) to maintain its orbit. A LEO generally extends from the Earth's surface up to 2000 km. For that reason, the

tropospheric effect is neglected when modelling these missions, however, in some cases the troposphere may have some effect in LEO missions, e.g. GPS occultation.

1.1 Formation Flying Using GPS

It is worthwhile to investigate the filter and ambiguity strategy used in this work before going into further detail. The Extended Kalman filter (EKF) was used and found to be very robust and suitable for highly precise relative navigation. For the ambiguity resolution technique, the Least-squares AMBiguity Decorrelation Adjustment (LAMBDA) method was used and is further discussed in detail in Chapter 3.

The navigation algorithm implemented for optimal estimation is based on a Kalman filter approach. The system estimates the position and velocity of the reference satellite and then the filter uses double difference (DD) measurements to estimate the position and velocity of the other nanosatellite relative to the reference. The use of DD observables can reduce or eliminate many major error sources (orbital, atmospheric and clock errors). However, the level of uncorrelated errors (multipath and noise) is doubled in the differencing process. In the prediction stage, the kinematic model selected is a random walk velocity model; here it assumes the acceleration input to be pure white noise. Although the random walk velocity model is too simple to describe the relative motion of a satellite over a long time span, it is still suitable for applications with high sampling rate and low dynamics scenarios, which is the situation for formation flying.

1.2 CanX Program Overview

At present, CanX-2 is nearing completion and is planned for launch into a low Earth orbit in June 30, 2007. However, the launch has been delayed to February 2008. This satellite will demonstrate some of the key technologies needed for the CanX-4 and -5 formation flight, but at the component level. CanX-4 and -5 are expected to be launched in late 2008 (Mauthe et al., 2005, Rankin et al., 2004) and is aimed to perform formation flying, where each satellite operates on less than ten watts of power and has a mass under 5 kg (Sarda et al., 2006). The CanX-4 and -5 mission objectives, as discussed in Sarda et al. (2006) and Caillibot et al. (2005), are to demonstrate centimetre-level accuracy for relative position determination and sub-metre relative position control accuracy. The satellites have cold gas propulsion, three-axis attitude stabilization, inter-satellite communications and dual-band GPS receivers. Table 1.1 shows the performance requirements and information for CanX-4 and -5.

Table 1-1: Performance Requirements for CanX-4 and -5 (3σ Error) (Caillibot et al., 2005)

Performance Indicator	Target
Position Determination	<10 cm (< 5 cm stretch goal)
Position Control	< 1 m (< 10 cm stretch goal)
Closest Relative Distance	<100 m (< 50 m stretch goal)
Attitude Determination	< 0.5° (< 0.1° stretch goal)
Attitude Control	< 1°
Intersatellite Link Data Rate	Between 32 kbps and 256 kbps
Satellite Mass (each)	<5 kg

1.3 Research Objectives and Motivation

GPS is capable of providing positional accuracy at the centimetre level when differential carrier phase measurements are used and this approach is implemented to determine the relative position of the nanosatellites. Testing the use of GPS for relative navigation can be divided into two areas: real data experiments, and software or hardware-in-the-loop simulation tests. Because of the low availability of real GPS data, most of the previous work is based on software or hardware simulations. As an example of a real data experiment, the relative positioning accuracy recorded with actual GPS data from the GRACE mission, is about 1 mm (3D Root Mean Square (RMS)) (Kroes, 2006). Kroes (2006) uses an EKF to process single difference GPS pseudorange and carrier phase observations, and uses ‘pseudo’ relative spacecraft dynamics to propagate the relative satellite state. In fact, there are no direct models that describe the relative dynamic models with a desired accuracy. To overcome this problem by obtaining the ‘pseudo’ relative spacecraft dynamics from the dynamical models of the individual spacecrafts, so that pseudo. In addition, the ‘pseudo’ relative spacecraft dynamics were generated using a high precision force model, to propagate the relative state. However, even though it is single difference parameterization, the integer nature of the DD ambiguities can still be exploited. The estimation of the integer ambiguities is accomplished by using the well known LAMBDA method. Out of the four processing schemes, batch estimators and a sequential kinematic filter were also implemented, but were found to have some limitations for use in real-world applications. These limitations were related to problems with integer ambiguity resolution, while the other two processing schemes (reduced

dynamic patch least squares estimator and EKF) show that there are no limitations regarding the ambiguity resolution process (see Kroes (2006) for details).

For hardware-in-the-loop simulation, Busse (2003) uses a modified version of the Zarlink Orion single frequency GPS receiver. These tests are performed using the NASA Goddard Space Flight Center (GSFC) formation flying test bed. In these tests, DD measurements were used but no efforts were made to fix the carrier phase ambiguities to integer values, though it is generally key for precise relative positioning. As a result of this study, a decision was made to use single difference measurements in the filter implementation. The conclusion drawn from this study was that any steady state error in the filter performance is not related to receiver clock state. This can be concluded from the fact that error level remains about the same using the DD process where the clock error is removed. Both approaches showed similar performance. Busse (2003) achieves less than 2 cm (3D RMS) relative position error and 0.5 mm/sec (3D RMS) relative velocity error for formations with 1-2 km separations using a single difference approach. However, ambiguity biases take at least five minutes to resolve, which is relatively long for a 1 km baseline separation.

Binning (1997) uses GPS data from both software and hardware in-the-loop simulators. He uses three different algorithms for determining the relative state between two spacecraft with two different separation distances. The first method is called the straight difference. In this method the relative state is found by differencing the two absolute positions. The second method is called correlated pseudorange; it is similar to the straight difference but with two distinctions. First an interpolation scheme is used to process

measurements from the same instant in time. Then, a correlated weight matrix and process noise matrix are used while processing two pseudorange measurements. The third method is called the single difference pseudorange approach. In this method, the relative state between two receivers is estimated. Furthermore, the measurement is changed to a combination of one pseudorange and one single difference pseudorange instead of two pseudoranges. Dual frequency TurboRogue receivers are used for both the software and hardware simulations. The Naval Research Laboratory's OCEAN orbital model, which is a very accurate and robust orbit propagator, is used. Using hardware-in-the-loop, the best case achieved using the correlated pseudorange method is less than 8 cm (3D RMS) relative position accuracy, and less than 0.3 mm/sec (3D RMS) relative velocity accuracy for a 5 km baseline. However, the multipath and noise errors are assumed to be small in comparison with the other errors.

In this work, the use of carrier phase differential GPS (CDGPS) is demonstrated to estimate the relative position and velocity between two spacecraft. A hardware-in-the-loop simulator is used to generate carrier phase and pseudorange measurements in single frequency mode. The reasons for using L1 only are the lower cost receiver and its simplicity since only the L1 carrier phase and pseudorange observations are used and no observation combination is formed. Also, it has lower noise and ionospheric error characteristics compared to widelane (WL) and L2. A DD approach is used whereby the carrier phase ambiguities are fixed to their integer values. The objective of this work is to demonstrate centimetre relative positioning accuracy based on a series of simulation tests. These test scenarios are chosen with different baseline separations varying between 100

m – 5 km. some of the associated errors (multipath, ionosphere, noise) were investigated using hardware simulation tests and scenarios in this work. To make these objectives possible, a significant enhancement was made to the relative navigation software, FLYKIN+™ developed at the University of Calgary by Liu (2003). The modified version is now capable of processing GPS measurements from moving base stations for space applications. However, since this version dealt with a specific data format (NovAtel OEM4-data), modifications regarding data extraction were modified by the author for the CanX-4 and -5 mission. Further details are discussed in Chapter 5.

1.4 Thesis Outline

- Chapter 2 presents an overview of the GPS observation types used throughout this research. Then a general idea on the relative positioning models, such as single and DD models is given. Various differential error sources are introduced, and the impact of these errors on relative positioning is investigated. Coordinate systems and coordinate transformation are shown as well.
- Chapter 3 presents an overview of relative spacecraft positioning phases for both the Chief and Deputy. In general both the Chief and Deputy should have more than four satellites (ideal case), however, sometime the number of satellite can be less than four, and in this case, positions and velocities are propagated from a previous epoch. An overview of the integer ambiguity estimation and validation is discussed in this chapter; the general idea is presented about Kalman filter's dynamic and measurements models.

- Chapter 4 describes the formation flying test bed (FFTB) environment, hardware connections and procedures. It also defines the simulation conditions for the results shown in Chapters 5 and 6.
- Chapter 5 describes availability test results for different antenna boresight angles.
- Chapter 6 describes the relative navigation tests and results in addition to the software development stages such as data extraction and code modifications.
- Chapter 7 lists the conclusions drawn from this study and recommendation for future work.

CHAPTER 2

GPS OBSERVATIONS AND ERROR SOURCES

2.1 Observation Types

In general GPS provides three types of measurements: pseudorange, carrier phase, and Doppler. All three measurements are used in this work, and are described in detail in the following subsections. The pseudorange measurements, at a specific moment from different satellites, have a common clock bias which results in the name of this observation. The carrier phase gives more precise measurements than pseudoranges, by estimating its instantaneous rate, or Doppler measurement (beat frequency) over time. Hence it is also known as the integrated Doppler, or the accumulated phase. The main differences and characteristics between pseudorange and carrier phase measurements are summarized in Table 2.1 (Hofmann Wellenhof et al., 1997). Additional signals are planned to enhance the ability of GPS to support users, provide a new military code and improve the over all performance. The first new signal will be a C code on the L2 frequency (1227.60 MHz). This new feature will enable dual channel civil receivers to correct for ionospheric errors. The L2C signal contains two codes of different length, CM-L2C which is the moderate length code contains 10,230 chips, repeats every 20 milliseconds. CL-L2C is the long code contains 767,250 chips, repeats every 1.5 seconds (Fontana et al., 2001). A third civil signal will be added on the L5 frequency (1176.45

MHz) for use in safety-of-life applications. L5 can serve as a redundant signal to the GPS L1 frequency (1575.42 MHz) with a goal of assurance of continuity of service potentially to provide precision approach capability for aviation users. The initial transmission of L5 signal is planned for 2008, with a full operational availability in 2012 (Qiu, 2007).

Table 2-1: Main Characteristics of Pseudorange and Carrier Phase Data (Hofmann Wellenhof et al., 1997)

	Code		Carrier
Wavelength	P-code	29.3 m	L1 19.03 cm
	C/A-code	293 m	L2 24.42 cm
Observation noise Classical receiver	P-code	0.1-0.3 m	1-3 mm
	C/A-code	0.1-3 m	
New development	P-code	2-5 cm	<0.2 mm
Propagation effect	Ionospheric delay		Ionospheric advance
	$+ \Delta T_{ION}$		$- \Delta T_{ION}$
Ambiguity	Non-ambiguous		Ambiguous

2.1.1 Pseudorange Measurements

Simply put, a pseudorange is the distance measurement based on the correlation of a satellite's transmitted code and the local receiver's reference code, which has not been corrected for errors in synchronisation between the transmitter's clock and the receiver's clock. Therefore a pseudorange measurement is a time error biased distance measurement. The precision of the measurement is a function of the resolution of the code; hence C/A-Code pseudorange measurements may have noise at the few metre level for standard GPS receivers and at the several centimetre precision level in the case of so-called "narrow correlator" GPS receivers (Raquet, 1998). Since the true time between the

GPS satellite and the receiver is not known, the satellite transmit time (t^S) and the receiver reception time (t_R) is given by

$$\begin{aligned} t^S &= T^S + \Delta t^S \\ t_R &= T_R + \Delta t_R \end{aligned} \quad (2.1)$$

where T^S and T_R are indicative of the true times, and Δt^S and Δt^R denote the satellite and receiver clock errors, respectively. Ideally, the pseudorange measurement is simply the speed of light times the difference between transmit and receive times in the satellite and receiver time scales, respectively.

$$P = \rho = c(t^S - t_R) \quad (2.2)$$

where P is the pseudorange in metres, ρ is the geometric range between the satellite and the receiver, and c is the speed of light in m/s. Equation 2.2 represents the ideal case where the pseudoranges are error free, but this is not the real case. The effect of clock errors, orbital errors, tropospheric and ionospheric errors, and receiver noise should be taken in consideration. When these error sources are accounted for, Equation 2.2 becomes (Lachapelle, 2005):

$$P = \rho + d\rho + c(\Delta t^S - \Delta t_R) + d_{ion} + d_{trop} + \varepsilon_{mp} + \varepsilon_p \quad (2.3)$$

where $d\rho$ is the orbital error in code measurements, d_{ion} and d_{trop} are the ionospheric and tropospheric errors in the code measurements, respectively, ε_{mp} is the error due to

multipath, and ε_p is the receiver code noise. In the case of a LEO the tropospheric effect is neglected, so Equation 2.3 becomes:

$$P = \rho + d\rho + c(\Delta t^S - \Delta t_R) + d_{ion} + \varepsilon_{mp} + \varepsilon_p \quad (2.4)$$

2.1.2 Carrier Phase Measurements

The carrier phase measurement is the difference between the phases of the receiver generated carrier signal and the carrier received from a satellite at the measurement instant. These measurements are made on the L1 or L2 carrier signal and may refer to the fractional part of the L1 or L2 carrier wavelength, expressed in units of metres and cycles. In carrier phase-based positioning, the carrier phase may also refer to the accumulated or integrated measurement which consists of the fractional part plus the whole number of wavelengths (or cycles) since signal lock-on. As mentioned previously, the carrier phase measurement is a direct measurement of the phase of the received signal. If the phase of the received carrier signal for the GPS satellite is denoted as φ^S and the phase of the reference carrier signal generated by the receiver as φ_R , (Hofmann Wellenhof et al., 1997) then,

$$\varphi_R(t_R) = \varphi_R(T_R) + \dot{\varphi}_R(\Delta t_R) \quad (2.5)$$

$$\varphi^S(t^S) = \varphi^S(T^S) + \dot{\varphi}^S(\Delta t^S) \quad (2.6)$$

The time t is an epoch considered from an initial epoch $t_0 = 0$. The carrier beat phase

$\varphi_R^S(t_R)$ is denoted as in Equation 2.7:

$$\begin{aligned}
\varphi_R^S(t_R) &= \varphi^S(t^S) - \varphi_R(t_R) \\
&= (\varphi^S(T^S) - \varphi_R(T_R) + f\Delta t^S - f\Delta t_R)
\end{aligned} \tag{2.7}$$

where the L1 carrier frequency $\dot{\varphi}$ has been replaced with f , and the appropriate terms from Equations 2.5 and 2.6 have been substituted in. The term f/c can be used to convert the geometric distance ρ into cycles. By accounting for all error sources affecting the carrier phase measurements, the observation equation in cycles is:

$$\phi = \rho + d\rho + c(\Delta t^S - \Delta t_R) - d_{ion} + \varepsilon_{mp} + \varepsilon_\phi + \lambda N \tag{2.8}$$

Where ε_ϕ is the receiver phase noise, λ is the wavelength of the GPS carrier, N is the number of integer cycles, and the rest of the terms are the same as mentioned in Equation 2.3.

2.1.3 Doppler Measurements

Since a GPS satellite is always in motion relative to the receiving body, the received frequency is Doppler shifted. The raw Doppler shift is linearly dependent on the radial velocity and for this reason velocity determination is very important in GPS navigation. The equation for the Doppler measurement scaled to units of range can be obtained by:

$$D(t) = \lambda \dot{\Phi} = \dot{\rho} + c(\Delta f_R^f - \Delta f^S) - \dot{\Delta}_{iono} + \delta \tag{2.9}$$

where $\dot{\rho}$ is the geometric range rate, Δf_R and Δf^s are the received and transmitted frequency (Hz), respectively, $\dot{\Delta}_{iono}$ is the ionospheric delay drift (m/s), and δ is the noise in Doppler measurements (m/s).

2.2 Relative Positioning Models and Orbit Configuration

For GPS positioning, to obtain the best possible navigation result, the integer nature of the DD carrier-phase ambiguities is exploited and resolved to their integer values. After fixing the DD ambiguities to integer wavelengths the relative position of both receivers at each epoch can be recovered with an accuracy determined essentially by the position dilution of precision (PDOP) and the measurement noise of the receivers. When only the relative position between two GPS receivers is required, use is made of GPS data differences between observations taken by both GPS receivers. Differenced GPS observation data has the advantage of eliminating or reducing common error sources, such as the GPS satellite clock offsets and common biases.

2.2.1 Single Difference Model

In this mode, a single difference (SD) observation is formed by subtracting two GPS observations of the same type and on the same frequency (L1 or L2), taken by two GPS receivers at the same instant and originating from a mutually observed GPS satellite. Considering two receivers C, D and satellite j at epoch t gives (Lachapelle, 2005)

$$\begin{aligned}\Delta\phi &= \phi_{rover} - \phi_{base} \\ &= \Delta\rho + \Delta d\rho - c\Delta dT + \lambda\Delta N - \Delta d_{ion} + \Delta\varepsilon_{mp} + \Delta\varepsilon_{\phi}\end{aligned}\tag{2.10}$$

where Δ is the SD operator. The SD operation between two receivers reduces orbital and atmospheric errors, and eliminates satellite clock error. However, it increases the noise by $\sqrt{2}$ compared to a single phase. Figure 2.1 shows the overall viewing geometry for relative positioning using differenced GPS observations. GPS satellites j and k are commonly observed by both receivers and thus SD and DD observations can be formed. This is not the case for GPS satellites h and m which are only observed by one receiver.

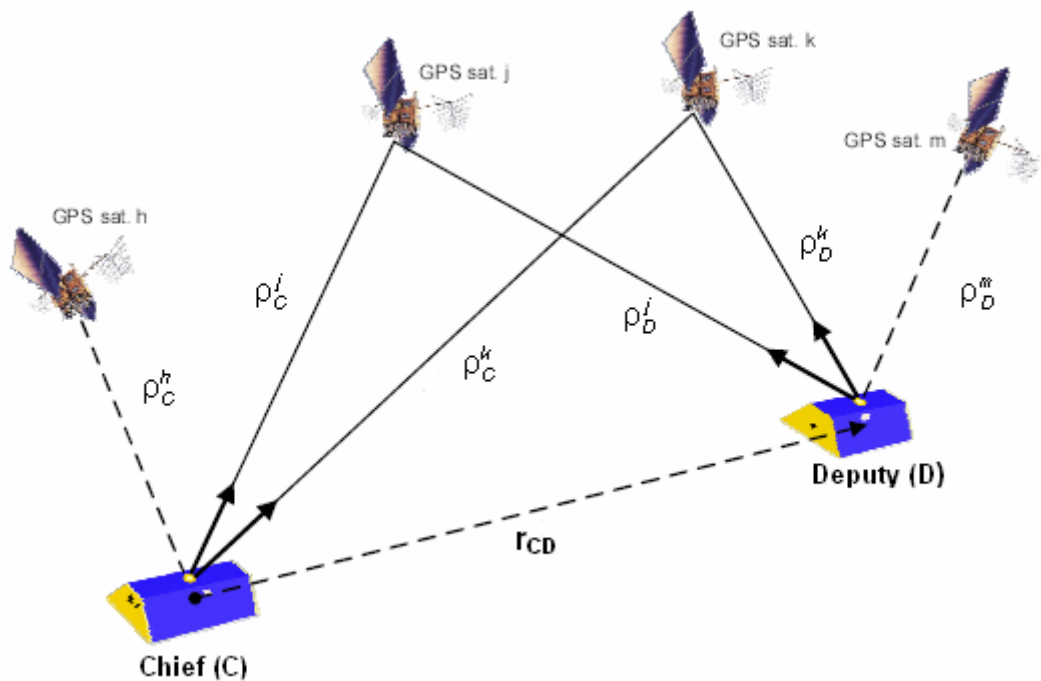


Figure 2-1: Overall Viewing Geometry for Relative Spacecraft Positioning Using Differenced GPS Observations (Kroes, 2006)

2.2.2 Double Difference Model

A DD observation is formed by subtracting two SD observations of the same type and frequency, taken by the same receivers and same epoch, but each relating to different

GPS satellites. If there are two satellites with one as a reference satellite, for the two receivers and epoch t , the DD equation will be:

$$\Delta\nabla\phi = \Delta\nabla\rho + \Delta\nabla d\rho + \lambda\Delta\nabla N - \Delta\nabla d_{ion} + \Delta\nabla\varepsilon_{mp} + \Delta\nabla\varepsilon_{\phi} \quad (2.11)$$

where $\Delta\nabla$ is the DD operator. The DD operation reduces orbital and atmospheric errors, and eliminates satellite and receiver clock errors, however, the DD noise and multipath ($\Delta\nabla\varepsilon_{mp}$ and $\Delta\nabla\varepsilon_{\phi}$) is twice compared to undifferenced measurements (Misra & Enge, 2001). From this fact, receiver noise and multipath are more significant errors in DD measurements.

2.2.3 Orbit Configuration

The orbits of the planets are ellipses with the sun at a common focus; orbits were first analyzed mathematically by Kepler who formulated his results in his three laws of planetary motion. As previously mentioned, this work will focus on nano-satellites rotating about the Earth in low Earth circular orbits. Furthermore, there is a 2-by-1 elliptical formation which is described by Tsoi (2007) in detail. The CanX-4 and -5 mission will be tested in stages. A simple coarse formation will be performed first, whereby the Deputy or the Chief satellite will simply try to negate secular drift in the separation distance between them (Sarda et al., 2006). Second, an along-track formation will be involved where both the Chief and Deputy satellites are flown in the same orbit with the Chief leading the Deputy by a specified distance and this is the case tested in this work. Once the nanosatellites have successfully completed this simple formation, one

satellite will be manoeuvred into a halo orbit around the other, by performing an orbital plane change. For a system of only two bodies that are only influenced by their mutual gravity, their orbits can be exactly calculated by Newton's laws of motion and gravity. Briefly, the sum of the forces will equal the mass times its acceleration. Gravity is proportional to mass, and falls off proportionally to the square of distance,

$$\ddot{r} = -\frac{\mu r}{\|r\|^3} \quad (2.12)$$

where r is the three-dimensional position vector of the satellite with respect to the centre of the Earth, μ is the Earth's gravitational parameter. To fully describe orbits, six parameters are required, and are called the Keplerian orbital parameters. These parameters shown in Figure 2.2 (Busse, 2002) and are defined below:

Ω	is the right ascension of ascending node
i	is the inclination of orbital plane
ω	is the argument of perigee
a	is the semi major axis of orbital ellipse
e	is the numerical eccentricity of ellipse
θ	is the mean anomaly, epoch of perigee passage

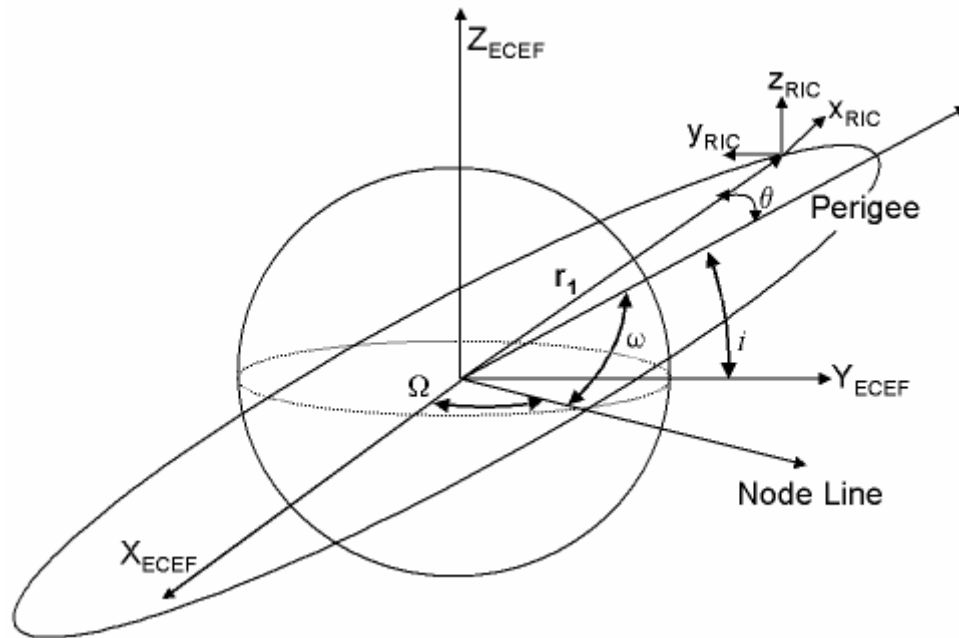


Figure 2-2: Keplerian Orbital Parameters (Busse, 2003)

2.3 GPS Error Sources

In this section and the following subsections a general background is given about the environment of the simulated errors and their properties. GPS errors can be classified into two categories - correlated and non-correlated. Spatially correlated errors can be reduced between a reference receiver and a rover receiver. However, correlated errors increase if the baseline length increased these errors such as atmospheric (troposphere and ionosphere) errors. The troposphere is the lowest part of the atmosphere, extending up to 50 kilometres in altitude above the Earth's surface. The tropospheric delay depends on the temperature, humidity, and pressure. It varies with the height of the GPS receiver. The total tropospheric delay can be separated into dry and wet components. The dry component, which reaches up to 90% of the total delay, is easier to determine than the wet component. Nanosatellites are considered as LEO satellites, which are often

distributed in satellite constellations, because the coverage area provided by a single LEO satellite is relatively small, and the satellite travels at a high speed (e.g. 7 km/s) to maintain its orbit. LEOs generally extend from the Earth's surface up to 2000 km. Non-correlated errors are those errors that are different for different receivers or their environments; these errors cannot be reduced using differencing techniques. These errors are multipath and receiver noise.

2.3.1 Orbital Error

Orbital errors result from inaccuracies in the broadcast ephemerides. These inaccuracies are the consequence of the inability to completely model the forces acting on a satellite and thus predict the satellite's orbit over time. Differencing observations from one satellite between receivers can reduce the error. As a rule of thumb, the effect of orbital errors on baseline determination is (Lachapelle, 2005):

$$\frac{db}{b} = \frac{d\rho}{\rho} \quad (2.13)$$

where db is the error in baseline, b is the length of baseline, $d\rho$ is the orbital error, and ρ is the satellite-receiver range. The range between the GPS satellites and the receivers varies from approximately 20,000 km, when the satellite is at the zenith, to about 26,000 km, when the satellite is close to the horizon. The typical RMS value of orbital error for the broadcast ephemerides is about 2 m (IGS, 2007); for a satellite at the zenith the corresponding baseline error is 0.1 ppm. For a baseline distance of 1 km, the corresponding baseline error would be 0.1 mm, which is negligible.

2.3.2 Clock Error

Clock errors occur in both the satellites and the receivers. Each satellite carries clocks that act as the time and frequency base for its realization of GPS system time. Satellite clocks are extremely accurate, but they suffer from slight clock drift. These clocks have a stability of about 1 part to 10^{13} over a day (Kaplan, 1996). The behaviour of the satellite clocks is monitored by the GPS ground control segment and the clock correction model is transmitted to users as part of the navigation message. The actual behaviour of the clock differs from this model because of unpredictable errors. These errors are mainly due to slowly changing signals of the clock and have no significant effect on receiver tracking. Receiver clock drift is generally larger than the satellite clock drift because of the lower quality of the oscillator. Differencing observations from one satellite between two receivers can eliminate the satellite clock error, while differencing observations from two satellites and one receiver can eliminate the receiver clock error.

2.3.3 Ionospheric Delay

The ionosphere is the band of atmosphere extending from about 50 to 1580 kilometres above the Earth's surface. The ionosphere can retard GPS signals from their velocity in free space by more than 300 ns in the worst case, corresponding to range errors of 100 metres (Bamford, 2004). The ionospheric delay depends on the Total Electron Content (TEC) along the signal path and on the frequency used, and this can be expressed in metres as in Equation 2.14. TEC is a function of solar ionizing flux, magnetic activity, user location, and viewing direction (Skone, 1998)

$$I_{\phi} = \frac{40.3 \cdot TEC}{f_{\phi}^2} \quad (2.14)$$

where the value of 40.3 is a derived constant and f_{ϕ} is the frequency of the carrier signal. Dual frequency receivers make use of the fact that the L1 and L2 signals experience different propagation delays in the ionosphere. However, the type of receivers used by the majority of civilian users is of the less expensive, single frequency kind, which does not measure on two frequencies. If dual frequency measurements are available, the Ionosphere-Free (IF) linear combination for code measurements can be computed as,

$$P_{IF} = P_{L1} - \frac{f_{L2}^2}{f_{L1}^2} \cdot P_{L2} \quad (2.15)$$

where P_{L1} and P_{L2} are the pseudorange measurement on L1 and L2, respectively. f_{L1} and f_{L2} are the corresponding frequency on L1 and L2, respectively. For more accurate estimation of the ionosphere, correction can be done by the ionosphere-free linear combination of the phase observation as,

$$\Phi_{IF} = \Phi_{L1} - \frac{f_{L2}}{f_{L1}} \cdot \Phi_{L2} \quad (2.16)$$

where Φ_{L1} and Φ_{L2} are L1 and L2 carrier phases. A couple of methods can be mentioned here to deal with ionospheric refraction. First, the satellite's navigation message includes an atmospheric refraction model that compensates for as much as 50% (RMS) of the error (Seeber, 2003). The second and more effective method to remove the

ionospheric delay is to use dual frequency GPS receivers. The value of the absolute ionospheric error is about 12 metres. When the level of ionospheric activity is low, a typical relative ionospheric error will be in the order of 1-2 ppm. In conditions when the ionosphere is more active, errors in the order of 10 ppm can be expected (Skone, 1998; Fortes et al., 2000).

2.3.4 Multipath

Multipath is the phenomena whereby a signal arrives at a receiver via multiple paths (Misra & Enge, 2001). Multipath propagation is almost inevitable in most GPS applications since many kinds of possible reflectors are normally present, such as the Earth's surface, buildings and other objects. However, in space applications, the case is different. The influence of these reflections depends on their signal strength and delay compared with that of the line-of-sight signal, the attenuation by the receiver antenna, and the measuring technique of the receiver. The theoretical maximum effect of multipath on C/A code pseudorange measurements can reach 0.5 ms when the reflected/direct signal strength ratio is one. Carrier phase measurements are not free from multipath either, though the effect is about two orders of magnitude smaller than in pseudoranges (Misra & Enge, 2001).

In the case of a spaceborne GPS receiver, multipath reflections are caused by the satellite surface, and the path delay thus depends on the spacecraft dimension (Kroes, 2006). To minimize the effect of multipath, choke-ring antennas maybe used for space missions. This is further discussed in Kroes (2006), however, Weiss et al. (2005) describe a new

advanced Global Navigation Satellite System (GNSS) multipath model that integrates reflector environment geometries, satellite almanac data, and antenna/receiver models to simulate multipath errors. This model has been developed to predict multipath error magnitudes, frequencies, and times of activity for many types of environments. These environments are the University of Colorado Engineering Center rooftop, an F-18 jet, and a C-5 large transport aircraft. Both real and simulated GPS multipath data are compared, and both results are promising (see Figure 2.3). For LEO missions, Kroes (2006) analyzed the multipath error for spacecraft from the GRACE mission and found that the C/A code multipath error in a spaceborne environment is at the decimetre level. Montenbruck & Kroes (2003) analyzed the effect of carrier phase multipath error for the CHAMP mission and found it to be at the millimetre level.

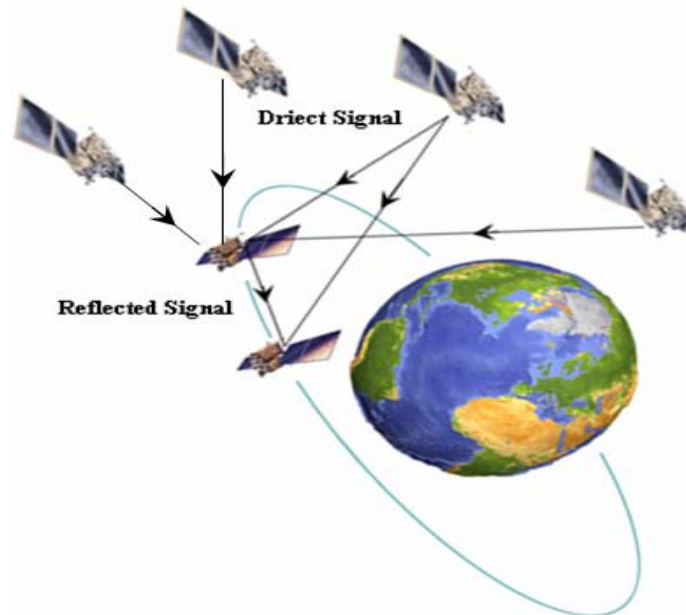


Figure 2-3: Direct and Multipath Signal

2.3.5 Receiver Noise

Carrier phase and code measurements are affected by noise which is considered to be white noise. This receiver noise is considered as one of the non-correlated errors due to the tracking loop (Raquet, 1998). All errors can be reduced by the DD process except for receiver noise and multipath. The magnitude of the receiver noise can be estimated using zero baseline tests (Raquet, 1998). The typical receiver noise level is summarized in Table 2.2. However, modern receiver technology tends to bring the internal phase noise below 1 mm, and reduces the code noise to the 10 cm level or lower. Montenbruck (2003) analyzed noise level of the phase measurements, using zero baseline tests with a NovAtel OEM4-G2L receiver and estimated the RMS error to be 0.8 mm for the L1 carrier, 1 mm for the L2 carrier, and 1.5 cm/s for the L1 Doppler measurement. Table 2.3 (Lachapelle, 2005) summarizes the magnitude of GPS error sources listed above.

Table 2-2: Receiver Noise for Different Observations (Hofmann Wellenhof et al., 1997)

Type of Obs.	Wavelength	Receiver Noise
C/A-code	300 m	3 m
P-code	30 m	30 cm
Carrier Phase	20 cm	2 mm

Table 2-3: GPS Error Sources and their Magnitudes. (Lachapelle, 2005)

Source	Comment	Residual Error (PPM)*
Orbital	Broadcast Eph.	0.1 ppm
Tropospheric	Model (e.g. Hopfield)	0.2-0.4 ppm
Ionospheric	L1 only	0.2-20 ppm
Ionospheric	Dual frequency	----
Multipath	Site dependent	3-15 mm
Noise	Receiver dependent	0.2-2 mm

* 1 PPM is 1 cm of relative error per 10 km of receiver spacing.

2.4 Coordinate Systems

To describe satellite motion, it is important to define a reference coordinate system. There is a direct relation between the accuracy of the observations from satellites and the accuracy of the reference system used (Seeber, 2003). Two different reference coordinate systems are used for describing satellite motion and terrestrial measurements. Global and geocentric coordinate systems are used to describe satellite motion, and these refer to the Earth's centre of mass. While terrestrial measurements can be described using any local coordinate system, it depends on where these measurements are taken. The relation between these two frames should be accurate (ibid). In this work, four coordinate systems are described as in the following four subsections. However, two systems are required in detail: (1) a space-fixed, for the description of satellite motion as the Local Orbiting Coordinate System (Hill Frame), and (2) an Earth-fixed, terrestrial reference frame for the positions, velocities and the analysis of results. A Geodetic Coordinate System is also called an Earth Centered Earth Fixed (ECEF) system. These are described below.

2.4.1 Inertial Coordinate System

The origin of the inertial frame is located at the Earth's centre of mass. The x_i vector is in the direction of the vernal equinox, the z_i vector pointing to the North Celestial Pole (NCP) and the y_i vector is perpendicular to the other axes forming a right-handed coordinate system (Schwarz, 1999) (see Figure 2.4 for details).

2.4.2 Orbital Coordinate System

The orbital coordinate system is commonly used to define the position and velocity of satellites on the Kepler ellipse. The origin of the orbital frame is located at the focus of the ellipse. The x_o vector points towards the perigee, the z_o vector is normal and pointing out from the orbital plane and the y_o vector is orthogonal to the other axes forming a right-handed coordinate system (Schwarz, 1999) (see Figure 2.4 for details).

2.4.3 Orbiting Coordinate System (Hill Frame)

This frame is defined as a right handed rotating coordinate system with its origin located at the reference satellite; although in practice this origin does not have to be occupied by a physical satellite (Sünkel, 1998). The orientation of this triad is defined with the x_h vector pointing in the radial direction, the y_h vector aligning to the velocity vector and the z_h vector pointing in the cross-track direction forming a right-handed coordinate system (see Figure 2.4 and Tsoi (2007) for details). The main reason for using the Hill frame and its equations is because these equations are easy to use. These equations are a set of linearized, constant coefficient differential equations and hence can be solved analytically to provide a solution that can be easily understood. The design of satellite control algorithms generally requires a set of constant coefficient and linearized equations, for this reason Hill's equations can be used since they are very effective (Schweighart, 2001). Transformation from Hill's frame to the ECEF frame is shown in Section 2.4.6.

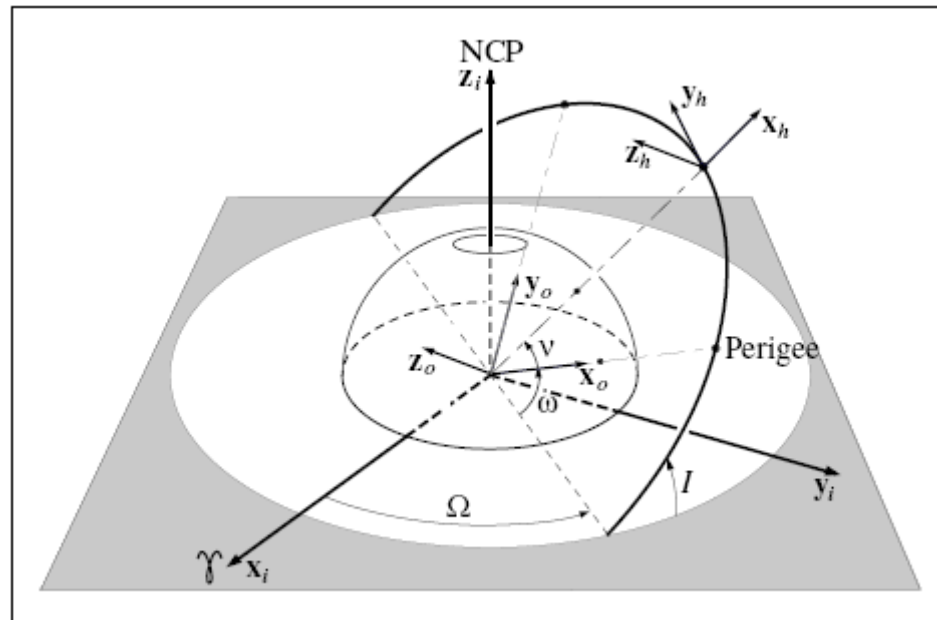


Figure 2-4: Representation of Orbital, Inertial and Hill Coordinate Systems (Schwarz, 1999)

2.4.4 Geodetic Coordinate System

The Earth-Fixed frame is a rotating coordinate system with its origin located at the Earth's centre of mass. The x_g vector is the intersection between the equator plane and the mean meridian plane of Greenwich, the z_g vector is aligned with the spin axis of the Earth and the y_g vector is orthogonal to the other axes forming a right handed coordinate system. With a datum ellipsoid defined, curvilinear measures are used for representation of the geodetic coordinates, where φ is the latitude, λ is the longitude, and h is the height above the datum ellipsoid (see Figure 2.5 for details).

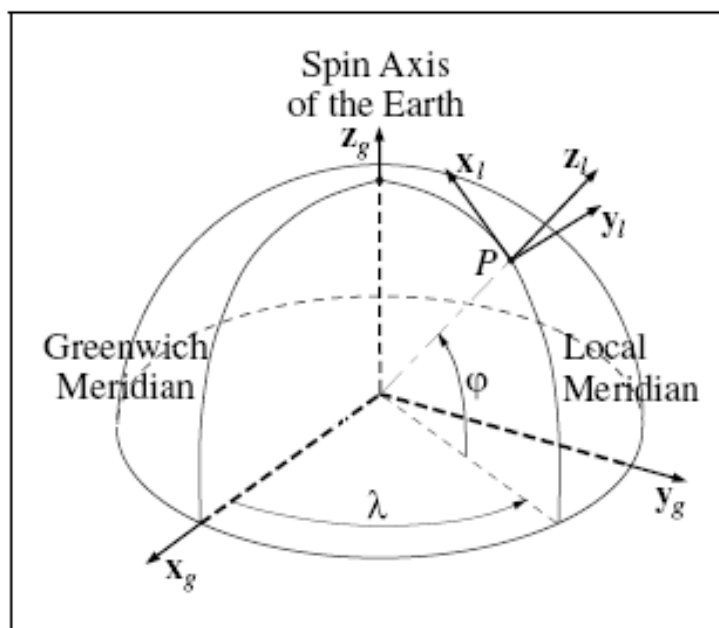


Figure 2-5: Representation of the Global and Local Geodetic Coordinate Systems (Moritz, 1980)

2.4.5 Local Geodetic Coordinate System

With the datum ellipsoid defined, a local geodetic coordinate system is established. The origin is located at the point of interest P , with the x_l vector tangent to the geodetic meridian pointing north, the z_l vector orthogonal to the ellipsoid at point P and y_l pointing east forming a left-handed system.

2.4.6 Coordinate Transformation

Coordinate transformations shown here deal only with orientation. Note that for coordinate systems with different origins, a translation vector must be applied. Using rotation matrices, the coordinate transformations between different frames are as follows:

- **Orbital to Inertial** (Seeber, 2003)

$$r_i = R_3(-\Omega)R_1(-I)R_3(-\omega)r_o$$

- **Inertial to Hill** (Sünkel, 1998)

$$r_h = R_3(u)R_1(I)R_3(\Omega)r_i$$

- **Local Geodetic to Geodetic** (Schwarz, 1999)

$$r_g = R_3(\pi - \lambda)R_2(\pi/2 - \varphi)P_2r_l$$

- **Inertial to Geodetic** (Schaub & Junkins, 2003)

$$r_g = R_3(GAST)r_i$$

- **Geodetic to Inertial** (Schwarz, 1999)

$$\begin{aligned} r_i &= R_3(\omega^e)r_g \\ &= \begin{pmatrix} \cos \omega^e t & -\sin \omega^e t & 0 \\ \sin \omega^e t & \cos \omega^e t & 0 \\ 0 & 0 & 1 \end{pmatrix} r_g \end{aligned}$$

- **Geodetic to Hill** (Sünkel, 1998)

$$\begin{aligned} r_h &= (R_g^i * R_i^h)r_g \\ &= R_g^h r_g \\ &= R_3(\omega^e)[R_3(u)R_1(I)R_3(\Omega)]r_g \end{aligned}$$

- **Hill to Geodetic**

$$r_g = R_h^g r_h$$

where

I is the inclination,

Ω is the right ascension of ascending node,

ω is the Perigee angle

u is the Argument of latitude

$GAST$ is the Greenwich apparent sidereal time

ω^e is the Earth's Rotation

R_g^i is the Rotation matrix from the geodetic frame to inertial frame

R_h^g is the rotation matrix from Hill frame to geodetic frame

R_1 is the rotation about X-axis, $R_1(\theta) = \begin{pmatrix} 1 & 0 & 0 \\ 0 & \cos(\theta) & \sin(\theta) \\ 0 & -\sin(\theta) & \cos(\theta) \end{pmatrix}$

R_2 is the rotation about Y-axis, $R_2(\theta) = \begin{pmatrix} \cos(\theta) & 0 & -\sin(\theta) \\ 0 & 1 & 0 \\ \sin(\theta) & 0 & \cos(\theta) \end{pmatrix}$

$$R_3 \quad \text{is the rotation about } Z\text{-axis, } R_3(\theta) = \begin{pmatrix} \cos(\theta) & \sin(\theta) & 0 \\ -\sin(\theta) & \cos(\theta) & 0 \\ 0 & 0 & 1 \end{pmatrix}$$

CHAPTER 3

RELATIVE SPACECRAFT POSITIONING

In traditional ground based relative positioning applications, the coordinates of an unknown receiver position is determined with respect to a known point which is usually stationary. In space-based relative navigation applications, both the Chief and Deputy receivers are orbiting around the Earth. Their initial positions and velocities are not initially well known, and they are both moving with respect to one another. To overcome this problem, the FLYKIN+™ software with Moving Base Station (MBS) ability was modified by Crawford (2005) and used to allow for relative positioning between two moving receivers. FLYKIN+™ is a C++ program developed by the PLAN Group at the University of Calgary for the purpose of processing pseudorange, carrier phase and/or Doppler measurements for relative navigation (PLAN, 2003). Furthermore, a new modification was added in this work based on the availability of GPS satellites for both the Chief and Deputy, for the purpose of spacecraft formation flying. In this chapter, details regarding availability will be discussed. However, further details about software capabilities and modifications can be found in Chapter 5.

3.1 Measurement Model

In this work, the measurement model used for relative navigation is based on DD observations which were discussed in Section 2.2.2. The DD operation reduces orbital and atmospheric errors, also eliminates satellite and receiver clock errors; however, the DD multipath and noise $\Delta\nabla\varepsilon_{mp}$ and $\Delta\nabla\varepsilon_\phi$ are twice that of undifferenced measurements (Misra & Enge, 2001). By using the DD observation model, all residual errors are put together in a single group without discrimination and are assumed to be white noise, although this is not generally true for multipath. The DD measurement model includes pseudorange, carrier phase, and Doppler measurements.

$$\Delta\nabla P_{CA} = \Delta\nabla\rho + \Delta\nabla\varepsilon_p \quad (3.1)$$

$$\Delta\nabla\phi = \Delta\nabla\rho + \lambda\Delta\nabla N + \Delta\nabla\varepsilon_\phi \quad (3.2)$$

$$\Delta\nabla\dot{\phi} = \Delta\nabla\dot{\rho} + \Delta\nabla\varepsilon_\phi \quad (3.3)$$

The use of the pseudorange measurement is only before ambiguity resolution, as it is not of great importance after the integer ambiguities are resolved for the carrier phase measurements. Doppler measurements have a great impact on relative velocity estimation. Tsoi (2007) discusses different combination of these measurements to determine the optimal observation set to be used for relative navigation.

3.2 Extended Kalman Filter

Within the significant toolbox of mathematical tools that can be used for stochastic estimation applications from noisy sensor measurements, one of the most well-known and often-used tools is the Kalman Filter (KF). Theoretically the KF is an estimator for what is called a linear quadratic problem, which is the problem of estimating the instantaneous state of a linear dynamic system perturbed by white noise, by using measurements linearly related to the state (Grewal & Angus, 2001). Note that the KF measurement model assumes a linear relationship between the observations and the state vector, which is generally not true for navigation applications. To overcome this problem, an EKF is implemented to linearize the measurement model.

The EKF is very robust for precise relative navigation in addition to the ability of estimating the state vector even in the face of non-linear relationships (Busse et al., 2002). Basically there are three steps used in the DD carrier phase positioning. These steps are float Kalman filter, ambiguity fixing and ambiguity validation. The float solution implemented uses the Kalman filter, which usually has two main steps: time update and measurement update. The time update equations can be thought of as predictor equations, where the state vector and error covariance matrix are projected ahead of the measurement update. The measurement update equations can be thought of as corrector equations, where the computation of the Kalman gain, updating of the estimates using measurements, and updating of the error covariance matrix are done. Related to the filter, two models were implemented: the dynamic model and measurement model. The dynamic model describes the state variable and their relation with each other and over

time, and in this case the state vector that usually contains three position states, three velocity states, and the DD ambiguity state for each double difference. It also describes the variance covariance matrix of the state vector. The measurement model describes the roots of the state through the design matrix (Grewal & Angus, 2001).

3.2.1 EKF Dynamic Model

As mentioned previously, there are three basic steps to differential positioning using carrier phase observables. The float Kalman filter has two main steps: time update and measurement update. The state vector is as follows (Liu, 2003):

$$\mathbf{x} = (\varphi, \lambda, h, \dot{\varphi}, \dot{\lambda}, \dot{h}, \Delta\nabla\hat{N}_1, \Delta\nabla\hat{N}_2, \Delta\nabla\hat{N}_3, \dots, \Delta\nabla\hat{N}_n) \quad (3.4)$$

where (φ, λ, h) which are the three position states (latitude and longitude in units of radians, height in metres), three velocity states $(\dot{\varphi}, \dot{\lambda}, \dot{h})$ (latitude rate and longitude rate in units of radians per second, height rate in units of metres per second), and the DD ambiguity states $\Delta\nabla\hat{N}$ (in units of cycles) for each satellite-receiver pair. The dynamics of the system used are modeled using a random walk model or a Gauss-Markov model, which makes the transition matrix easily obtained.

3.2.2 EKF Measurement Model

The measurement model in the Kalman filter relates the state vector to the GPS measurements through the design matrix, H . The state vector should be regularly updated by measurements as the system will diverge if there is no measurement update

over a long period of time, driven by the system input noise. Strategy 1 is used in these tests; however, the software supports eight different strategies, and the observations for the float filter are the carrier phase observables and pseudorange observables (CP and P). Providing the DD pseudorange observations can reduce the time for the Kalman filter to converge and resolve ambiguities to integers easily. In this work, DD pseudoranges are also used to speed up the filter convergence, which aids ambiguity fixing.

3.3 Integer Ambiguity Resolution

Integer ambiguity resolution is essential for high precision relative GPS positioning (Tiberius et al., 1995). In this work the LAMBDA method is used for integer ambiguity resolution which gives the highest possible success rate for estimating the correct integers (Teunissen, 1995). However, a validation test should be performed after fixing these ambiguities and this is usually done based on a ratio test called F-Ratio test. In this test, there is a comparison of the smallest sum of squared ambiguity residuals against the second smallest, and this should be greater than a specific value called “Ratio threshold” which is often selected as three (Teunissen, 1999). The FLYKIN+™ software supports eight different strategies for ambiguity fixing, with each one using a different set of pseudorange and carrier phase measurements. In this work the simplest one is used (Strategy 1), where only the L1 carrier phase and pseudorange measurements are used and only L1 ambiguities are estimated. In addition, the ionospheric error is not taken into account, as it assumes that the effect of the ionospheric error is sufficiently minimized in the DD process (Liu, 2003). This strategy works well for short baselines (< 5 km). An

advantage of this strategy is its simplicity. Another advantage is the low noise and ionospheric error in comparison with L2 and WL, if the ambiguities are fixed correctly. But this strategy has the disadvantage of solving integer ambiguities in the presence of high ionospheric error, because of the short wavelength of L1.

3.3.1 Integer Ambiguity Estimation

Teunissen (1999) describes the integer ambiguity estimation procedure which includes the following steps. First, is the estimation of the real valued ambiguities (float ambiguity) using the least square estimation method. This method gives good position accuracy, especially for short baselines and low ionospheric effects. These values are then mapped to their integer values using LAMBDA. By using Equation 3.5, a check on the ratio is performed as follows:

$$\frac{v^T P v_{\text{secondbest}}}{v^T P v_{\text{best}}} \quad (3.5)$$

Where v is the residual vector and P is the inverse of the ambiguity covariance matrix. After estimating the real valued ambiguities and fixing them to their integer values, a validation of the set of integers should be tested using $v^T P v$. Lastly, the ratio between the second best and the best is calculated and then compared to a threshold value. If they are less than this threshold, the values will be accepted. During ambiguity resolution some challenges can be faced such as efficiency, reliability, and cycle slips (Lachapelle, 2005). Efficiency is important especially when the search space is chosen, i.e. if the search space is large it will take a longer time to find integers, and the uncertainty in the

position is increased especially in kinematic mode. For reliability $v^T P v$ is an optimal measurement of the ambiguity validation based on certain assumptions. Finally, cycle slips reset the integer ambiguity resolution search and this may cause problems depending on the number of satellites affected and the frequency of the slips.

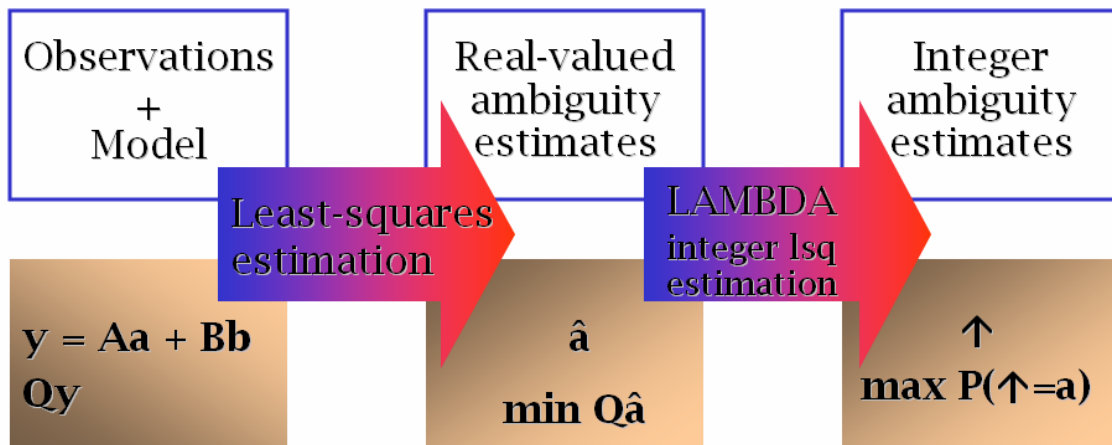


Figure 3-1: Integer Ambiguity Estimation Procedure (Teunissen, 1999)

3.4 Availability of Chief and Deputy Positions and Velocities

In the ideal case, the Chief and Deputy positions and velocities are estimated according to Section 3.4.1 (i.e. absolute positions and velocities of the Chief are determined using pseudorange and Doppler measurements), and relative positions and velocities are determined using DD carrier phase and Doppler data. Since both sets of positions and velocities are needed at the Deputy satellite in order to facilitate the guidance and control function, under these circumstances described above, the highest levels of position and velocity accuracy are obtained at a consistent data rate (e.g. every 1-5 seconds). In some

circumstances, the positions and velocities of the Chief and Deputy may be compromised in terms of accuracy and availability at the Deputy location. The following subsections below summarize the ideal case, followed by three scenarios where there is degradation in performance. Note that the following is for the information available at the Deputy which is transmitted to the guidance and control algorithm, see Table 3.1 for details.

3.4.1 Case I (Ideal): Chief and Deputy Each Track ≥ 4 SVs and the Data Link is Available

In this case both the Chief and Deputy track more than four satellites. This is considered as the ideal case. In Chapter 4 some GPS satellite availability tests versus antenna boresight angle from the zenith are analysed. These tests show that 99% of the time there are more than four satellites in view. But in some cases, the number of satellites may be less than four. For this reason the modification regarding data extraction and position and velocity propagation was added to the FLYKIN+™ software. In this case, Chief and Deputy position will be propagated as follows:

- The Chief absolute position and velocity are determined from pseudorange and Doppler data in single point mode with an accuracy of 2-5 m (RMS) and 5-10 cm/s (RMS).
- The Deputy position and velocity are determined from DD carrier phase and Doppler data with a relative accuracy of 1-2 ppm (RMS) and 1-3 cm/s (RMS).

3.4.2 Case II: Chief and Deputy Each Track ≥ 4 SVs and the Data Link is not Available

For this case, and the following two cases, the positions are propagated when there are less than four satellites. The Chief and Deputy positions are determined as follows:

- The Chief absolute position at the current time is propagated forward using the position and velocity from the previous epoch. The accuracy is dependent on the validity of the constant velocity assumption and will degrade over time relative to the initial accuracy of 2-5 m (RMS).
- The Deputy position at the current time is propagated forward using the relative position and velocity from the previous epoch. The accuracy is dependent on validity of constant velocity assumption and will degrade over time relative to the initial accuracy of 1-2 ppm (assuming the start is a fixed DD solution).
- Chief and Deputy velocities will have the same values as the previous epoch due to the constant velocity assumption.

3.4.3 Case III: Chief Tracks ≥ 4 SVs, Deputy Tracks < 4 SVs and the Data Link is Available

- The Chief absolute position is determined from pseudorange and Doppler data with an accuracy of 2-5 m (RMS) and 5-10 cm/s (RMS).
- The Deputy position at the current time is propagated forward using the relative position and velocity from the previous epoch. The accuracy is dependent on validity of constant velocity assumption and will degrade over time relative to the initial accuracy of 1-2 ppm (assuming the start is a fixed DD solution).

- If data link is not available, this reverts to Case II.

3.4.4 Case IV: Chief Tracks <4 SVs, Deputy Tracks ≥ 4 SVs and the Data Link is Available

- The Chief absolute position at the current time is propagated forward using the position and velocity from the previous epoch. The accuracy is dependent on the validity of the constant velocity assumption.
- The Deputy position at the current time is propagated forward using the relative position and velocity from the previous epoch. The accuracy is dependent on the validity of the constant velocity assumption.
- The above are the same if the data link is not available since there is no new Chief position and velocity transmitted that has the same effect as < 4 satellite tracking.

Table 3.1 shows a summary of the above four phases.

Table 3-1: Scenarios Description Summary of Available Information at the Deputy

Chief Satellite (≥ 4 SV's)	Data Link	Deputy Satellite (≥ 4 SV's)	Forwarded to G&C Algorithm
Case I			
Absolute Position $P_{Che}^{abs}(GPS)_{t_k}$ *	Available	Relative Position $P_{Dep-Che}^{rel}(GPS)_{t_k}$ **	Absolute Position $P_{Che}^{abs}(GPS)_{t_k}$
Absolute Velocity $V_{Che}^{abs}(GPS)_{t_k}$		Relative Velocity $V_{Dep-Che}^{rel}(GPS)_{t_k}$	Absolute Velocity $V_{Che}^{abs}(GPS)_{t_k}$
			Relative Position $P_{Dep-Che}^{rel}(GPS)_{t_k}$
			Relative Velocity $V_{Dep-Che}^{rel}(GPS)_{t_k}$
Chief Satellite (≥ 4 SV's)	Data Link	Deputy Satellite (≥ 4 SV's)	Forwarded
Case II			
Absolute Position $P_{Che}^{abs}(PROP)_{t_k}$ ***	Not Available	Relative Position $P_{Dep-Che}^{rel}(PROP)_{t_k}$	Absolute Position $P_{Che}^{abs}(PROP)_{t_k}$
Absolute Velocity $V_{Che}^{abs}(PROP)_{t_k}$		Relative Velocity $V_{Dep-Che}^{rel}(PROP)_{t_k}$	Absolute Velocity $V_{Che}^{abs}(PROP)_{t_k}$
			Relative Position $P_{Dep-Che}^{rel}(PROP)_{t_k}$
			Relative Velocity $V_{Dep-Che}^{rel}(PROP)_{t_k}$
Chief Satellite (≥ 4 SV's)	Data Link	Deputy Satellite (< 4 SV's)	Forwarded
Case III			
Absolute Position $P_{Che}^{abs}(GPS)_{t_k}$	Available	Relative Position $P_{Dep-Che}^{rel}(PROP)_{t_k}$	Absolute Position $P_{Che}^{abs}(GPS)_{t_k}$
Absolute Velocity $V_{Che}^{abs}(GPS)_{t_k}$		Relative Velocity $V_{Dep-Che}^{rel}(PROP)_{t_k}$	Absolute Velocity $V_{Che}^{abs}(GPS)_{t_k}$
			Relative Position $P_{Dep-Che}^{rel}(PROP)_{t_k}$
			Relative Velocity $V_{Dep-Che}^{rel}(PROP)_{t_k}$
Chief Satellite (< 4 SV's)	Data Link	Deputy Satellite (≥ 4 SV's)	Forwarded
Case IV			
Absolute Position $P_{Che}^{abs}(PROP)_{t_k}$	Available	Relative Position $P_{Dep-Che}^{rel}(PROP)_{t_k}$	Absolute Position $P_{Che}^{abs}(PROP)_{t_k}$
Absolute Velocity $V_{Che}^{abs}(PROP)_{t_k}$		Relative Velocity $V_{Dep-Che}^{rel}(PROP)_{t_k}$	Absolute Velocity $V_{Che}^{abs}(PROP)_{t_k}$
			Relative Position $P_{Dep-Che}^{rel}(PROP)_{t_k}$
			Relative Velocity $V_{Dep-Che}^{rel}(PROP)_{t_k}$
* Chief absolute position from pseudorange and Doppler data at current time.			
** Deputy position from DD carrier phase and Doppler data.			
*** Chief absolute position at current time is propagated forward using position and velocity from previous epoch.			

3.5 Summary

Ambiguity resolution is essential for high precision relative GPS positioning. In order to achieve high precision results, the integer nature of the ambiguities has to be exploited. The DD operator reduces orbital and atmospheric errors, and eliminates satellite and receiver clock errors. However, the DD noise and multipath are twice that compared to undifferenced measurements. In reality, the Chief and Deputy satellites track more than four satellites most of the time. However, availability tests were performed and are reported in Chapter 5.

CHAPTER 4

HARDWARE-IN-THE-LOOP DEMONSTRATION

This chapter presents the conditions and setup of a Hardware-In-The-Loop (HWIL) signal simulator using the NovAtel FFTB. A brief overview of the GPS receiver used and some fundamentals for orbital dynamics will be also introduced; however, many references exist and are cited.

4.1 OEM4-G2L Receiver Overview

Spacecraft receivers are almost the same as ground-based receivers, but ground-based receivers are programmed with altitude and speed limits because of US COCOM restrictions (OEM4-G2L 2003). Spacecraft receivers operate at high velocities and altitudes; therefore, these restrictions must be removed. The GPS receiver to be used in this research is the NovAtel OEM4-G2L dual-frequency unit (OEM4-G2L, 2003 - see Figure 4.1). The OEM4-G2L is a small, high-performance, self-contained receiver which is used in a wide variety of demanding applications including aircraft applications; see Table 4.1 for receiver performance.



**Figure 4-1: NovAtel OEM4-G2L Dual-Frequency GPS Receiver (125X85 mm)
(OEM4-G2L, 2003)**

Table 4-1: GPS Receiver Performance (OEM4-G2L, 2003)

Receiver Performance	
Position Accuracy	1.8 m L1 only Absolute Position
	1.5 m L1/L2 Absolute Position
	2-5 cm RMS Relative Position
Velocity Accuracy	3 cm/s RMS Absolute
	0.1-0.3 cm/s Relative
Time Accuracy	20 ns RMS
Measurement Precision	6 cm RMS C/A pseudorange

4.2 NOVATEL FFTB Environment

The FFTB simulates a GPS constellation and a formation for two vehicles (Chief and Deputy). It produces actual RF signals that are transmitted to the receivers such that they respond to conditions similar to a field environment. The benefits of using an HWIL simulator is to test the GPS receiver to be used in this mission on the ground instead of in orbit, such that the hardware and algorithms used in the software for relative

navigation can be evaluated. Figure 4.2 shows a block diagram of the FFTB setup, while Table 4.2 shows the hardware configuration used in these tests. The FFTB can be divided to three parts, with the first part being the software interface (SimGEN), where it is considered as the control panel for the hardware simulator (STR 4760 GPS Simulator), where all the parameters and conditions specified. STR 4760 is the hardware part of the FFTB, where the GPS signal are simulated and sent to the GPS receivers through the EF400 Cables. The third part is the GPS receiver, where all data are collected and saved to cards for later data processing.

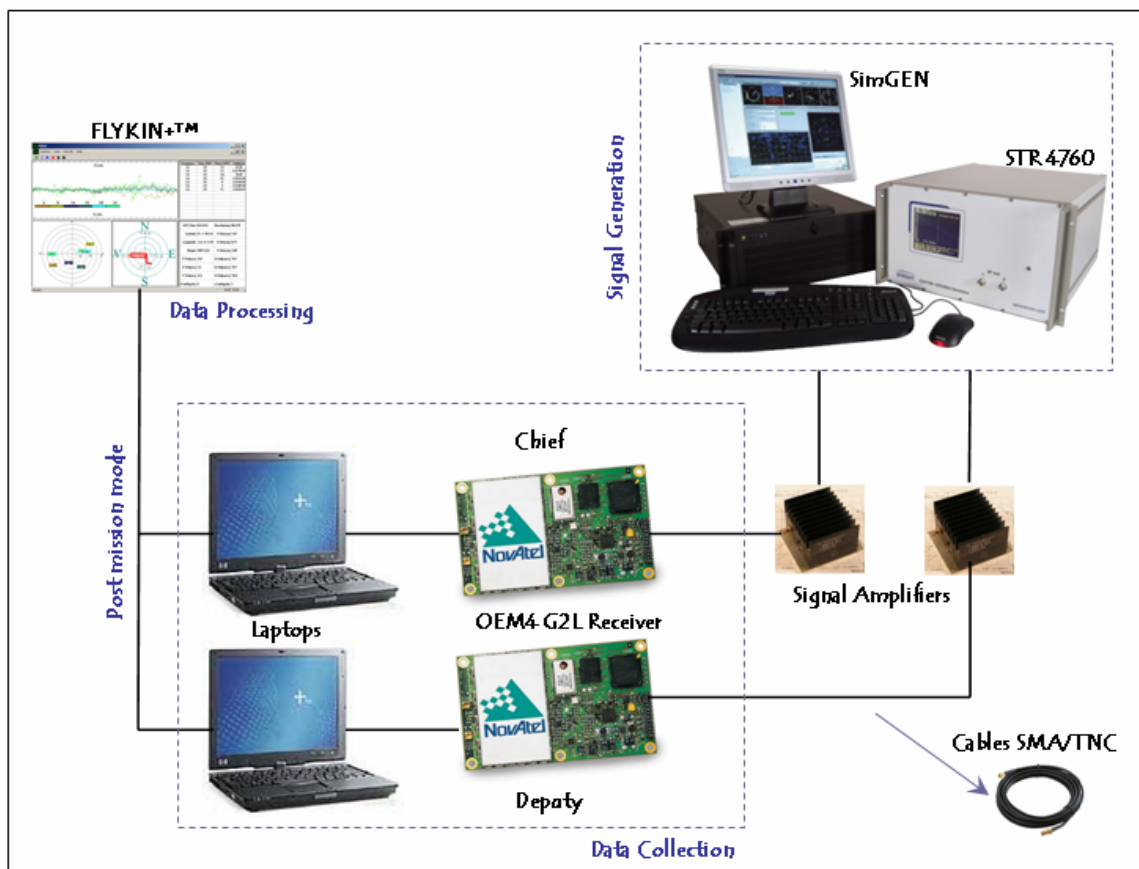


Figure 4-2: FFTB Setup

Table 4-2: Hardware Configuration Used in These Tests

Item	Description
Receiver	OEM4-G2L
Simulator	STR 4760 GPS Simulator
Amplifier	MINI-CIRCUIT 15542, Model No. ZHL-1217HLN
Cables	EF400 Cables (SMA/TNC)

SimGEN is able to generate an RF signal that simulates the GPS receiver to be tested. A simulator of 12 channels can generate a direct signal or reflected (multipath) signal. Normal signal level power is in the range of -20 to +20 dB, but multipath signals may go down to -49 dB (Spirent, 2005). Currently there are five different multipath types supported by the SimGEN software: ground reflection, fixed offset, Doppler offset, vertical plane, and reflection pattern. The most appropriate type for our application is the vertical plane type, as it reflects the real life multipath for space application. The vertical plane model assumes that the reflected signal, with respect to a vertical plane, is located on either side of the GPS receiver (the only reflected surface in space). The location and dimensions of the vertical plane can be specified by the user.

Moreover, the process begins with inserting the parameters to the simulator software (SimGEN); however, the software has three options for determining the user motion (Spirent, 2005):

- **Stored Files:** The user motion can be taken from stored files from previous and actual missions. These files contain the state information of the vehicles.
- **External Source:** The state information of the vehicles is provided in real time from external sources.

- **Simulated Motion:** The software is capable of simulating the user's motion.

In this work the simulated motion option was used, with all the parameters inserted by the user. These parameters include:

- Spacecraft property for the two simulated vehicles: These properties include mass of the spacecraft, the cross-sectional area for use in drag calculations, and moments of inertia.
- Trajectory parameters: These parameters include a reference frame to be used, and orbital parameters to be used including semi-major axis, inclination angle, eccentricity, and mean anomaly.
- Gravity model: The number of terms used in the gravity model (1 to 70). More terms make the gravity model more precise but require more computational time.
- GPS constellation: The ephemeris parameters are loaded from an external file or are created by the simulator internally.
- Ionosphere properties: The default case is to use the ionospheric model specified in ICD-GPS-200
- Antenna characteristics: Noise characteristics and gain pattern are set.

The previously mentioned information is used to simulate the motion of the vehicles and to form the signals that are observed by the receivers.

As mentioned previously, SimGEN is connected to the hardware simulator where it feeds the GPS receiver with the signal. In between the receiver and the simulator, an RF amplifier is connected to compensate for the noise from the cables used. The GPS

receiver is connected to a computer for data collection and monitoring. All the data from the receiver are saved as binary files. For data analysis, the FLYKIN+™ software is used with the software developed by PLAN group at the University of Calgary. This software package is capable of processing two moving base stations, where the reference and the rover satellites are both moving (PLAN, 2003).

4.3 NOVATEL FFTB Setup

The FFTB has many parameters in its simulation environment, with the parameters entered by the user and related to vehicle motion, dynamics, and signal generation. For the dynamics, the simulation scenario uses a tenth-order gravity model; however, more terms can be used thus making the gravity model more precise but requiring more computational time. Both vehicles are modeled identically, with a surface area of 1 m^2 , a drag coefficient of zero, and 0.001 tonne (the smallest mass simulator can model). For spacecraft attitude mode, the spacecraft may be set to maintain an Earth-pointing or sun-pointing attitude or to maintain its initial attitude with respect to the inertial reference frame. In this work the spacecraft maintains an earth-pointing attitude which results in almost identical drag forces on all vehicles. The reason for choosing the spacecraft as Earth pointing is to keep the GPS antenna pointing upward, so more GPS satellites are tracked. The mask angle is chosen to be five degrees (common value), where all the GPS satellites below this angle are not simulated.

For the ionosphere, there are two options for the model (Off or Modeled). If the Off option is selected, then the effect of the ionosphere is neglected (not simulated),

otherwise if the Modeled option is selected, then the ionospheric effect is simulated. There are three options when the effect of ionosphere is on: Terrestrial, Spacecraft or Switched. If Switched is selected then the height and the transition rate which switch from terrestrial to spacecraft model should be specified. The ionosphere is modeled using the following equation, where this equation represents that standard model for ionospheric noise (Parkinson et al., 1996),

$$I_i^m = \frac{82.1 \times TEC}{f_c^2 \times \sqrt{\sin^2 \gamma_i^m + 0.076} + \sin \gamma_i^m} \quad (4.1)$$

where f_c is the frequency of the GPS signal (L1 or L2) and γ_i^m is the elevation angle of the GPS satellite m as measured by receiver i .

The TEC is difficult to determine, and for this work it was assumed to be constant at 10^{17} electron/ m^2 . This represents an unrealistic simplification, since the TEC will normally vary depending on many different conditions, such as day or night. The GPS constellation ephemeris parameters are created by the simulator internally.

For multipath, the most appropriate type for the spacecraft application is the vertical plane type. The vertical plane model assumes that the reflected signal with respect to a vertical plane is located on either side of the GPS receiver. The location and dimensions of the vertical plane can be specified by the user. In the case of CanX-4 and -5, particularly when they are close to each other, a multipath signal may occur whereby the signal may hit one of the spacecraft and be received as a multipath signal by the other receiver. By assuming one of the spacecraft as a vertical plane with the same dimensions

and displacement, then a multipath signal may occur, however multipath is not expected to be a significant error source for nanosatellites. In addition, the effect of multipath was investigated in Chapter 6, and shows that the effect of multipath is substantially negligible.

4.4 Formations

For the formations simulated, the orbit altitude was set at about 650 km, the eccentricity was set to zero, and the inclination angle was set to 98 degrees. Three different formations were simulated based on the following parameters:

- *100 m in-track.* In this scenario both the Chief and Deputy are in the same orbital path, with a 100 m separation in the in-track direction. The separation between the two vehicles is because of the difference in the mean anomaly.
- *1 km in-track.* This is the same as the previous scenario, but the baseline separation is approximately 1 km, with the difference purely related to a change the mean anomaly between Chief and Deputy.
- *5 km in-track.* Similar to the previous scenario, with a 5 km separation and both Chief and Deputy in the same orbital path.

The orbital parameters used are similar to the parameters used in the CanX-2 mission (Caillibot et al., 2005). Most planetary orbits in the solar system have relatively small inclination angles. However, a high inclination angle has been chosen for CanX-4 and -5 to give a near polar retrograde orbit similar to CanX-1. As for the remaining elements, they are set to zero arbitrarily (Caillibot et al., 2005) (see Table 4.3).

Table 4-3: CanX-4 and -5 Orbital Parameters (Caillibot et al., 2005)

Orbital Parameter	Value
Semi-major axis	ae + 650 km
Inclination	98°
RAAN	0°
Eccentricity	0
Mean anomaly	0°
Arg. of Perigee	0°

4.5 Summary

In this chapter the conditions and setup of HWIL signal simulator using the NovAtel FFTB were discussed in details. The following tests in Chapters 5 and 6 were done by using the NovAtel FFTB. The hardware was provided in this work (STR 4760 GPS Simulator, OEM4-G2L GPS Receiver, and EF400 Cables (SMA/TNC)) by the NovAtel Inc. Laboratory, Calgary AB, Canada.

CHAPTER 5

TEST SCENARIOS AND AVAILABILITY TEST RESULTS

In this chapter, availability tests of GPS satellites were done to analyze the number of GPS satellites' in view versus the GPS antenna boresight angle which was measured from zenith. As previously discussed in Section 3.4, the Chief and Deputy receivers should track at least four satellites to determine the absolute and relative position and velocity with the desired accuracy. However, in the case of tracking less than four satellites, the software is still capable of propagating positions and velocities from the previous epoch. Six different scenarios with different antenna boresight angles were tested using an HWIL signal simulator.

5.1 Analysis of GPS Satellites in View versus GPS Antenna Boresight Angle from Zenith

In the following, the use of an HWIL signal simulator was demonstrated to analyze the GPS satellites' availability with different antenna boresight angles. Each test shows different antenna position for zero to 270 degrees from zenith. A simulation time of three hours was chosen to cover a full orbit around the Earth.

5.1.1 Test Concept

This test is designed to analyze the number of GPS satellites in view versus the GPS antenna boresight angle measured from zenith. The use of a signal simulator provides

realistic signal dynamics including high Doppler shifts and line-of-sight accelerations. In addition it allows a separate study of individual error sources (e.g. broadcast ephemeris errors or ionosphere) that may affect the quality of the resulting tracking data. In this case no errors were simulated since only the geometry is to be determined, not the position accuracy (position accuracy is measurement accuracy times the position dilution of precision - PDOP).

5.1.2 Simulation Scenario

The simulation is configured for a spacecraft orbiting the Earth in a circular orbit. The time chosen for this simulation (09-Aug-2002 12:00:00 to 09-Aug-2002 15:00:00 local time) provides three hours of data collected, the reason of using such time is for security purposes determined by NovAtel Inc.. Although a full 24-hour period is not simulated because of simulator time constraints, the collected data still provides insight into potential availability/geometry issues. The subsequent test description is based on the use of a GSS STR4760 GPS signal simulator with one (or two) R/F outlet(s) and 12 dual (L1, L2) channels. In these tests both L1 and L2 signals are simulated for a 12 dual frequency GPS receiver. However, in Chapter 6, L1 only was used, as the signal simulator is not capable of simulating both L1 and L2 in real time mode.

5.1.3 Satellite Availability

The HWIL signal simulator has the capability of changing satellite selection criteria. These options are (Spirent, 2005):

- *DOP*: Satellites giving best DOP are selected first.

- *Power Level*: Satellites with highest power level (at the receiver) are selected first.
- *Range*: Satellites with the shortest range (to the receiver) are selected first.

In these tests, the DOP criteria were selected; in this case satellites giving the best GDOP were selected first. Figure 5.1 has two parts; the first part shows all simulated GPS satellites by the software simulator (SimGEN). It is clear that most of the time there were 12 satellites in view, because it is a 12 channel hardware simulator. The second part of Figure 5.1 shows the simulated GPS satellites above the cutoff angle (5 degrees). In this case, the number of GPS satellites varies between 4 to 10 most of the time. Figure 5.2 shows the positions in the sky of the currently simulated satellites, relative to the current vehicle position. Each satellite position is denoted by a + with its satellite identification adjacent.

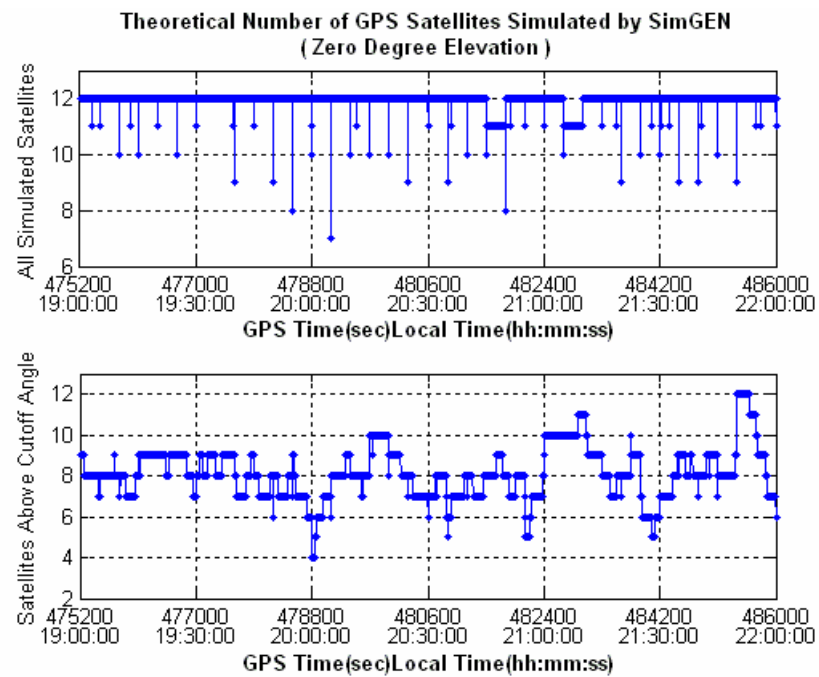


Figure 5-1: Theoretical Number of GPS Satellites Simulated by SimGEN

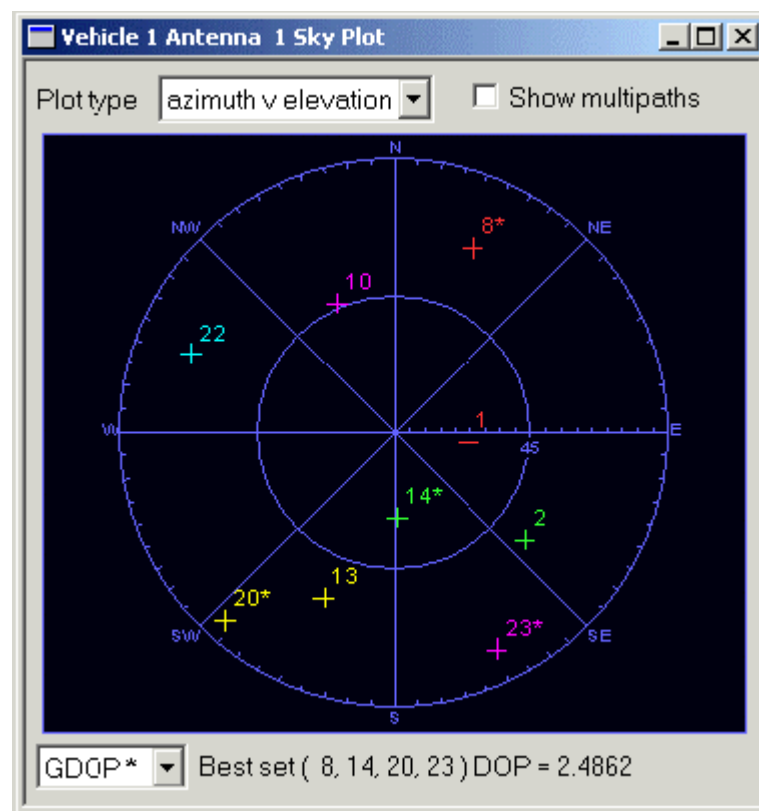


Figure 5-2: Sky Plot (Spirent, 2005)

5.2 Test Results and Analysis

In this section results for six different elevation angles from zenith were shown, and discussed. In Section 5.2.6 analysis of the percentage of time with required number of GPS satellites in view versus GPS antenna boresight angle from zenith is also shown in detail.

5.2.1 Test Results for Zero Degree Elevation

Figure 5.3 shows the total number of GPS satellites in view versus the GPS antenna boresight angle from zenith for a zero degree elevation. This is the best case for the position of the antenna whereby for 99% of the simulation time there is more than four satellites in view. Figure 5.4 shows the number of satellites used in the position solution, which requires at least four satellites. The difference between Figures 5.3 and 5.4 is that Figure 5.3 shows the total number of satellites tracked, while Figure 5.4 shows the number of satellites that are used in the calculation of the position solution. The reason why the number of satellites used in the solution is less than the number of satellites tracked is because during processing, a check on the measurements must be done to ensure that there are no blunders. Measurements with detected blunders are removed.

Figures 5.5 and 5.6 show an analysis of position and geometric Dilution of Precision (DOP) values. During processing, a maximum value is chosen for the DOP whereby DOPs above this value are neglected (at threshold, $DOP \geq 20$, are removed). DOP values are reported in three bins, where with the first bin, the geometry is very good (between 1 and 3)*. This is the desired level to be used for applications demanding the highest

possible precision. The second bin is where the geometry is deemed satisfactory (between 4 and 6) **. At this level, positions are considered accurate enough to meet many application requirements. The last bin is where the values are more than six. This represents a low level of geometry and gives generally poor positioning results. Section 5.2.6 gives an analysis of the quality of the DOP values, whereby Figures 5.22 to 5.25 provide summaries for four different positions of the GPS antenna. Figure 5.22 shows that 77.5% is in the first bin, where the geometry is very good, 18.8% is in the second bin where the geometry is good; and 3.7% is in the last bin, where the geometry is considered poor. As a result 96.3% of the DOPs are in the range of good to very good.

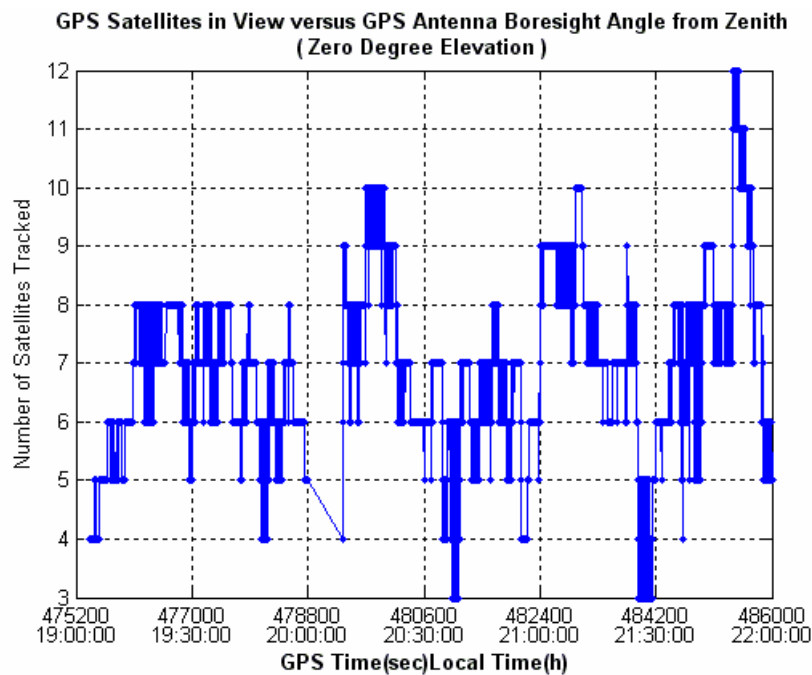


Figure 5-3: Number of Satellites Tracked for a Zero Degree Angle

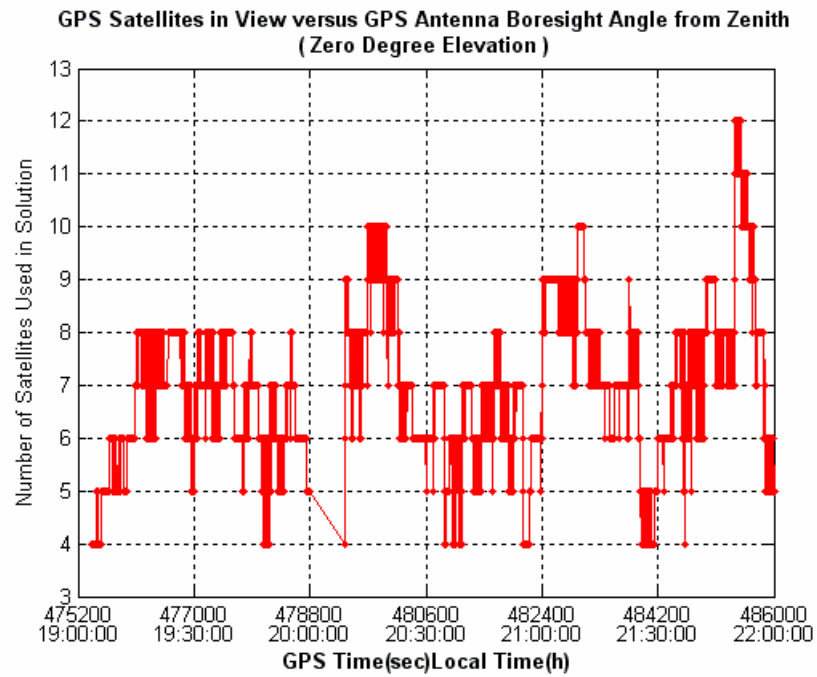


Figure 5-4: Number of Satellites Used in Solution for a Zero Degree Boresight Angle

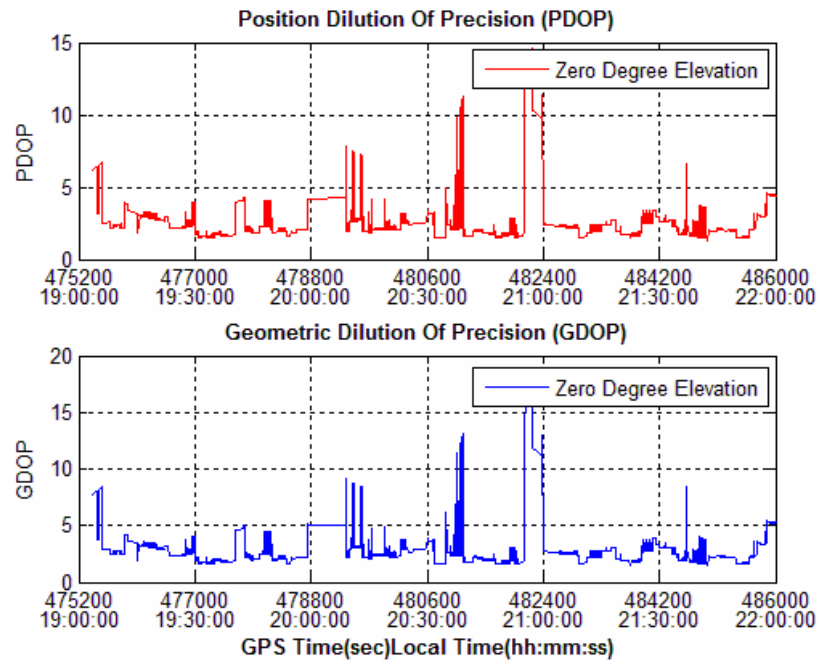


Figure 5-5: Position and Geometric Dilution of Precision for a Zero Degree Boresight Angle

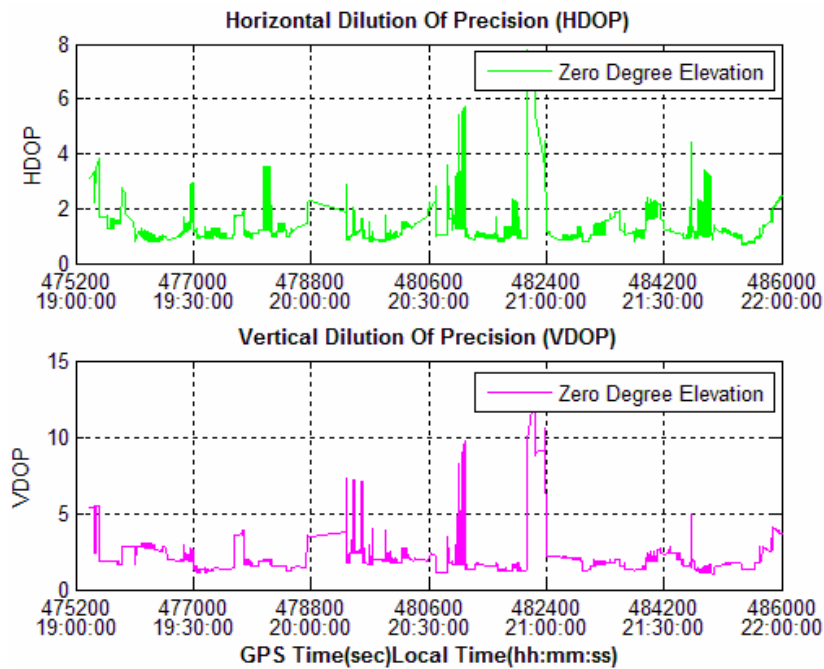


Figure 5-6: Horizontal and Vertical Dilution of Precision for a Zero Degree Boresight Angle

* $1 \leq \text{DOP} \leq 3$

** $3 < \text{DOP} \leq 6$

5.2.2 Test Results for 45 Degree Elevation

Figure 5.7 shows the total number of GPS satellites in view versus the GPS antenna boresight angle from zenith for a 45 degree elevation. Relative to a zero degree elevation, it can be seen that there is a slight degradation in satellites tracked according to the tilted antenna, whereby for 95% of the simulation time there are more than four satellites in view. Figure 5.8 shows the number of satellites used in the position solution, which requires at least four satellites. The difference between Figures 5.7 and 5.8 is that Figure 5.7 shows the total number of satellites tracked, while Figure 5.8 shows the number of satellites that are used in the calculation of the position solution. Figures 5.9

and 5.10 show an analysis of position and geometric DOP values. While Figure 5.23 in Section 5.2.6 shows that 79.4% are in the first bin, where the geometry is very good, 16.5% are in the second bin where the geometry is good; and 4.1% are in the last bin, where the geometry is considered poor. As a result 95.9% of the DOPs are in the range of good to very good.

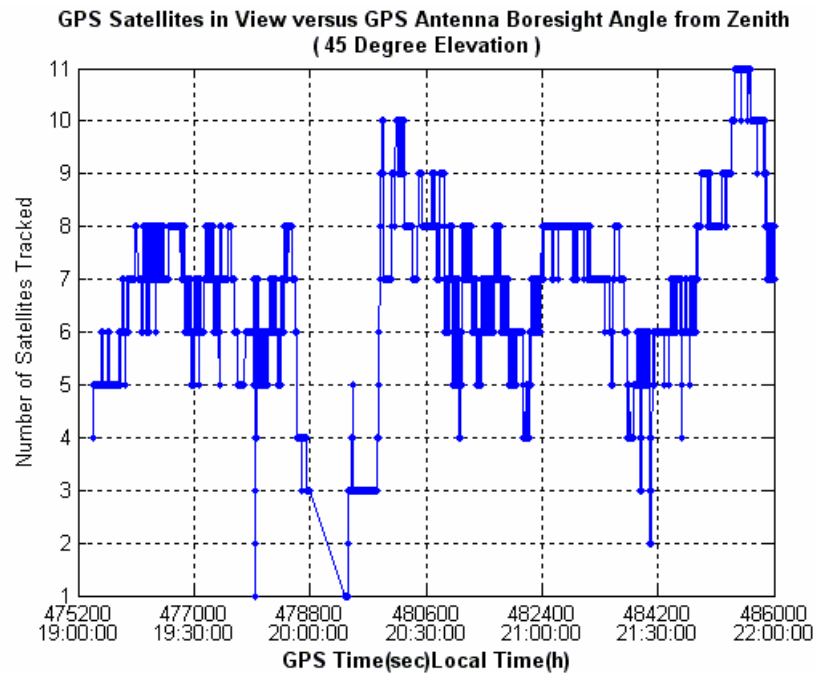


Figure 5-7: Number of Satellites Tracked for a 45 Degree Boresight Angle

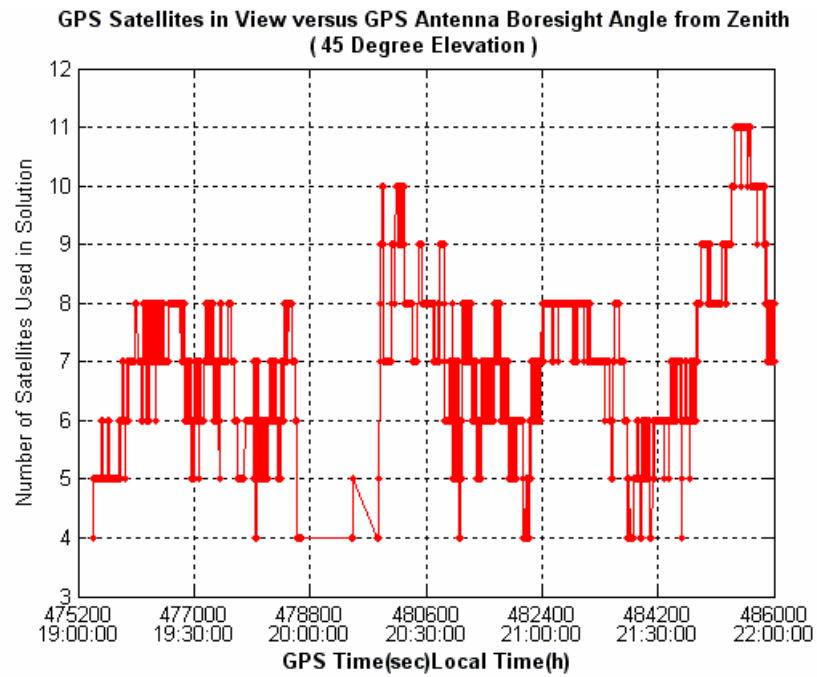


Figure 5-8: Number of Satellites Used in Solution for a 45 Degree Angle for 45 Degree Boresight Angle

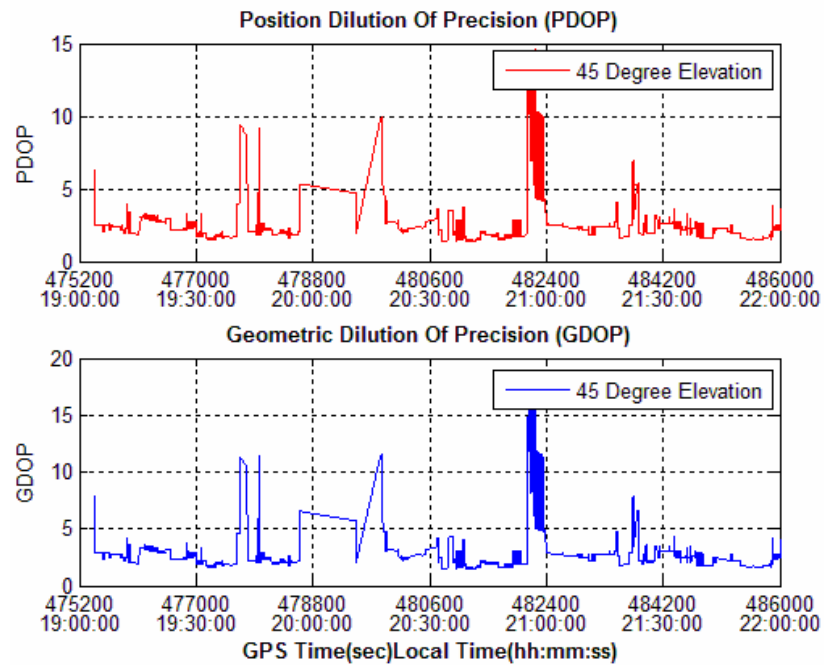


Figure 5-9: Position and Geometric Dilution of Precision for a 45 Degree Boresight Angle

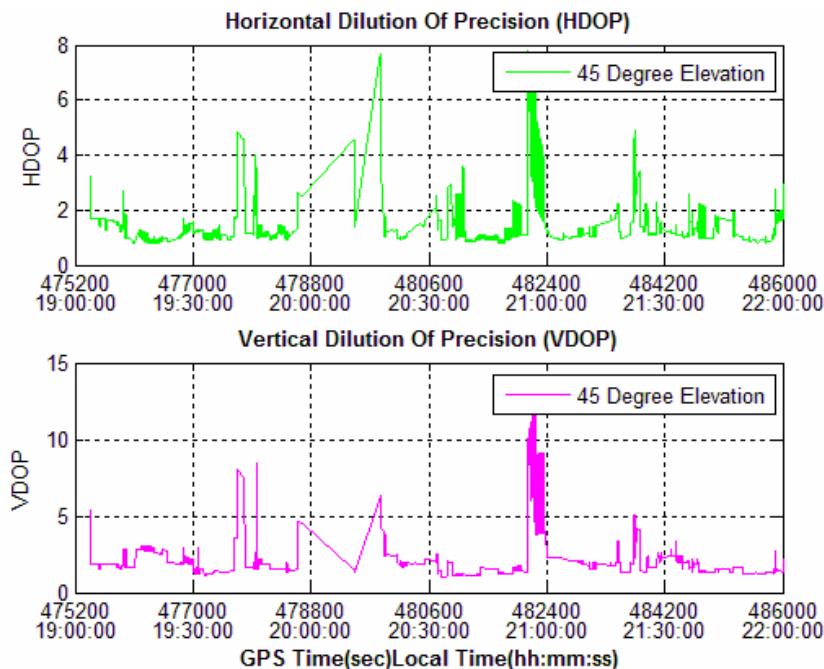


Figure 5-10: Horizontal and Vertical Dilution of Precision for a 45 Degree Boresight Angle

5.2.3 Test Results for 90 Degree Elevation

It is clearer now how the satellites tracked were degraded relative to the antenna boresight angle. Figure 5.11 shows the total number of GPS satellites in view versus the GPS antenna boresight angle from zenith for a 90 degree elevation. Relative to the previous two cases, it can be seen that there is degradation in satellites tracked according to the tilted antenna, whereby for 80% of the simulation time there are more than four satellites in view. Figure 5.12 shows the number of satellites used in the position solution. It also can be seen that these result are close to the results shown in Section 5.2.5, where the antenna boresight angle is 270 degree. The only difference between these two cases that the antenna position is located in different directions relative to the zenith. In the case of 270 degrees, for 77% of the simulation time there were more than

four satellites. Figures 5.24 and 5.25 show an analysis of the position and geometric DOP values.

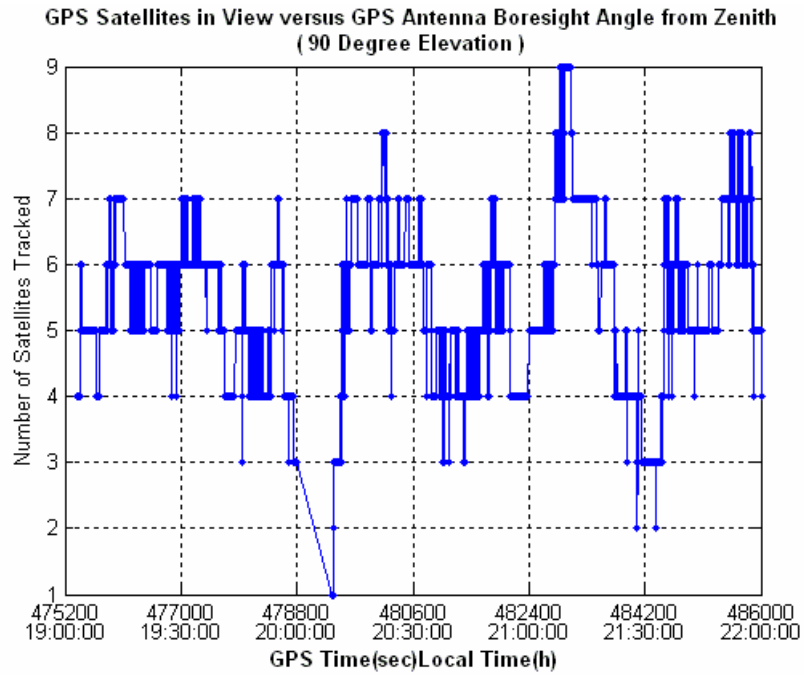


Figure 5-11: Number of Satellites Tracked for a 90 Degree Boresight Angle

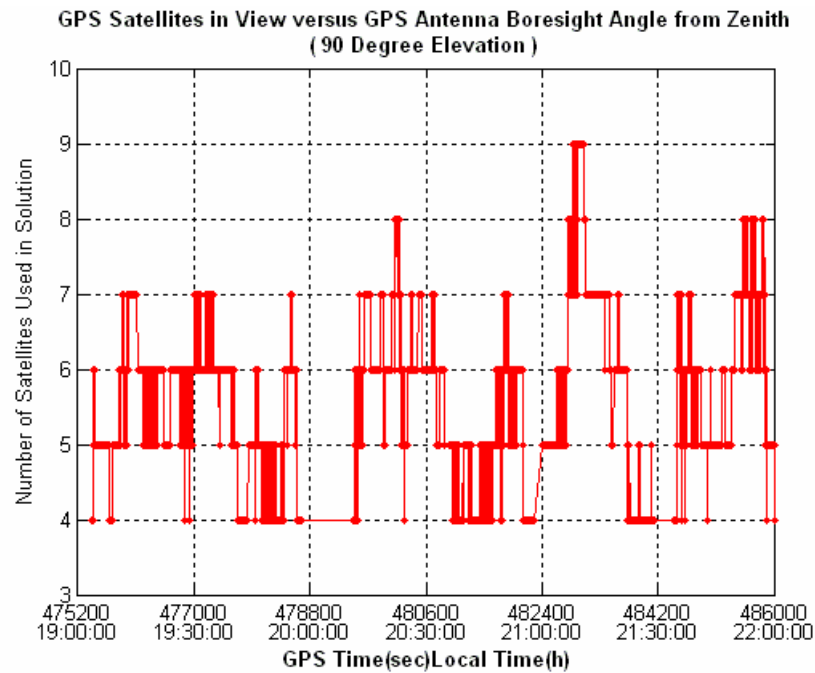


Figure 5-12: Number of Satellites Used in Solution for a 90 Degree Boresight Angle

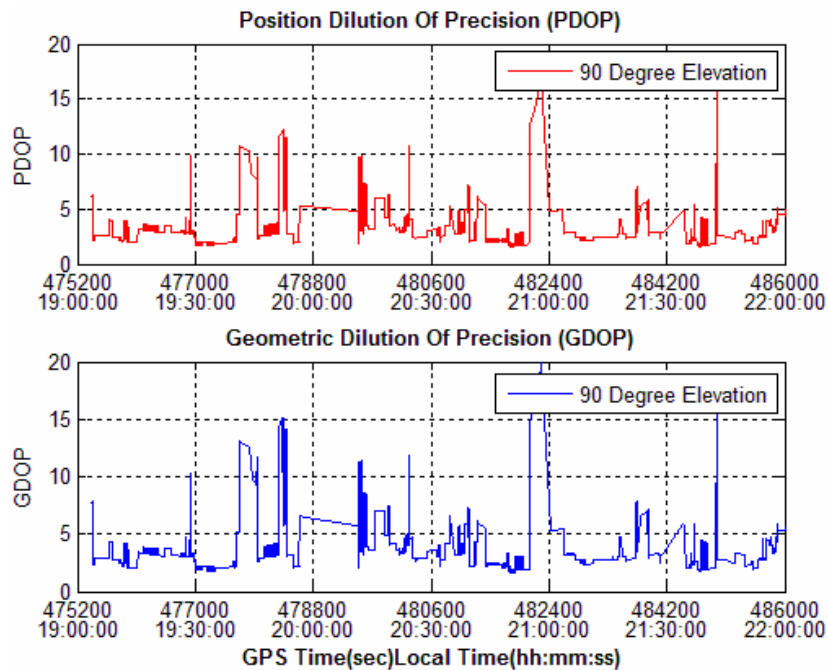


Figure 5-13: Position and Geometric Dilution of Precision for a 90 Degree Boresight Angle

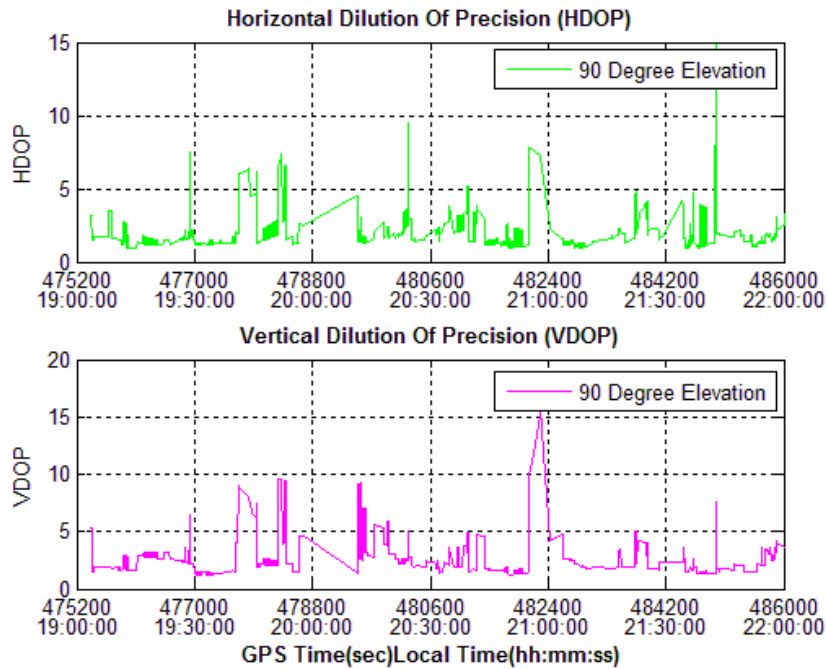


Figure 5-14: Horizontal and Vertical Dilution of Precision for a 90 Degree Boresight Angle

5.2.4 Test Results for 180 and 225 Degree Elevation

In this and the following test, figures for the GPS satellites in view versus the GPS antenna boresight are only shown. From these figures it is clear that for most of the time the total number of satellites is less than four, so the receiver is not able to determine position. Figure 5.15 shows that for 23% of the time there were four satellites and this is the case when the antenna was pointing downward. Figure 5.16 shows the number of satellites tracked when the antenna boresight angle from zenith is 225 degrees. Also the percentage availability is about 30% which is also low.

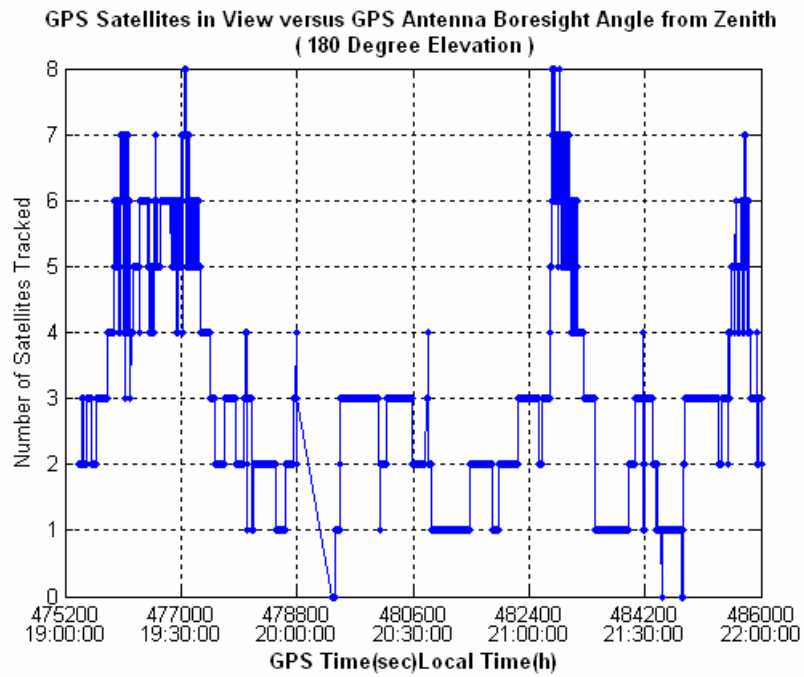


Figure 5-15: Number of Satellites Tracked for a 180 Degree Boresight Angle

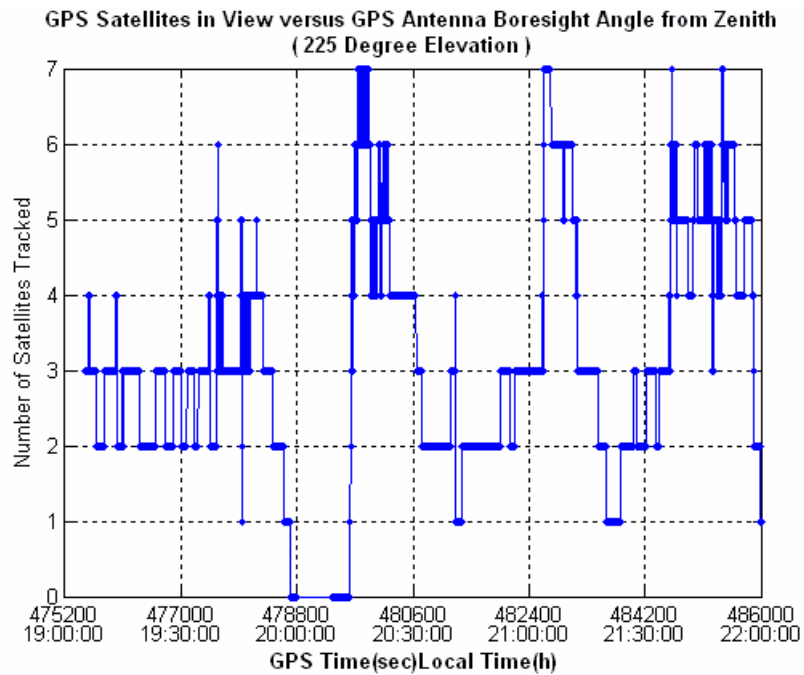


Figure 5-16: Number of Satellites Tracked for a 225 Degree Boresight Angle

5.2.5 Test Results for 270 Degree Elevation

Figures 5.17 to 5.20 summarize the last test where the antenna boresight angle is 270 degrees from zenith. In this case, for 77% of the simulation time there are more than four satellites in view used in the solution. Figures 5.17 and 5.18 show the total number of satellites tracked and used in the solution, respectively. Figures 5.19 and 5.20 show a DOP analysis where most of the time these values are below five, meaning that the satellites in view provide reasonably strong geometry.

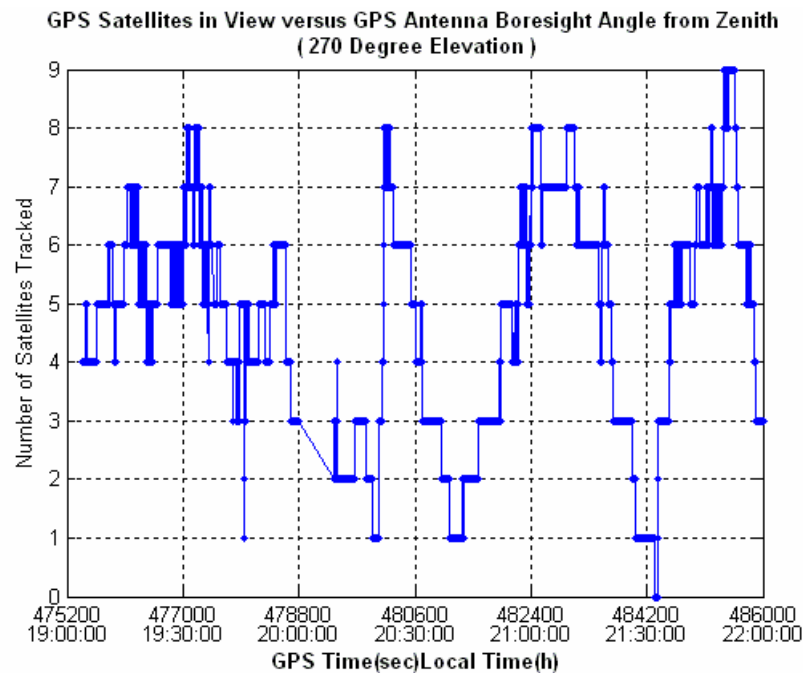


Figure 5-17: Number of Satellites Tracked for a 270 Degree Boresight Angle

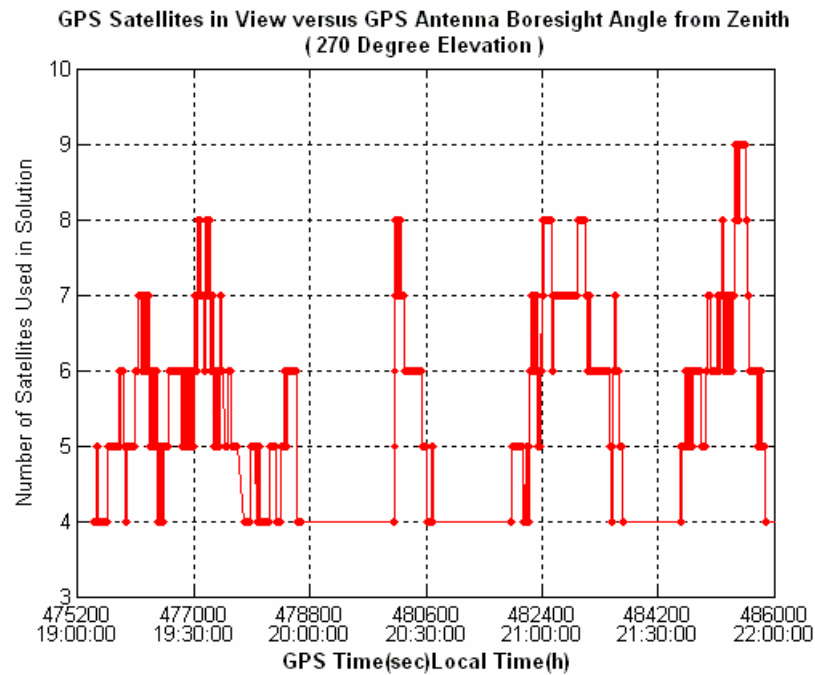


Figure 5-18: Number of Satellites Used in Solution for a 270 Degree Boresight Angle

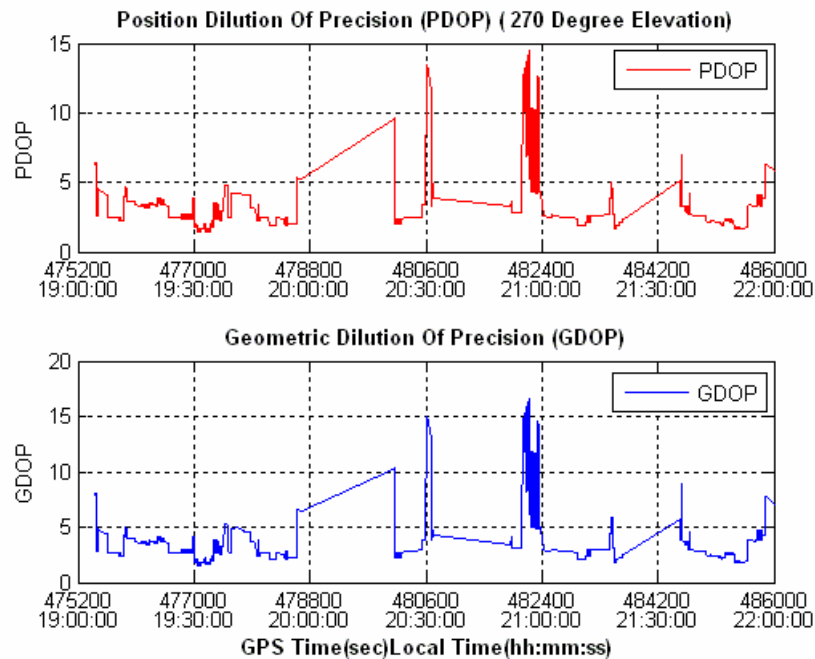


Figure 5-19: Position and Geometric Dilution of Precision for a 270 Degree Boresight Angle

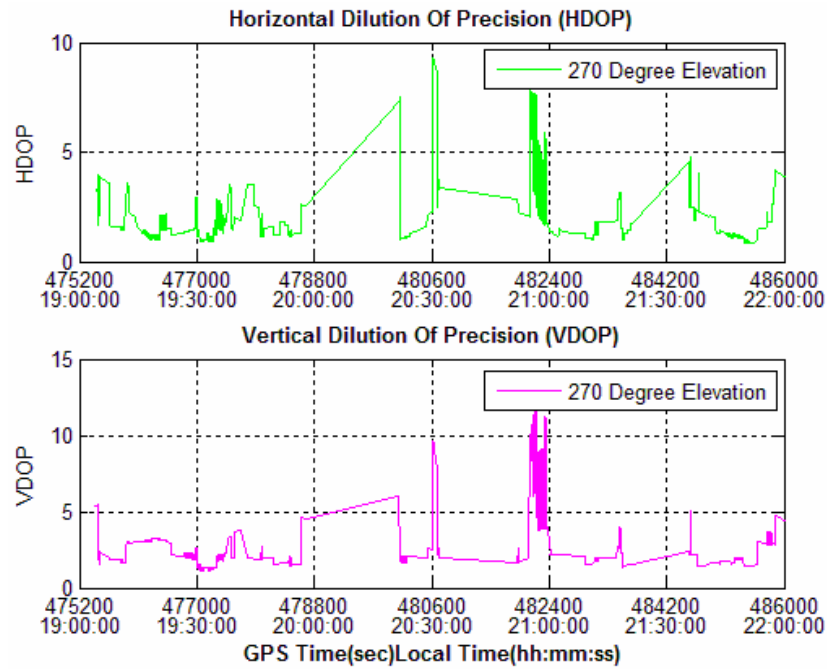


Figure 5-20: Horizontal and Vertical Dilution of Precision for a 270 Degree Boresight Angle

5.2.6 Analysis

- **Percentage of Time with Required Number of GPS Satellites in View versus GPS Antenna Boresight Angle from Zenith**

Table 5.1 shows the percentages of GPS satellites in view versus the GPS antenna boresight angle from zenith. In this case the number of GPS satellites should be greater than four. Table 5.2 shows the same relation but for different numbers of satellites. As a result of this analysis, the best case to use for the antenna position is clearly the first case, whereby the antenna boresight angle from zenith is zero.

Table 5-1: Satellites in View versus Antenna Boresight Angle

Angle	0°	45°	90°	180°	225°	270°
Percent	99%	95%	80%	23%	30%	77%

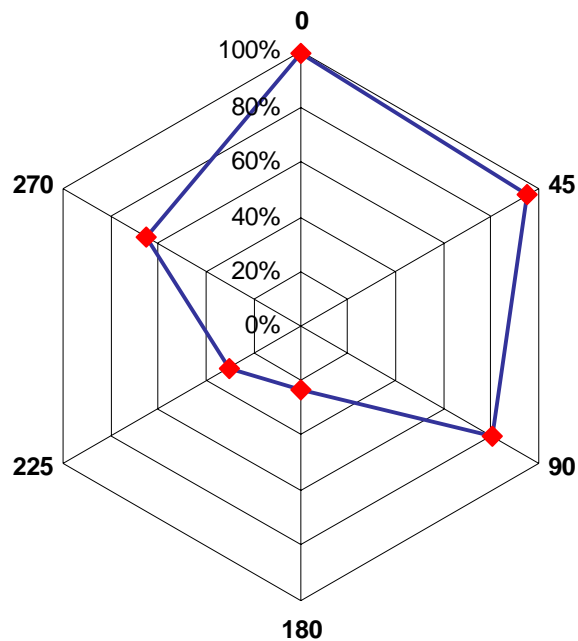


Figure 5-21: Satellites in View versus Antenna Boresight Angle

- **Percent of satellites in view “as a function of number of satellites tracked” versus GPS Antenna Boresight Angle from Zenith**

Table 5.2 summarizes the percentages of satellites in view for different numbers of satellites with different positions of the GPS antenna. As shown in Table 5.2 the best case is when the angle is zero, whereby four satellites are available for 99% of the time. In this case the receiver is able to determine position most of the time. From this analysis it is clear that as the number of satellites increases, the DOP will decrease (i.e. better geometry).

Table 5-2: Percentage of Satellites in View versus Antenna Boresight Angle

Percentage of Satellites in View versus Antenna Boresight Angle						
Angle ► No. of SV ▼	0°	45°	90°	180°	225°	270°
0	0.04	0.00	0.00	0.75	6.02	0.31
1	0.00	0.41	0.18	19.28	7.12	2.69
2	0.00	0.20	6.49	26.28	28.01	7.94
3	1.30	5.06	13.24	31.01	28.74	13.28
4	3.00	2.80	12.93	5.10	9.69	10.99
5	7.51	7.51	23.56	5.78	8.66	19.52
6	24.00	18.18	26.91	7.45	9.07	26.80
7	27.41	26.39	12.87	3.77	2.69	13.80
8	23.16	25.55	2.53	0.58	0.00	4.49
9	8.58	6.59	1.29	0.00	0.00	0.18
10	4.00	4.63	0.00	0.00	0.00	0.00
11	1.00	2.68	0.00	0.00	0.00	0.00

- **Analysis of the Quality of Dilution of Precision for GPS Antenna Boresight Angle from Zenith**

For the DOP analysis three bins are chosen, where with the first bin, the geometry is very good (between 1 and 3). The second bin is where the geometry is satisfactory (between 4 and 6), while the last bin is when the values are more than 6 (considered marginal to poor). Figure 5.22 shows that for 77.5% of the simulated time, the GDOP is very good and for 18.8% of the time it is satisfactory, while for the PDOP it is 85.0% and 11.3%, respectively. Figures 5.23 to 5.25 summarize the DOP analysis for 45, 90 and 270 degree elevations, respectively.

Analysis of DOP (Zero Elevation)



Figure 5-22: Analysis of DOP for Zero deg Elevation

Analysis of DOP (45 Degree Elevation)

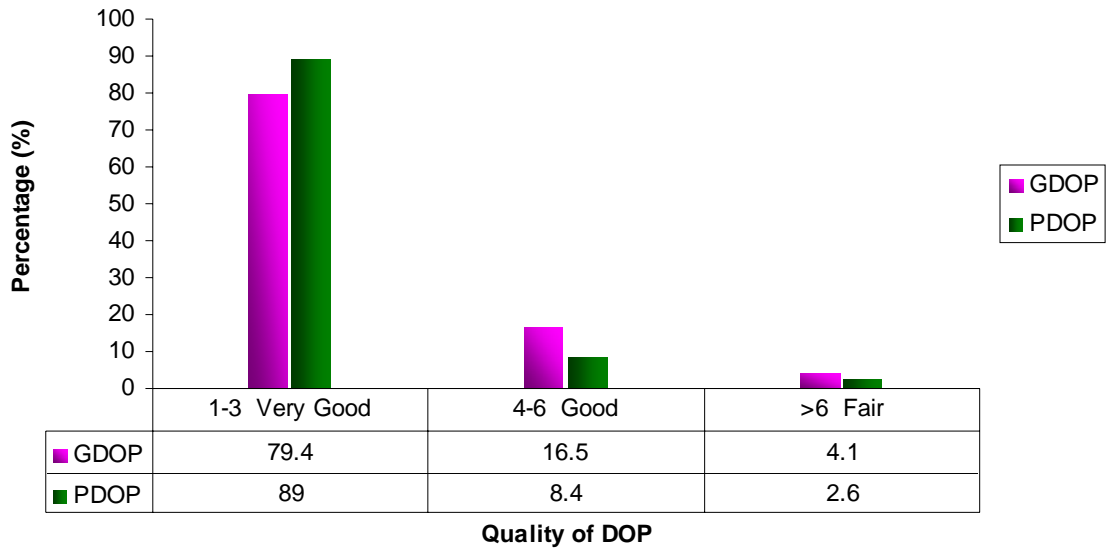


Figure 5-23: Analysis of DOP for 45 deg Elevation

Analysis of DOP (90 Degree Elevation)

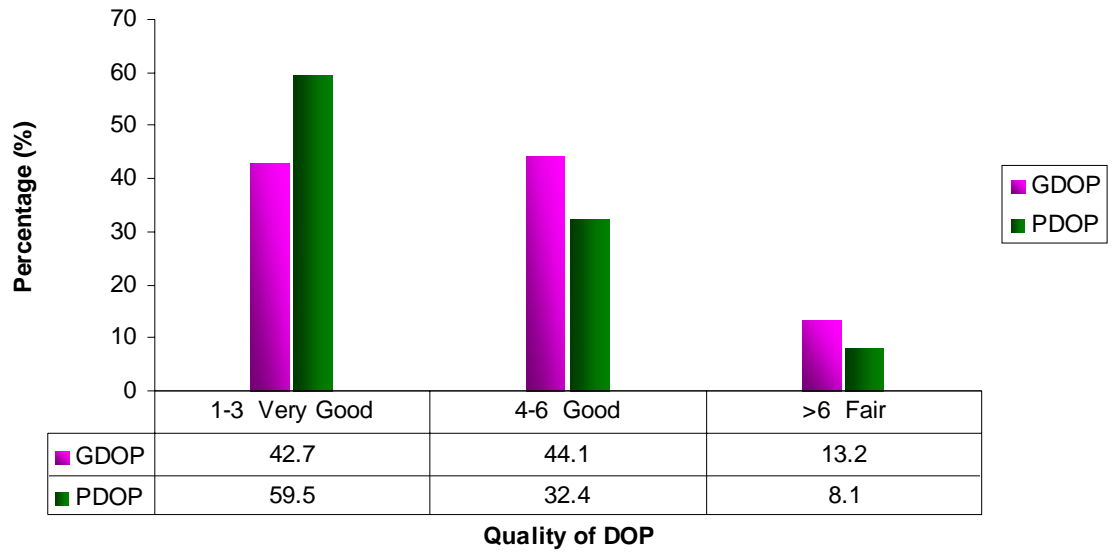


Figure 5-24: Analysis of DOP for 90 deg Elevation

Analysis of DOP (270 Degree Elevation)



Figure 5-25: Analysis of DOP for 270 deg Elevation

5.3 Summary

An analysis of the GPS satellites in view versus the GPS antenna boresight angle from zenith was performed. As expected, the zero angle case performs the best case and the coverage is 99%. The use of a signal simulator provides a realistic signal dynamics including high Doppler shifts and line-of-sight accelerations. In addition it allows a separate study of individual error sources that may affect the quality of the resulting tracking data. In Chapter 6 two sets of results are shown based on two different trajectory files. First, the reference trajectory (reference coordinates) is generated from the output files provided by the simulator (STR4760). While the second data set based on coordinates extracted from the OEM4-G2L receiver.

CHAPTER 6

RELATIVE NAVIGATION TESTS AND RESULTS

As mentioned previously, much of the research in the field of relative navigation for formation flying of satellites is based on HWIL or software simulation tests. In both cases the actual accuracy of the resulting relative position estimates can be computed since the reference trajectories are exactly known. In order to find the relative position and velocity errors, reference station coordinate should be known. Usually in FLYKIN+™ software the reference station coordinates are inserted manually from an external source; however, this option was modified to make the software capable of extracting the reference station coordinate from the receiver during processing (see appendix for details).

6.1 Test Scenarios

6.1.1 HWIL Demonstration

Before discussing the main thrust of the chapter, it is worthwhile to give a summary of how the FLYKIN+™ program works. This program is initialized by an option file that specifies the processing methods to be used, reference station (Chief) coordinates, and data filenames. In this chapter two sets of results are shown. First, the reference trajectory for the Chief satellite is generated from the output files provided by the simulator (STR4760). These trajectory files are fed to the software to find the relative

position and velocity errors through differencing of the ‘truth’ trajectories. The second set of results is based on modifying the FLYKIN+™ software by using the Chief absolute positions and velocities from the receiver itself, without need for any external source to provide the reference data, as the FLYKIN+™ software needs that to start processing. In the appendix, the software development steps are shown are the data extraction from the NovAtel logs. For the scenarios shown in this work, there are three different baselines: 100 m, 1 km, and 5 km.

6.1.2 GPS Errors

In this section a description of the GPS errors simulated using the HWIL simulator is given; however, the major error sources affecting the GPS measurements have been discussed in detail in Chapter 3 and so they are only mentioned briefly in this section. One of the main concerns for GPS navigation is the effect the ionosphere has on the pseudorange and carrier phase measurements. When the level of ionospheric activity is low, a typical relative ionospheric error will be on the order of 1-2 ppm. In this work the simulated value for ionospheric error was 3 ppm as a moderate ionospheric condition (see Table 6.1).

Other sources of errors were also simulated including multipath. For receiver noise the DD RMS value from the OEM4-G2l receiver was found to be 0.8 mm, and 1.0 mm for L1 and L2, respectively. The effect of multipath error was studied and analyzed in this work and found to be at the millimetre level. Table 6.1 is a summary of the error levels drawn from the output observations.

Table 6-1: RMS Level of GPS Errors

Orbital [PPM]	Ionosphere [PPM]	Multipath [mm]			Receiver Noise [mm]		
		P_{CA}	ϕ_{L1}	ϕ_{L2}	ϕ_{L1}	ϕ_{L2}	$\dot{\phi}_{L1}$
0.5	3	216	3.0	4.5	0.8	1.0	15

The GPS satellite availability and the corresponding DOP values are shown in Figure 6.1. In these tests the GPS antenna is assumed to be pointing upward (zero degree elevation from zenith) at all times. As mentioned previously the cutoff angle was chosen to be 5 degrees. This low cutoff angle is achievable because there are no obstructions at low elevation in space. It also can be seen that most of the time the number of GPS satellites varies between five and ten. The GDOP value ranges between 1.5 and 3.5 and this is considered very good geometry. Note that the number of GPS satellites visible changes quite rapidly over time which is due to the high velocity of the LEO spacecraft.

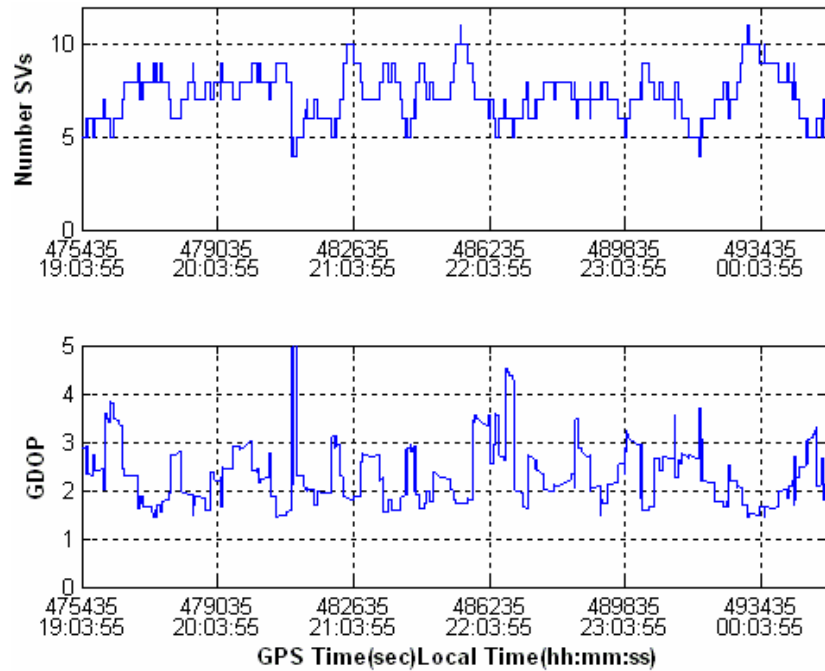


Figure 6-1: GPS Satellite Availability and GDOP for LEO Spacecraft

6.1.3 Processing Procedure

The process begins with inserting the parameters to the simulator software (SimGEN). However, the software has three options for determining the user motion (see Section 4.2). In these tests, the user's motion was internally simulated by the software. This is followed by two options; the first one is taking the Chief absolute coordinates from the HWIL simulator. While the other option which is considered the core of this work is to take the Chief absolute coordinates internally from the GPS receiver. Finally, the absolute coordinates are fed into FLYKIN+TM to estimate the relative position and velocity of the spacecraft based on precise carrier phase measurements. In the following section, an overview of the modifications done previously by the author will be shown.

6.2 Modifications

FLYKIN+™ is a C++ program that processes GPS pseudorange and/or carrier phase data from two receivers in both static and kinematic modes. Usually there are two stations: reference and rover.

- **Conventional:** In this version the reference station coordinates should be precisely known (Static). The rover station can be either static or moving, and usually its position unknown, as it was designed for terrestrial applications with a static reference station.
- **Modification:** The modified version has the capability of using a moving base station (MBS). These modifications were previously done by Crawford (2005).

In the appendix, data extraction was discussed in detail, and this is considered as one of the modifications done to the FLYKIN+™ software. However, the four cases discussed in Chapter 3 also applied in FLYKIN+™. The next section shows two sets of results with the first set of results showing the relative position and velocity errors using precise reference trajectories from the hardware simulator. Multipath effects are also shown for the 100 m baseline. The second set of results show the relative position and velocity errors using internal reference trajectory from the GPS receiver.

A modified version of FLYKIN+™ software is used for this work; however, the modifications mentioned previously are added to this software, to be compatible with a formation-flying mission.

6.3 Results and Analysis

The following sets of results show the relative position and velocity errors, using precise reference trajectories taken from the hardware simulator. The maximum baseline limit is 5 km as the limits of the datalink between Chief and Deputy satellites are limited to 5 km (Foisy et al., 2007). For the 100 m baseline separation, multipath may occur between the Chief and Deputy, due to the surface of the satellite itself. However, in the case where the two satellites are close to each other, such as 100 metres in distance, a signal may hit one satellite and be received by the other as discussed in Section 2.3.4. This scenario is simulated in the hardware simulator, and it is assumed that there are multipath signals from two GPS satellites, SV#9 and SV#19.

6.3.1 Test Results Using SimGEN Trajectory

1) Test 1 Results: 100 m Separation

Figure 6.2 shows the relative position errors and ambiguity resolution states for Test 1 with 100 m baseline. The green colour shows the relative position error when all the ambiguities are fixed, while the red colour represents all float ambiguities. At the beginning it takes about eight seconds to fix ambiguities to their integer values. At this time the relative error is at the centimetre level until fixing is done.

Table 6.2 gives the mean and RMS values of the errors shown in Figure 6.2. The values are given for the north, east, and height directions. As expected, the errors in all directions are small. Relative position error has a zero mean for all three directions; the RMS errors were 1, 2, and 2 mm respectively, and the 3D RMS value is approximately 3

mm. In this case these results are less accurate from Kroes (2006); however, Kroes (2006) uses real GPS data from the GRACE mission. But these results are better than the results achieved by Busse (2003) in terms of positions. Busse achieved better results in terms of velocity errors with a 1 km baseline separation.

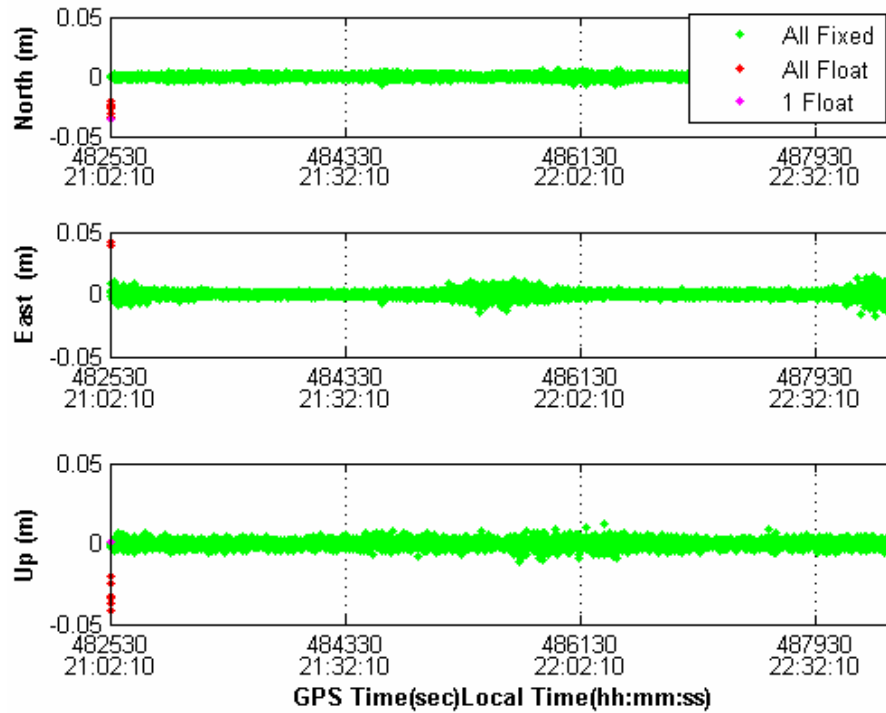


Figure 6-2: Test 1 Relative Position Errors (100m Baseline)

Table 6-2: Statistics for Relative Position Errors

	Mean	RMS
North (mm)	0	1
East (mm)	0	2
Height (mm)	0	2

Figure 6.3 shows relative the velocity errors while Table 6.3 shows the means and RMS of these errors. The 3D RMS velocity error achieved is about 22 mm/s. The RMS value for the north direction is 2 mm/s and is 22 mm/s in the east direction. For up direction the RMS value is equal to 1 mm/s. It also can be seen that the east velocity is noisier. This is directly related to the spectral density (SPD) of the KF that have been set for the east direction. An SPD analysis was carried out by comparing the navigation performance in terms of position and velocity accuracies. Based on this analysis the best SPD values chosen in the north and up direction is $10^{-3} \text{ m}^2/\text{s}^3$. For the east direction, the best value was found to be $10^{-1} \text{ m}^2/\text{s}^3$. Due to the higher SPD level the weight of the KF is shifted more towards the measurement compare to the other direction. For such a reason, less smoothing is achieved and a noisier velocity estimate was observed. If the value of the SPD was decreased to a lower value, better results would be shown. However, some jumps would appear in such configuration which is related to the parameterization problem, where singularity would occur as you get near the poles.

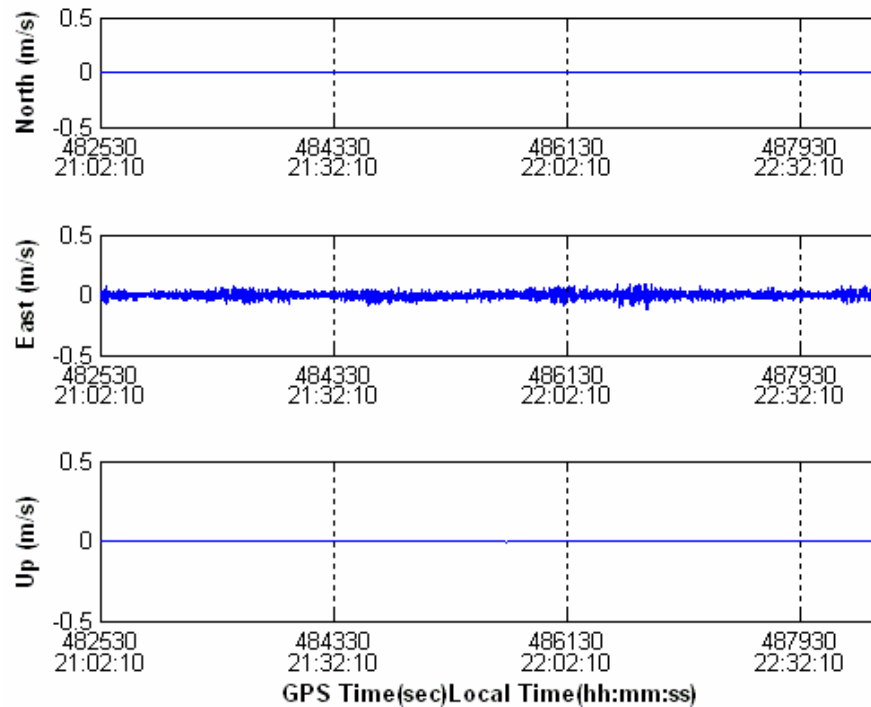


Figure 6-3: Test 1 Relative Velocity Errors (100m Baseline)

Table 6-3: Statistics for Relative Velocity Errors

	Mean	RMS
Velocity N (mm/s)	0	2
Velocity E (mm/s)	0	22
Velocity H (mm/s)	0	1

Figures 6.4 and 6.5 show the DD measurement residuals with the value of these residuals range from -3 to +3 mm. These two figures reflect the quality of data for each satellite, and hence the measurement reliability. Figures 6.6 and 6.7 show L1 Doppler residuals, with the value of the residuals ranging from -5 to +5 cm/s. These two figures reflect the quality of data for each satellite and hence the measurement reliability. Note that Montenbruck (2003) analyzed noise level of the phase measurements, using zero baseline test with a NovAtel OEM4-G2L receiver and estimated the RMS error to be 1.5

cm/s for the L1 Doppler measurement. However, in these tests the mean value of Doppler measurements is about 3 cm/sec.

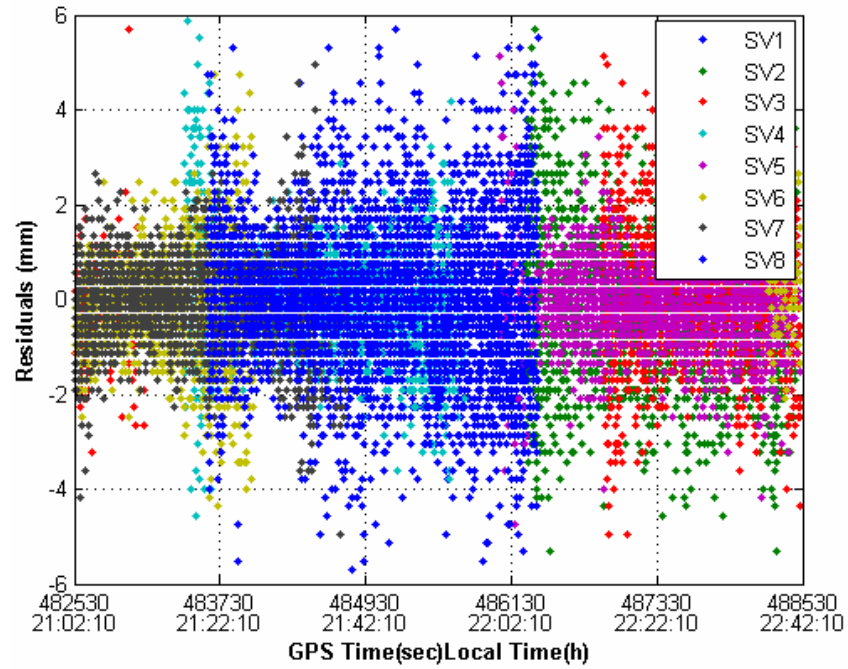


Figure 6-4: L1 Phase Residuals Error for Satellites 1-8

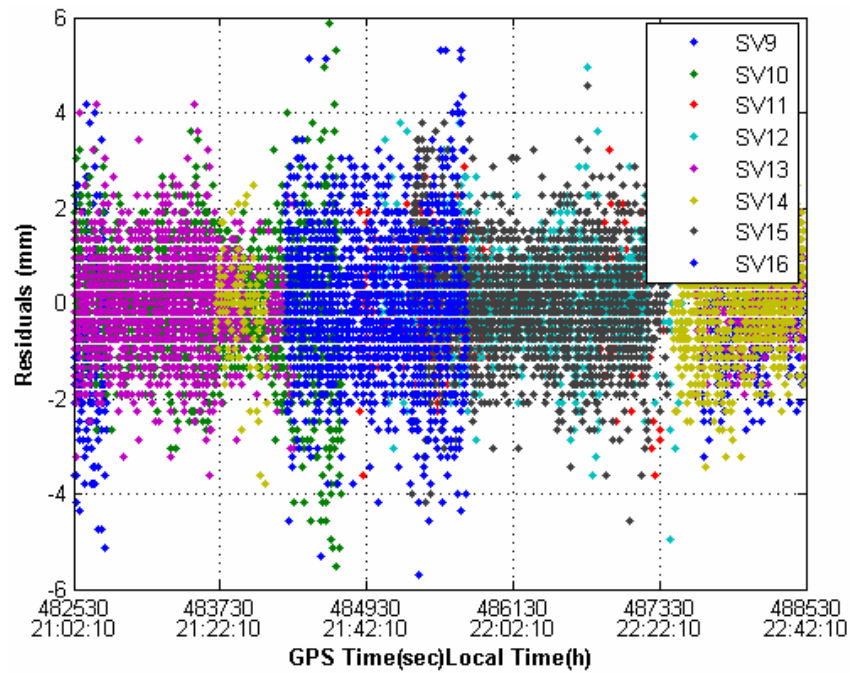


Figure 6-5: L1 Phase Residuals Error for Satellites 9-16

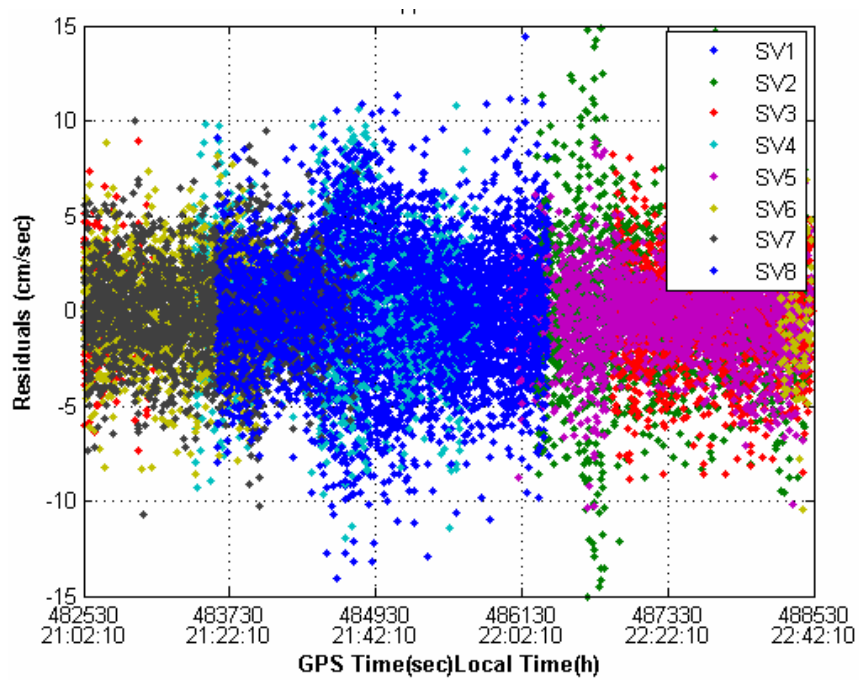


Figure 6-6: L1 Doppler Residuals Error for Satellites 1-8

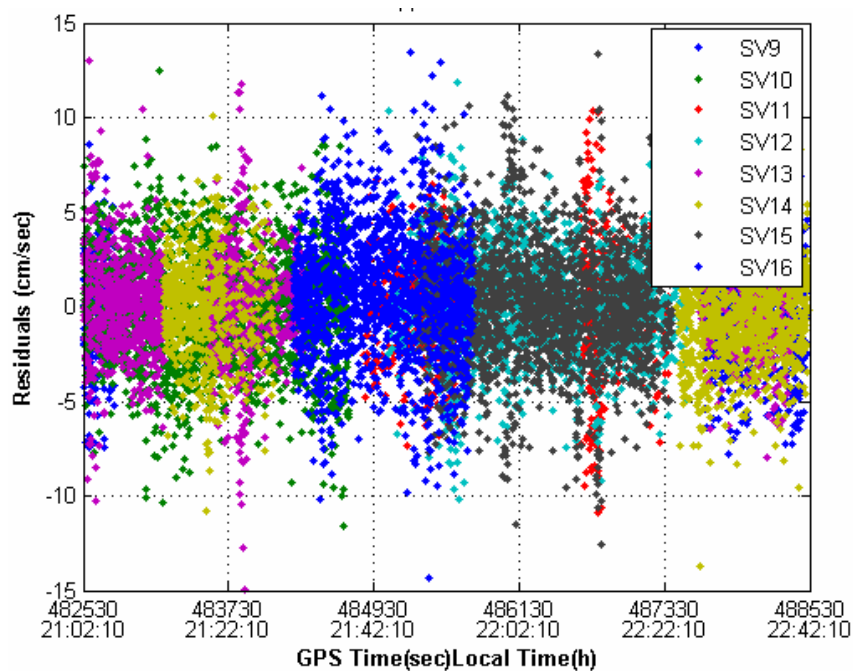


Figure 6-7: L1 Doppler Residuals Error for Satellites 9-16

2) Test 1 Results: 1 km Separation

Figure 6.8 shows the relative position errors and ambiguity resolution states for Test 1 with a 1 km separation distance. The green colour shows the relative position error when all the ambiguities are fixed, while the red colour represents all float ambiguities. At the beginning it takes about eight seconds to fix ambiguities to their integer values. At this time the relative error is at the centimetre level until fixing is done. Table 6.4 gives the mean and RMS values of the errors shown in Figure 6.8. However, these values are calculated when the fixed solution started. The values are given for the north, east, and height directions. As expected, the errors in all directions are small. Relative position error has a zero mean and at the millimetre level for all three directions; the RMS errors were 2, 3, and 2 mm respectively, and a 3D RMS value is approximately 4 cm.

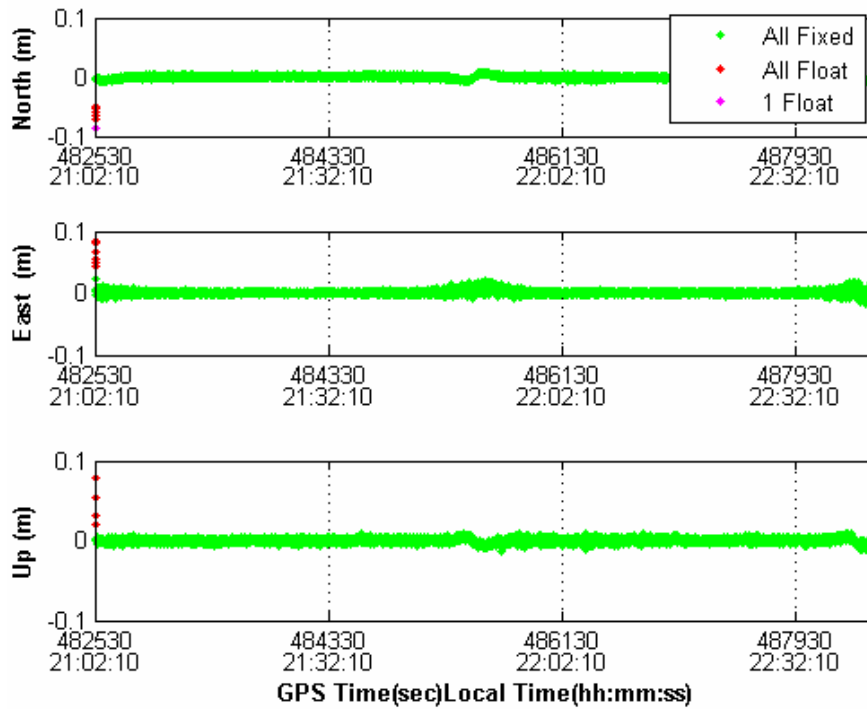


Figure 6-8: Test 1 Relative Position Errors (1 km Baseline)

Table 6-4: Statistics for Relative Position Errors

	Mean	RMS
North (mm)	0	2
East (mm)	0	3
Height (mm)	0	2

Figure 6.9 shows relative the velocity errors while Table 6.5 shows the mean and RMS values of these errors. The 3D RMS velocity error achieved is approximately 25 mm/s. The RMS value for the north direction is 8 mm/s, and is 23 mm/s in the east direction. For the same reason mentioned previously, the east velocity is still nosier. Several tests were done to tune the filter and to achieve better results, and in these tests the best case achieved is shown in this work. Again by looking at the north velocity error, it can be seen that between 484330 to 486130 s GPS time these jumps will start to appear as the Chief and Deputy satellites get near the poles. The best solution in this case was chosen

and to be smaller SPD for the east velocity. For up direction the RMS value is equal to 2 mm/s.

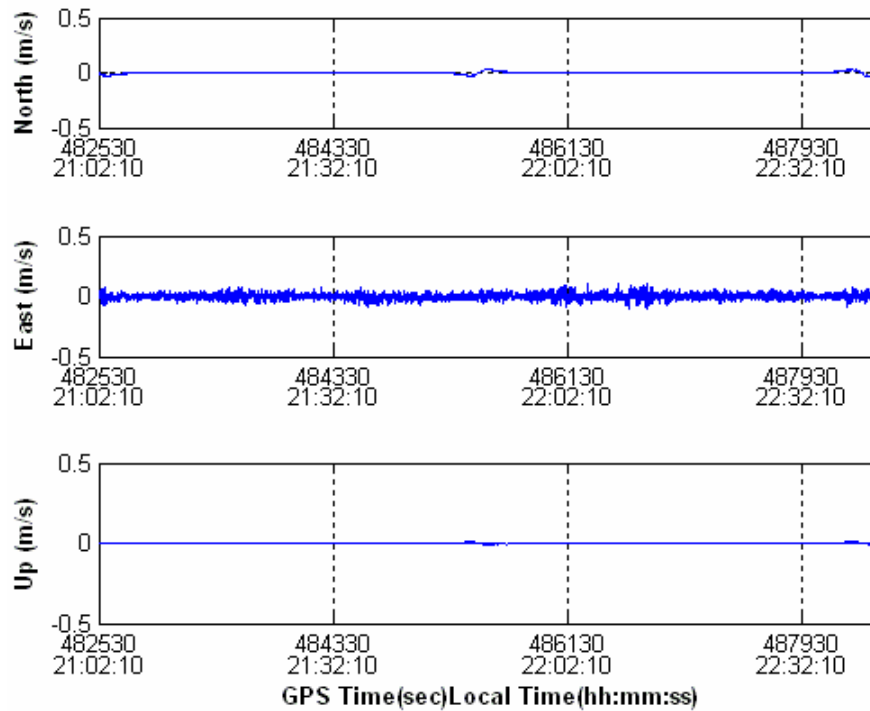


Figure 6-9: Test 1 Relative Velocity Errors (1km Baseline)

Table 6-5: Statistics for Relative Velocity Errors

	Mean	RMS
Velocity N (mm/s)	0	8
Velocity E (mm/s)	0	23
Velocity H (mm/s)	0	2

3) Test 1 Results: 5 km Separation

Figure 6.10 shows the relative position errors and ambiguity resolution states for Test 1 with a 5 km separation distance. The green colour shows the relative position error when all the ambiguities are fixed, while the red colour represents all float ambiguities. The blue colour represents the ambiguity when there is just one float. If there are two or more float ambiguities, this is represented by the magenta colour. At the beginning it

takes about 12 seconds to fix ambiguities to their integer values. At this time the relative error is at the centimetre level until fixing is done. Table 6.6 gives the mean and RMS values of the errors shown in Figure 6.10. The values are given for the north, east, and height directions. As expected, the errors in all directions are small. The relative position error has a zero mean for all three directions; the RMS errors are 5, 8, and 7 mm respectively, and a 3D RMS value is approximately 12 mm.

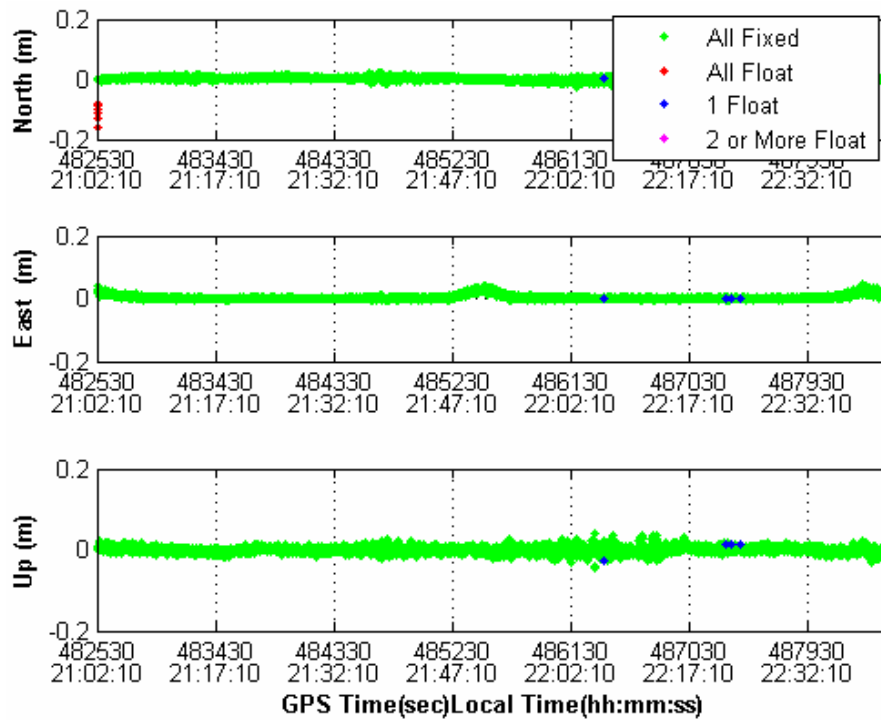


Figure 6-10: Test 1 Relative Position Errors (5km Baseline)

Table 6-6: Statistics for Relative Position Errors

	Mean	RMS
North (mm)	0	5
East (mm)	0	8
Height (mm)	0	7

Figure 6.11 shows relative velocity errors while Table 6.7 shows the mean and RMS values of these errors. The 3D RMS velocity error achieved is approximately 34 mm/s.

The RMS value for the north and up directions is 18 mm/s, and is 22 mm/s in the east direction. It can be seen that according to the baseline length (5 km), the north, east, and up directions are relatively close to each other and are at the centimetre level

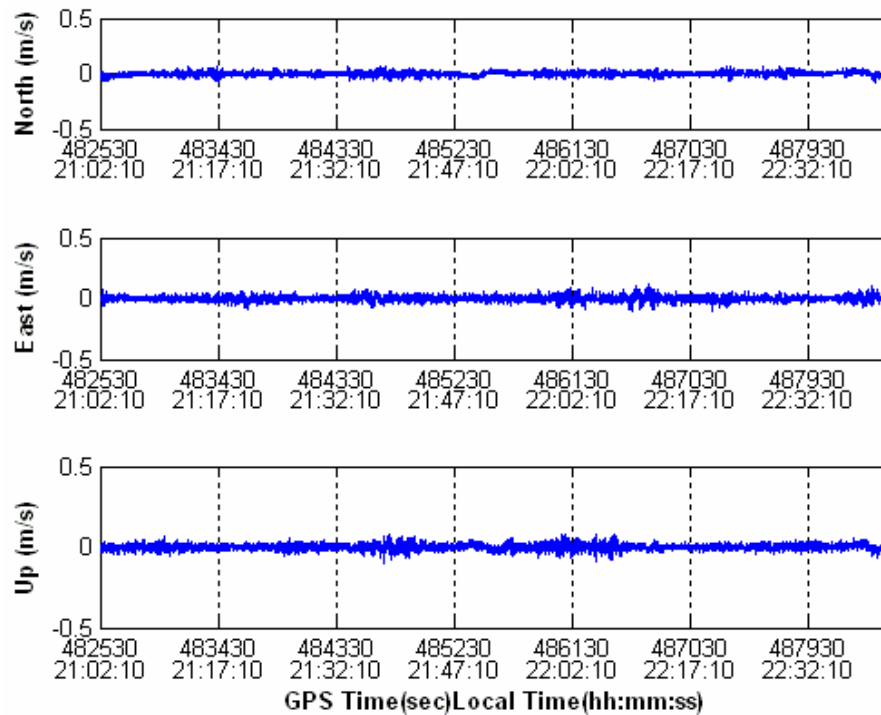


Figure 6-11: Test 1 Relative Velocity Errors (5km Baseline)

Table 6-7: Statistics for Relative Velocity Errors

	Mean	RMS
Velocity N (mm/s)	0	18
Velocity E (mm/s)	0	22
Velocity H (mm/s)	0	18

4) Test 1 Results: 100 m Separation with Multipath added

Figure 6.12a shows the effect of multipath with the duration of the multipath being about 30 minutes. This test is similar to the first test done previously with a 100 m baseline, but multipath signals from two satellites were added. The simulated multipath signal starts at the epoch 478950 to 480750 GPS Time. In this period of time the relative

position accuracy degrades, but there is still less than a millimetre difference from the first test. The relative velocity errors change by about 4 mm/s the first test. As discussed previously, the RMS value of the simulated multipath signal is about 3 mm. The 3D RMS for position is about 3 mm, while in the presence of multipath; it is 7 mm which gives a 4 mm degradation in position accuracy.

Table 6.8 gives the mean and RMS values of the errors shown in Figure 6.12a. The values are given for the north, east, and height directions. As expected, the errors in all directions are small. Relative position error has a zero mean for all three directions; the RMS errors are 2, 4, and 5 mm respectively, and a 3D RMS value is approximately 7 mm. It also can be seen that the trends in the relative positions errors are correlated to the differential multipath errors. Sample results taken from Ray (1998) (see Figure 6.12 b) represent the carrier phase multipath errors for satellites 17 and 31 on October 1998, and found to be similar to what achieved in this work.

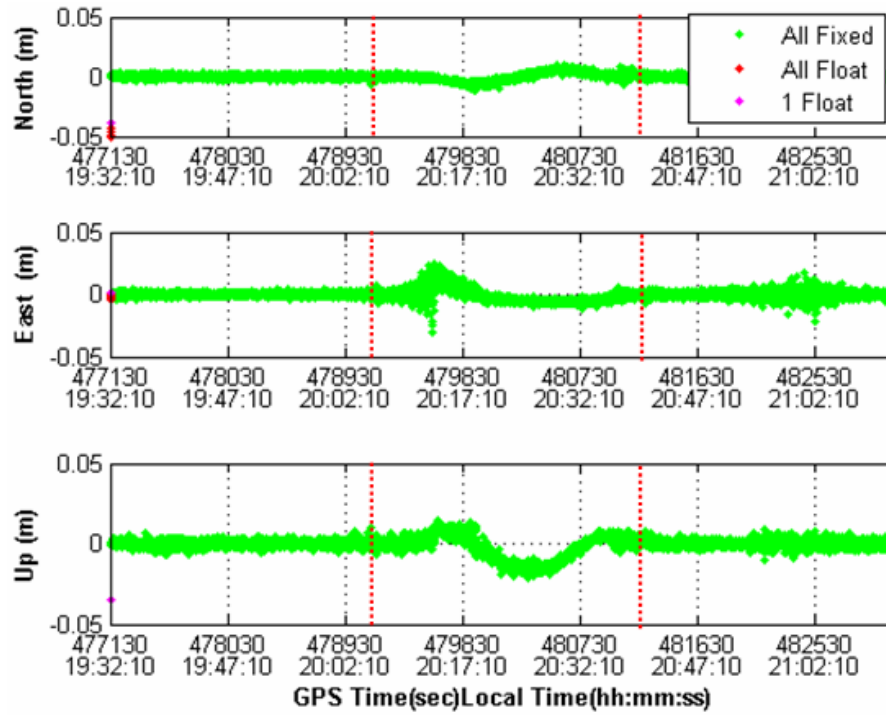


Figure 6-12a: Test 1 Relative Position Errors (Multipath)

Table 6-8: Statistics for Relative Position Errors

	Mean	RMS
North (mm)	0	2
East (mm)	0	4
Height (mm)	0	5

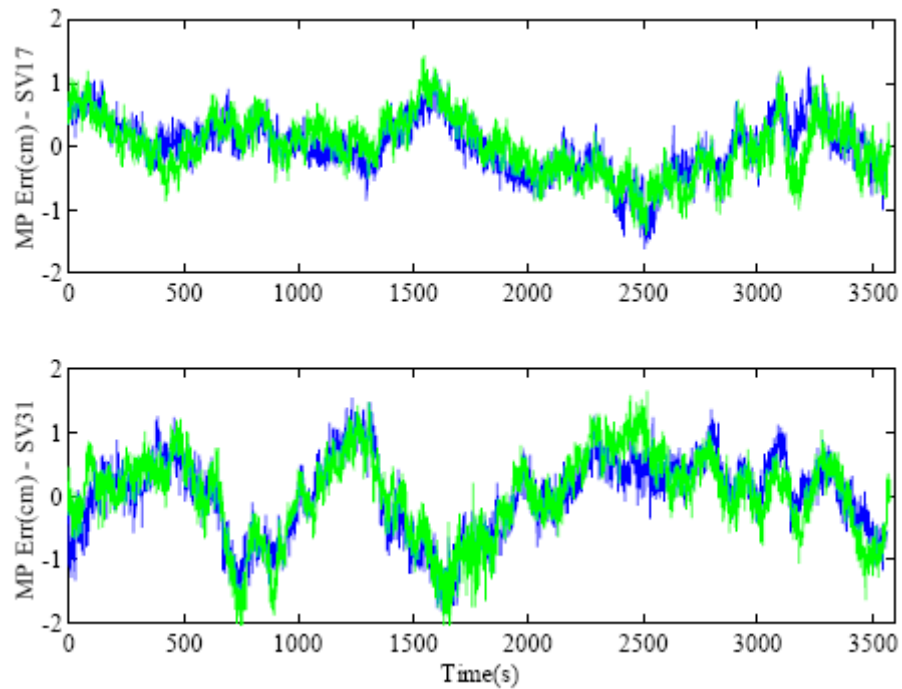


Figure 6-12b: Carrier phase multipath errors for satellites 17 and 31 (Ray, 1998)

Figure 6.13 shows the relative velocity errors while Table 6.9 shows the mean and RMS values of these errors. The 3D RMS velocity error achieved is approximately 27 mm/s. The RMS value for the north direction is 2 mm/s, and is 27 mm/s in the east direction. For the up direction the RMS value is equal to 1 mm/s.

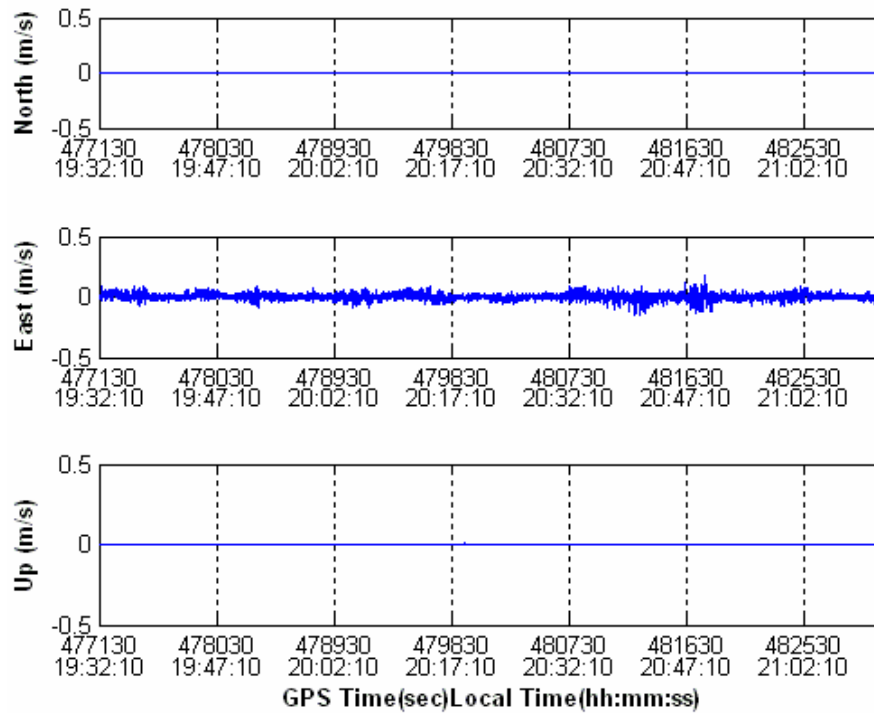


Figure 6-13: Test 1 Relative Velocity Errors (Multipath)

Table 6-9: Statistics for Relative Velocity Errors

	Mean	RMS
Velocity N (mm/s)	0	2
Velocity E (mm/s)	0	27
Velocity H (mm/s)	0	1

Figures 6.14 and 6.15 show the DD measurement residuals with the value of these residuals ranging from -2 to +2 mm. However, it can be clearly seen that the residual values increase to about ± 15 mm, where the multipath signal occurs (as it is simulated multipath). These two figures reflect the quality of data for each satellite, and hence the measurement reliability. Figures 6.16 and 6.17 show the L1 Doppler residuals with a mean value of 3 cm/s. This value is still high in comparison with the 1.5 cm/s from Montenbruck (2003), and considered as a main reason of relative velocity high error (centimetre level). As the multipath signal comes from two satellites in particular (Sv#9

and SV#19) it can be seen the residual values are much higher than the other satellites.

This may help to figure out if there is a multipath signal or not when analyzing data.

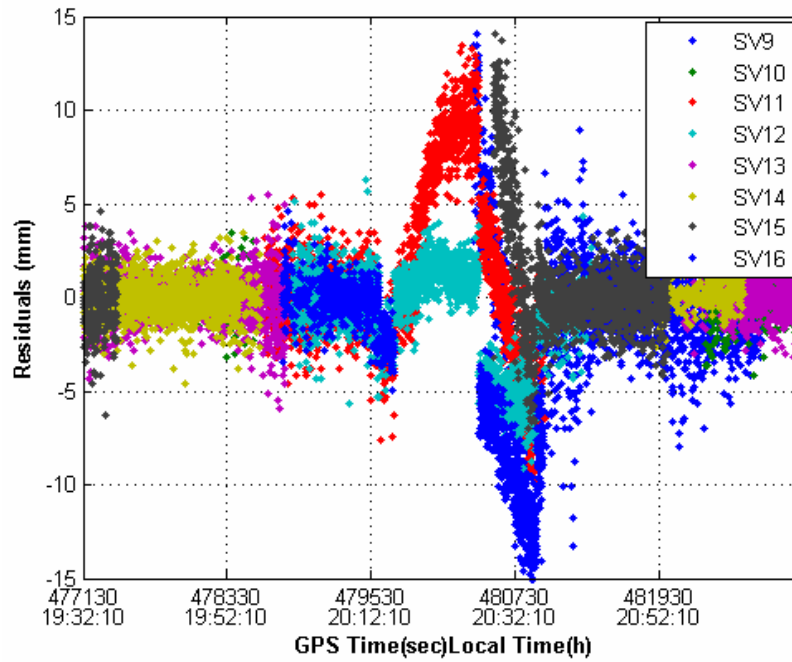


Figure 6-14: L1 Phase Residuals Error for Satellites 9-16

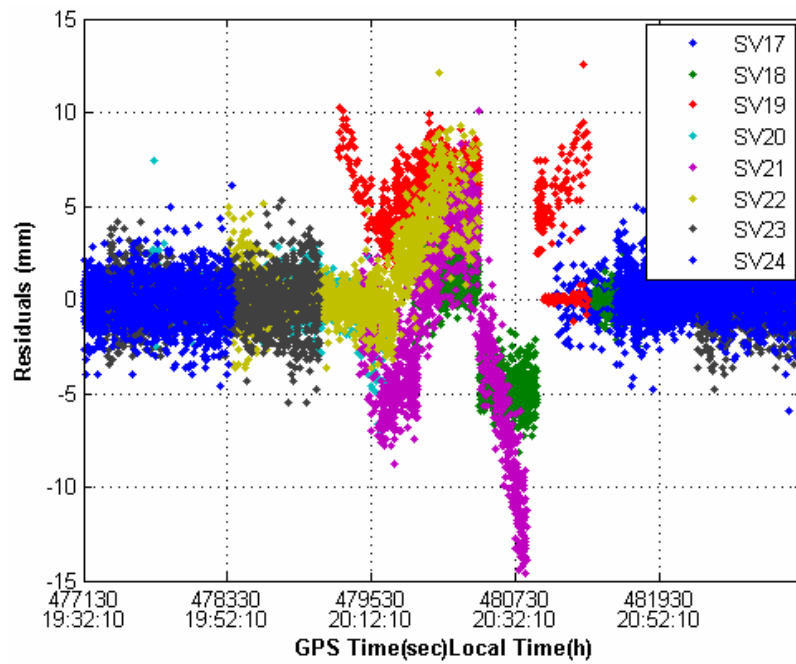


Figure 6-15: L1 Phase Residuals Error for Satellites 17-24

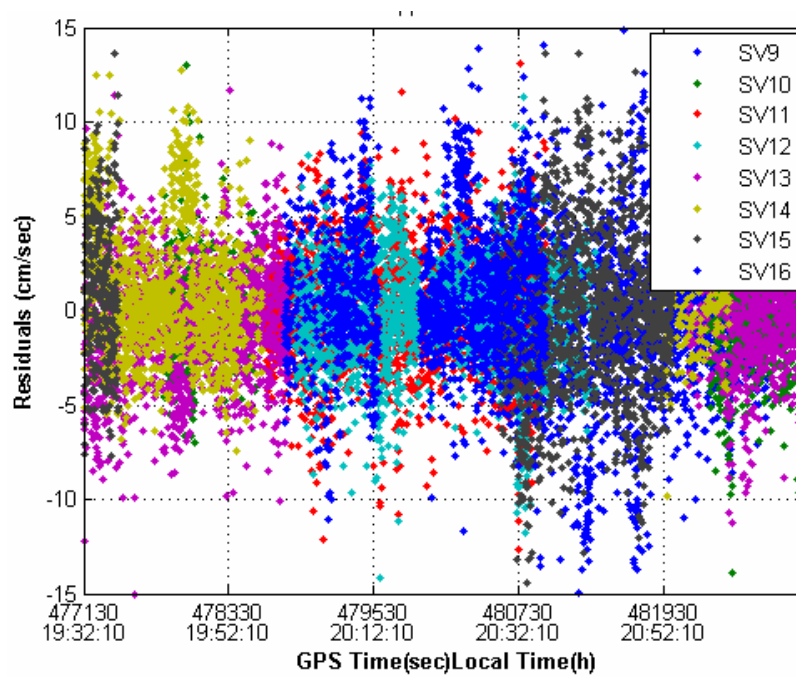


Figure 6-16: L1 Doppler Residuals Error for Satellites 9-16

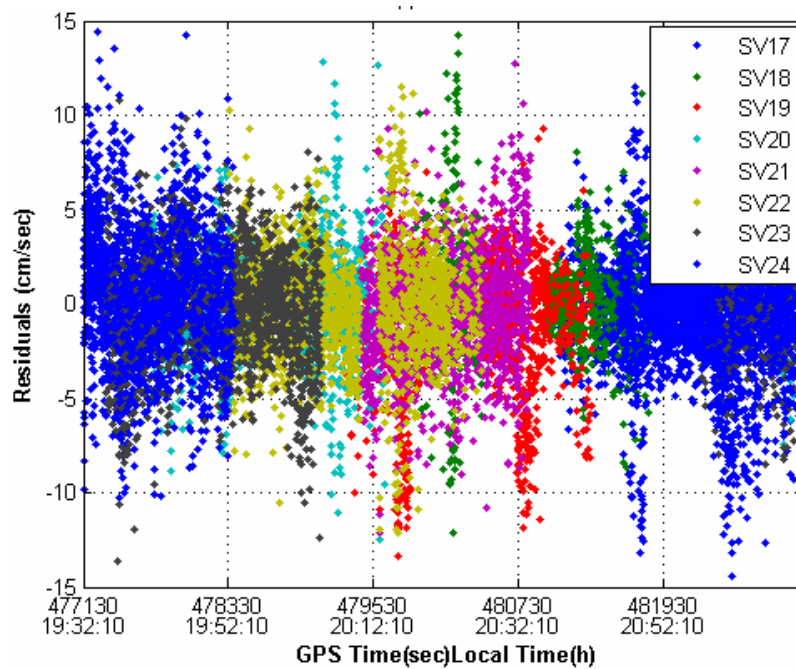


Figure 6-17: L1 Doppler Residuals Error for Satellites 16 -24

6.3.2 Test Results Using OEM4-G2L Trajectory

In this set of tests, the absolute positions and velocities of the Chief satellite are extracted from the NovAtel message and are used to update the software internally without the need for any external source. These tests are based on the modifications done to FLYKIN+™. As discussed previously, in the previous sets of tests the Chief absolute position (reference trajectory) is taken from the output files of the hardware simulator. These coordinates are accurate and in millimetre level as it is internally simulated by the simulator, so the exact position is well known. The positions and velocities from OEM4-G2L receiver is in the metre and centimetre level accuracy, respectively. For the absolute position errors for the Chief satellite a 3DRMS value of about 2.5 m was achieved.

1) Test 2 Results: 100 m Separation

Figure 6.18 shows the relative position errors and ambiguity resolution states for Test 2 with 100m baseline. The green colour shows the relative position error when all the ambiguities are fixed, while the red colour represents all float ambiguities. It takes less than 8 seconds to fix ambiguities to their integer values. At this time the relative error is at the centimetre level until fixing was done. Table 6.10 gives the mean and RMS values of the errors shown in Figure 6.18. The values are given for the north, east, and height directions. As expected, the errors in all directions are small. Relative position error has a zero mean for all three directions; the RMS errors are 1, 3, and 2 mm respectively, and the 3DRMS value is approximately 4 mm. These results are almost the same as the results from the previous tests with the absolute Chief positions taken from the simulator. This is show that the modifications done to the software give similar and reliable results.

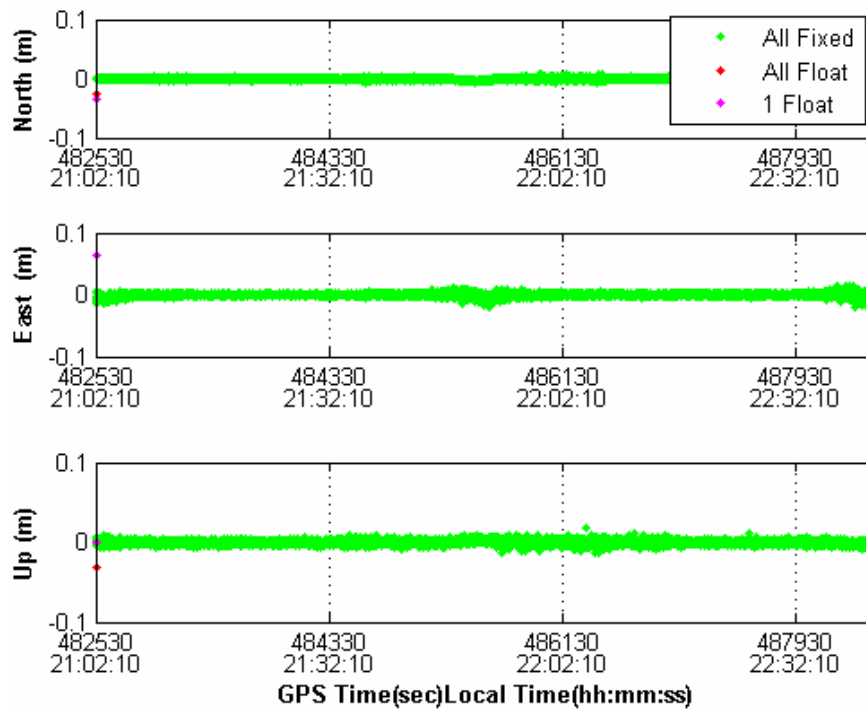


Figure 6-18: Test 2 Relative Position Errors (100 m Baseline)

Table 6-10: Statistics for Relative Position Errors

	Mean	RMS
North (mm)	0	1
East (mm)	0	3
Height (mm)	0	2

In Figure 6.19 the relative velocity errors were shown, while Table 6.11 shows the means, and RMS of these errors. The 3DRMS velocity error achieved is approximately 59 mm/s. The RMS value for the north direction is 44 mm/s, and is 40 mm/s in the east direction. For the up direction the RMS value is equal to 8 mm/s. These values are relatively high in comparison with the values from the previous tests. As said, the absolute velocity from the GPS receiver is relatively high (centimetre level), however, the velocity update assumed in the modification based on the constant velocity

assumption. In reality, velocity change from epoch to epoch but not constant. However, these results still acceptable for the CanX-4 and CanX-5 missions.

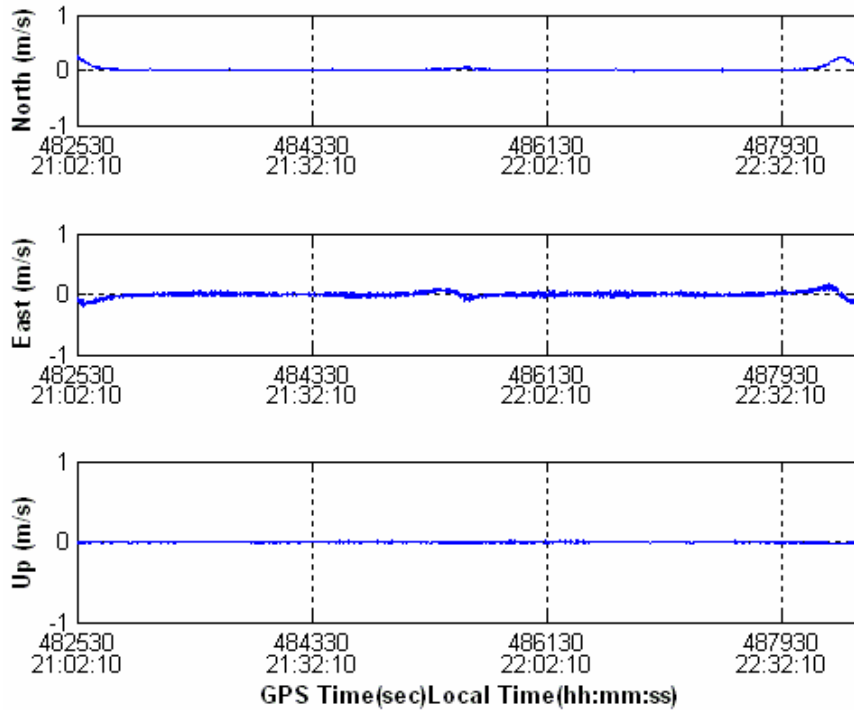


Figure 6-19: Test 2 Relative Velocity Errors (100 m Baseline)

Table 6-11: Statistics for Relative Velocity Errors

	Mean	RMS
Velocity N (mm/s)	0	44
Velocity E (mm/s)	0	40
Velocity H (mm/s)	0	8

2) Test2 Results: 1km Separation

Figure 6.20 shows the relative position errors and ambiguity resolution states for Test 2 with 1km baseline. The green colour shows the relative position error when all the ambiguities are fixed, while the red colour represents unfixed ambiguities. At the beginning it takes less than 7 seconds to fix ambiguities to their integer values. The

magenta color shows the ambiguity status when new GPS satellites come into view and new ambiguities are introduced to the estimation process. Table 6.12 gives the mean and RMS values of the errors shown in Figure 6.20. The values are given for the north, east, and height directions. As expected, the errors in all directions are small. Relative position error has a zero mean for all three directions; the RMS errors were 2, 6, and 3 mm respectively, and the 3DRMS value is approximately 7 mm. These sets of results are close to the previous results using the SimGEN trajectory files with a 3 mm difference.

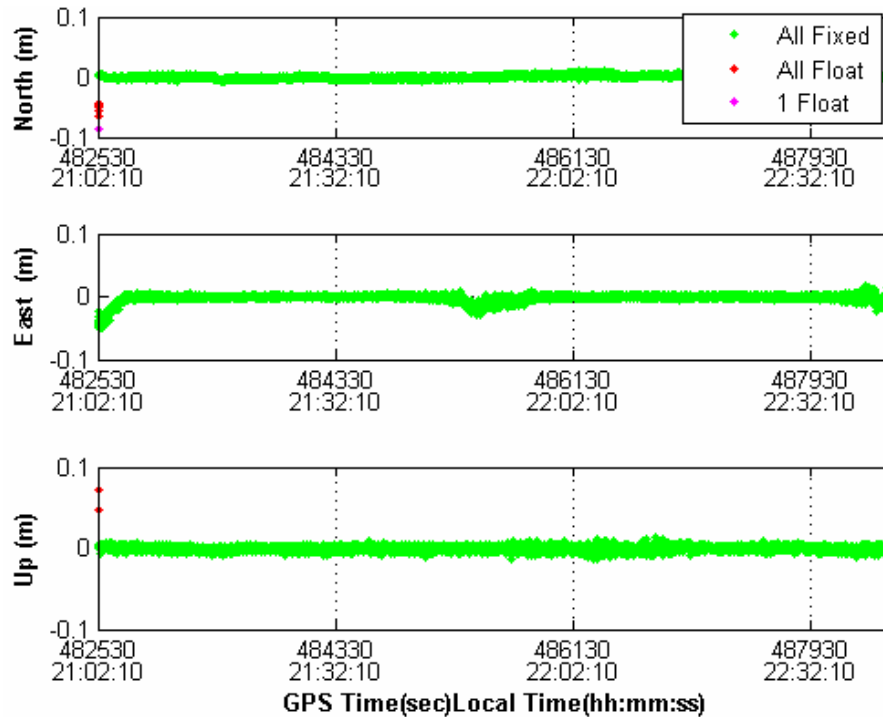


Figure 6-20: Test 2 Relative Position Errors (1 km Baseline)

Table 6-12: Statistics for Relative Position Errors

	Mean	RMS
North (mm)	0	2
East (mm)	0	6
Height (mm)	0	3

Figure 6.21 shows relative the velocity errors while Table 6.13 shows the means and RMS of these errors. The 3DRMS velocity error achieved is approximately 61 mm/s. The RMS value for the north direction is 45 mm/s, and is 40 mm/s for the east direction. For the up direction the RMS value is 9 mm/s.

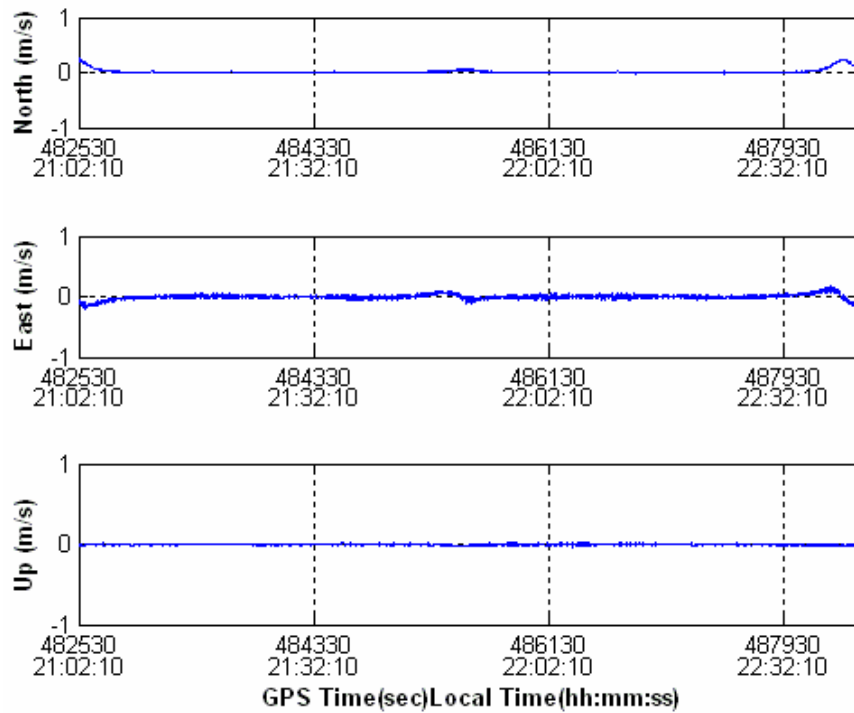


Figure 6-21: Test 2 Relative Velocity Errors (1km Baseline)

Table 6-13: Statistics for Relative Velocity Error

	Mean	RMS
Velocity N (mm/s)	0	45
Velocity E (mm/s)	0	40
Velocity H (mm/s)	0	9

6.3.3 Signal Outages Tests and Results

This section shows the relative position and velocity errors during signal outages. Three different tests were performed with 5, 30 and 60 second outage durations every 10 minutes with one second data rate. For the first test, within every 10 minutes there were 5 seconds of full GPS signal outage. Figure 6.22 shows the relative position errors during signal outages. The black colour shows the error when there is no signal. It can be seen that the RMS values for the north, east and up directions are at the centimetre level. However, it is seen (in red) that the ambiguities are float. The average time to fix ambiguities to their integer values after signal outages is about 2 seconds. Figure 6.23 shows the relative velocity errors with signal outages. The 3DRMS value is about 25 mm/s, and this value is very close to the results without signal outages.

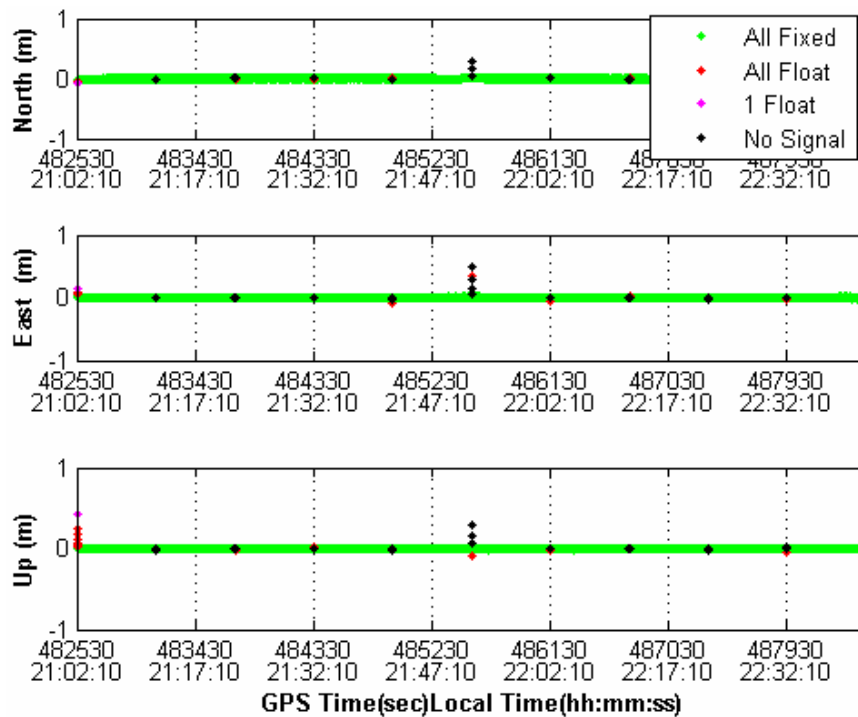


Figure 6-22: Relative Position Error During Signal Outages (5 sec)

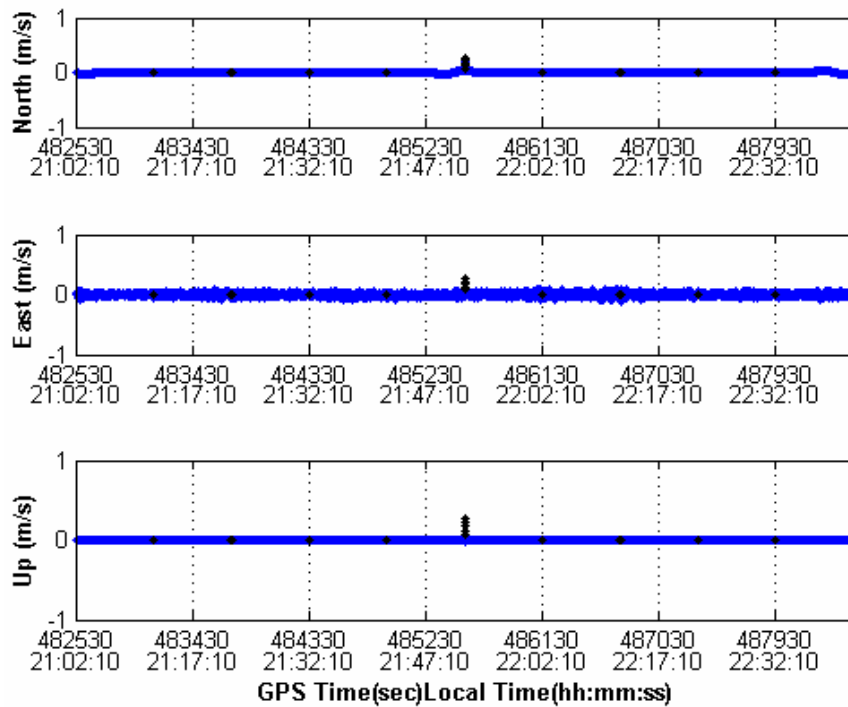


Figure 6-23: Relative Velocity Error During Signal Outages (5 sec)

Figure 6.24 shows the relative position errors during the 30 s signal outages. The black colour shows the error when there is no signal. It can be seen that the RMS values for the north, east and up directions reach approximately 50 cm in some cases, otherwise the relative errors are still at the centimetre level. The average time to fix ambiguities to their integer values after signal outages is about 5 seconds. Figure 6.25 shows the relative velocity errors with signal outages. The 3DRMS value is about 64 mm/s; a value that is higher than the value from the previous test. As a conclusion, the more signal outage the more time is needed to fix ambiguities to their integer values, and the higher relative position and velocity errors. This is clearly seen in the next test where 60 second signals outages were simulated.

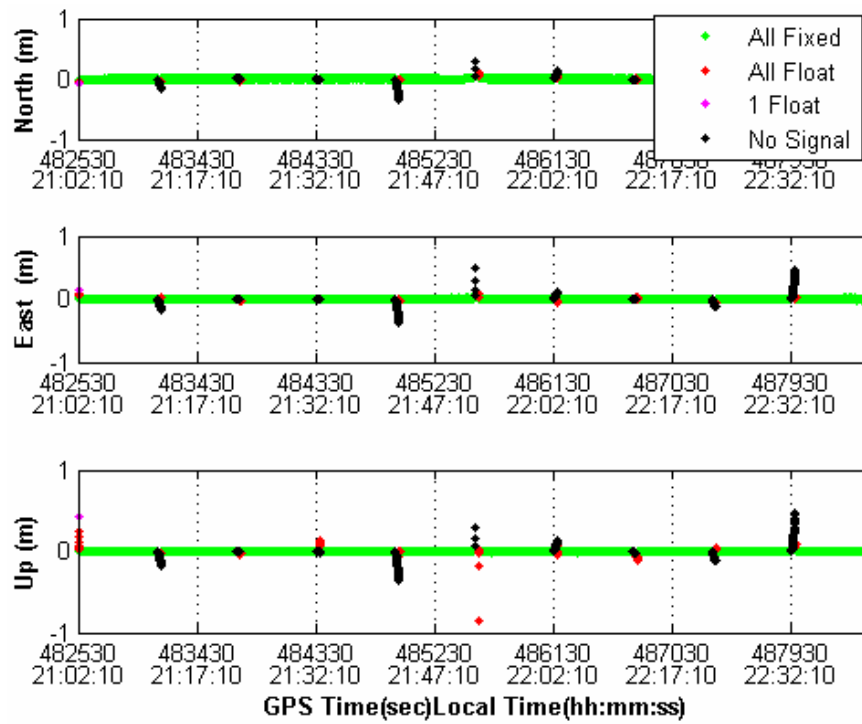


Figure 6-24: Relative Position Error During Signal Outages (30 sec)

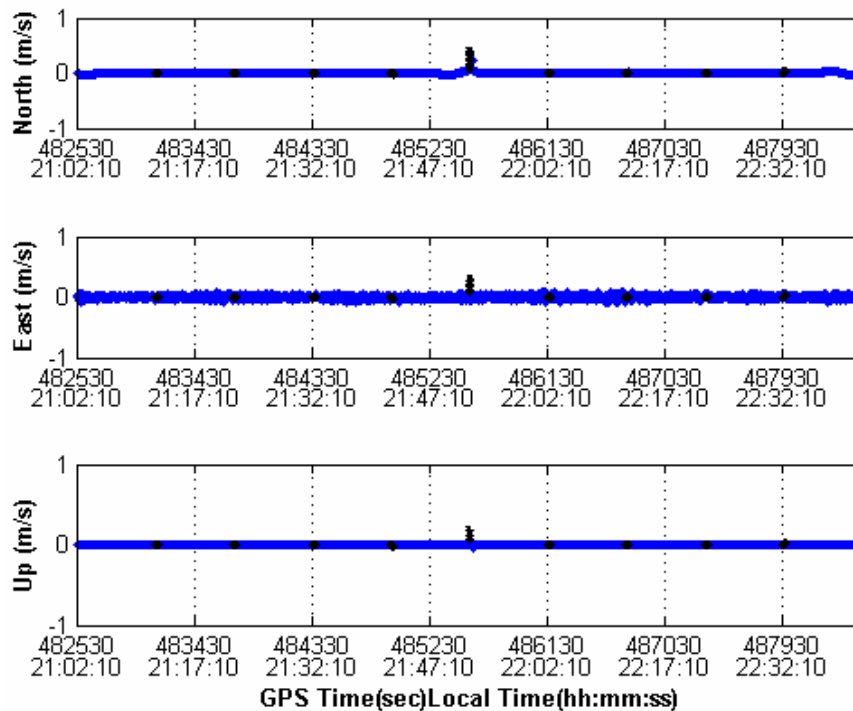


Figure 6-25: Relative Velocity Error During Signal Outages (30 sec)

In Figure 6.26 relative position errors during 60 s signal outages are shown. The black colour shows the error while there is no signal. It can be seen that the RMS values for the north, east and up directions grow to about one metre and higher in some cases. Close to the black dots there are the red dots where the ambiguities are float (unfixed), and the average time to fix ambiguities to their integer values after signal outages is about 9 seconds. Figure 6.27 shows the relative velocity errors with signal outages. The 3DRMS value is about 15.0 cm/sec, this value is higher than the values from the previous tests. This is in regards to the longer time needed to fix ambiguities to their integer values. As a conclusion, the software is still capable of fixing ambiguities to their integer values within a short time. Finally, relative position and velocity errors during signal outages are still acceptable.

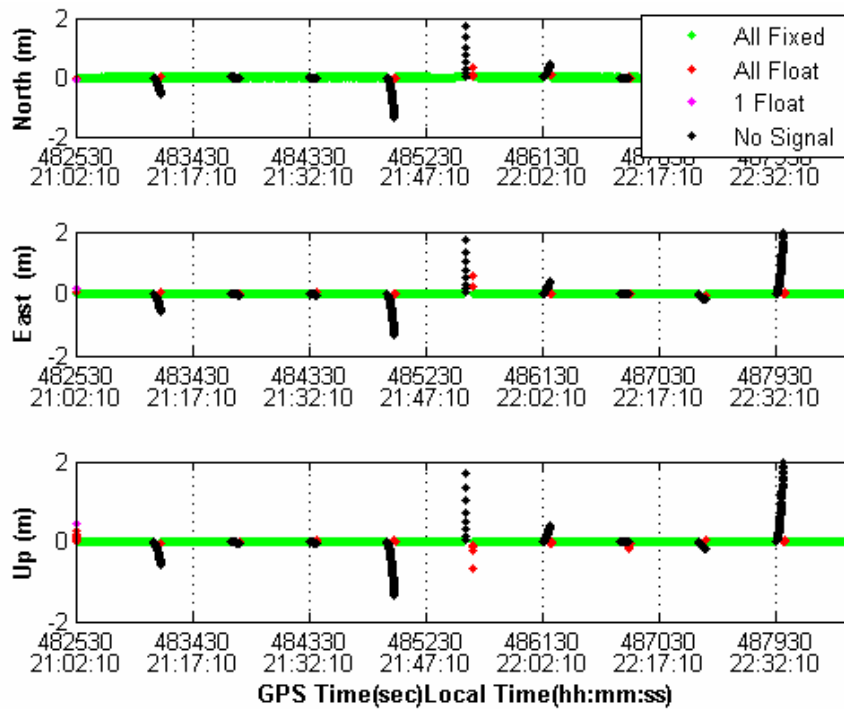


Figure 6-26: Relative Position Error During Signal Outages (60 sec)

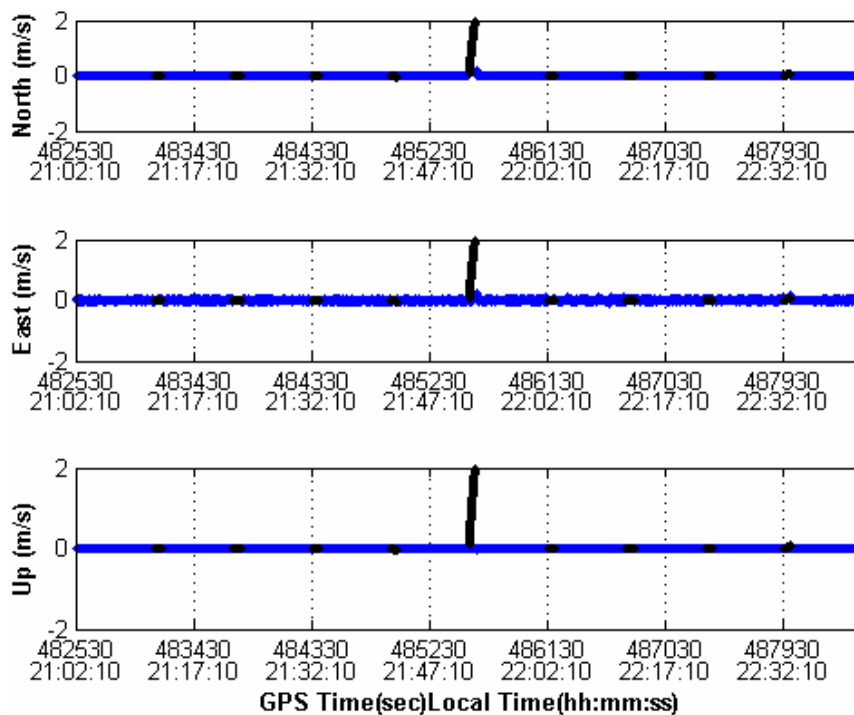


Figure 6-27: Relative Velocity Error During Signal Outages (60 sec)

6.4 Summary

In this work two sets of data were tested and analyzed for satellite formation flying. The first data set was based on using absolute trajectory coordinates from the HWIL signal simulator, while for the second data set, the coordinates were extracted from the GPS receiver internally, and based on the modifications done to the FLYKIN+™ software in this work. Relative position and velocity accuracies were at the millimetre and centimetre levels, respectively.

The results shown in the second tests, are close the results from the first test with some differences, relative to the method of modification. Chapter 7 summarizes the conclusions and recommendations

CHAPTER 7

CONCLUSIONS AND RECOMMENDATIONS

Formation flying of LEOs has great potential in the upcoming years. A simple precise relative navigation system is needed to enable the benefits from LEO formation flying. The primary objective of this research work was to develop, implement, and test a method for relative positioning of formation flying spacecraft. Based on the results from the previous chapter it can be concluded that this objective has been fulfilled.

7.1 Conclusions

- The focus of the work was to use carrier phase GPS observables to measure the inter-satellite position and velocity with millimetre relative position accuracy that are achieved when L1 ambiguities are correctly resolved, giving the following accuracies

- 3D RMS 100 m baseline: 3 mm
- 3D RMS 1 km baseline: 4 mm
- 3D RMS 5 km baseline: 12 mm

while centimetre relative velocity accuracy can be achieved, namely

- 3D RMS 100 m baseline: 2.2 cm/s

- 3D RMS 1 km baseline : 2.5 cm/s
- 3D RMS 5 km baseline : 3.4 cm/s

Using relative carrier phase observables with known ambiguities are required to reach this level of accuracy. However, the east velocity SPD value needs more investigation.

- During signal outages, the random walk approach was shown to provide metre level accuracy (3D RMS) for outages lasting up to 60 s. As for the accuracy of the velocity estimates, the 3D RMS errors were kept in the centimetre per second level. However, the software is still capable of fixing ambiguities to their integer values after signal outages with a time of less than 10 seconds.
- An analysis of GPS satellites in view versus GPS antenna boresight angle from zenith is performed. A zero angle is the best case where the coverage is 99%. For a 45 degree elevation there is a slight degradation in satellites tracked according to the tilted antenna, whereby for 95% of the simulation time there are more than four satellites in view. For a 180 degree elevation, the antenna was pointed downward. In this case 23% of the time there were four satellites.
- Multipath effect is studied; as a result multipath is not a major error for nanosatellite missions. As the only reflecting surface in space is the satellites' surface. In the case of CanX-4 and -5 the surface dimensions is about 20 cm X 20 cm which is a very small reflecting surface; in addition, Kroes (2006) analyzed the multipath error for

spacecraft from the GRACE mission and found that the C/A code multipath error in a spaceborne environment is at the decimetre level.

7.2 Recommendations

Based on the results from the previous chapter, the following recommendations can be made to address the limitations of this research:

- The multipath model used in this research was reasonable for LEO applications since the only available reflective source is the spacecraft surface. Using an HWIL signal simulator, multipath errors were assumed to be uncorrelated between spacecraft. This is shown in the results of the previous chapter, as 4.0 mm position degradation according to multipath. However, Kroes (2006) illustrated that multipath errors of the GRACE spacecraft are correlated, but no values were provided to quantify this relationship. More research is needed to address this matter of the multipath errors on formation flying missions.
- In this work the maximum baseline separation was 5 km based on the limits of the data link. In the future, more advanced dynamic models should be studied for use in long baseline separations up to 220 km. Kroes (2006) used a numerical integration approach for such separations. A complex dynamic model was incorporated into the Kalman filter, which resulted in a sub millimetre positioning accuracy for GRACE Mission.

- Using real data from both Chief and Deputy satellites and verify the results achieved in this work is recommended as they are scheduled to be launched in mid 2008.

REFERENCES

- Axelrad, P., C. Comp, and P. MacDoran (1994), Use of Signal-To-Noise Ratio for Multipath Error Correction in GPS Differential Phase Measurements: Methodology and Experimental Results, Proceedings of ION GPS-94, Salt Lake City, September 20-23, pp. 655-666.
- Bamford, W.A. (2004). Navigation and Control of Large Satellite Formations. Ph.D. Thesis, Faculty of the Graduate School. The University of Texas at Austin.
- Barrena, V. and Colmenarejo P. (2003). Ambiguity Dilution of Precision for Radio Frequency Based Relative Navigation Determination. Proceedings of the fifth international ESA Conference on spacecraft guidance, Navigation and Control Systems, Frascati, Italy. October 22-25.
- Binning, P. W. (1997). Satellite to Satellite Relative Navigation Using GPS Pseudoranges. Proceedings of the ION NTM, Santa Monica, January 14-16, pp.407-415.
- Bourga, C., C Mehlen., P. Colmenarejo, J.M Lopez., V. Barrena, A. Rodriguez (2003), Autonomous Formation Flying RF Ranging Subsystem, Proceedings of the ION GPS/GNSS-03. Portland, Oregon, September 9-12, pp. 2194-2200.
- Breger, L., and Jonathan P. How (2004), GVE-Based Dynamics and Control for Formation Flying Spacecraft, 2nd International Symposium on Formation Flying Missions & Technologies, Washington, DC, September 14-16, 2004
- Brown, A., and Stolk K. Rapid Ambiguity Resolution using Multipath Spatial Processing for High Accuracy Carrier Phase. NAVSYS Corporation.
- Busse, F. D. (2003). Precise Formation-State Estimation in Low Earth Orbit Using Carrier Differential GPS. Ph.D. Thesis. Department of Aeronautics & Astronautics .Stanford University.

- Busse, F. D. and J. P. How (2002). Real-Time Experimental Demonstration of Precise Decentralized Relative Navigation Formation Flying Spacecraft. American Institute of Aeronautics and Astronautics. pp. 1-11
- Busse, F., Jonathan H., and James S. (2002). Demonstration of Adaptive Extended Kalman Filter for Low Earth Orbit Formation Estimation Using CDGPS. Proceedings of the ION GPS Meeting, Portland, September 24-27, pp.2047-2058.
- Caillibot, E.P., C. Cordell Grant, and Daniel D. Kekez (2005), Formation Flying Demonstration Missions Enabled by CanX Nanosatellite Technology, 19th Annual AIAA/USU Conference on Small Satellites. Logan, Utah.
- Cannon, M. E. (2002). GPS Positioning, ENGO 561 Lecture Notes. Department of Geomatics Engineering, The University of Calgary, Canada.
- Cannon, M. E., and G. Lachapelle (2004). SimGNSSITM Operating Manual. Department of Geomatics Engineering, The University of Calgary, 10 pages.
- Cannon, M. E., G. Lachapelle, M. Olynik, M. Petovello, W. Gelatka, and J. Davis (2001), P3 Aircraft Buffeting Measurement Using Precise Carrier Phase Techniques, Proceedings of ION GPS-01 (Session D2, Salt Lake City, 11-14 September), Institute of Navigation, Alexandria, VA, pp. 1009-1016.
- Crawford S. (2005) Performance Evaluation of Sensor Combinations for Mobile Platoon Control. Master's thesis, Department of Geomatics Engineering, University of Calgary.
- Dong, L. (2003). IF GPS Signal Simulator Development and Verification. MSc. Thesis. UCGE Report #20184, Department of Geomatics Engineering, The University of Calgary.
- Dong, L. (2004). SimGNSSITM Algorithm Design Document. Department of Geomatics Engineering, The University of Calgary, 27 pages.

- El-Sheimy, N. (2006). ENGO 623 Lecture Notes: Inertial Techniques and INS/DGPS Integration. Department of Geomatics Engineering, University of Calgary.
- Foisy, D., C. Grant, T. Tuli, N. Orr, and N. Deschamps (2007). CanX-4/5 Systems Overview. UTIAS/SFL 4925 DUFFERIN ST., TORONTO, ON M3H 5T6, CANADA. 24 pages.
- Fontana, R.D., W. Cheung, P. M. Novak, and T.A. Stansell (2001). The New L2 Civil Signal, Proceedings of ION GPS 2001, 11-14 September 2001, Salt Lake City, UT, pp.617-631.
- French, G. T. (1996). Understanding the GPS: An Introduction to the Global Positioning System. USA. ISBN 0-9655723-0-7 p.p 87-97.
- Grewal, M.S. and Angus P.A. (2001). Kalman Filtering: Theory and Practise Using MATLAB. 2nd Editoin. John Wiley & Sons, Inc. ISBN 0-47126638-8
- Hofmann, B., Lichtenegger H., and Collins J. (1997). Global Positioning System Theory and Practice.
- IGS (2007) International GNSS Service Data and Products. <http://igsb.jpl.nasa.gov/components/compindex.html>, last accessed August 20, 2007.
- Kroes, R. (2006). Precise Relative Positioning of Formation Flying Spacecraft using GPS. Ph.D. thesis. Delft University of Technology, ISBN 90-8559-150-3.
- Lachapelle, G. (2005). Advanced GPS Theory and Applications, ENGO625 Lecture Notes. Department of Geomatics Engineering, University of Calgary.
- Lachapelle, G., H. Sun, M.E. Cannon and G. Lu (1994), Precise Aircraft-to-Aircraft Positioning Using a Multiple Receiver Configuration, Can. Aeronautics and Space Journal, Vol. 40, No.2, pp. 74-78.

- Lee, H. Wang J., and Rizos C. An Integer Ambiguity Resolution Procedure for GPS/Pseudolite/INS Integration. School of Surveying and Spatial Information Systems, the University of New South Wales, Sydney NSW 2052 Australia.
- Liu, J. (2003). Implementation and Analysis of GPS Ambiguity Resolution Strategies in Single and Multiple Reference Station Scenarios. M.Sc. Thesis, UCGE Report no. 20168 , Department of Geomatics Engineering, The University of Calgary.
- Long A., D. Kelbel, T. Lee, D. Leung, J. R. Carpenter and C. Gramling (2005), Relative Navigation of Formation-Flying Satellites, The Leading Edge Forum. Computer Sciences Corporation.
- Marji, Q., R. Tsoi, M.E. Cannon, and R.E. Zee (2007). Software Simulation Tests and Results for Nano-Satellites Formation Flying. Proceedings of the ION NTM, San diego, CA, January 22-24, pp.628-636.
- Marji, Q., S. Shiekh, and R. Basheer (2004). Global Positioning System for Establishing Geodetic Networks. B.Sc. Thesis, Department of Surveying and Geomatics Engineering, Al-Balqa' Applied University, Jordan.
- Mauthe, S., F. Pranajaya and R.E. Zee (2005).The Design and Test of a Compact Propulsion System for CanX Nanosatellite Formation Flying. Proc.19th Annual AIAA/USU Conference on Small Satellites. Logan, Utah.
- Misra, P., and P. Enge. (2001), Global Positioning System. Signals, Measurements, and Performance, Published by Ganga-Jamuna Press, P.O. Box 692, Lincoln, Massachusetts 01773. pp. 126-128.
- Montenbruck, O., and R. Kroes (2003) In-Flight Performance Analysis of the CHAMP BlackJack GPS Receiver. In: EGS - AGU - EUG Joint Assembly.
- NovAtel Inc. (2002). OEM4 Family of Receivers, USER MANUAL - VOLUME 1– Installation and Operation, Publication No. OM-20000046, Canada, 184 Pages.

- NovAtel Inc. (2002). OEM4 Family of Receivers, USER MANUAL - VOLUME 2— Command and Log Reference, Publication No. OM-20000047, Canada, 272 Pages.
- OEM4-G2L Data Sheet, NovAtel. (2003)
. <<http://www.novatel.ca/Documents/Papers/oem4g2.pdf>>, Last accessed, Feb28, 2007.
- Olsen, E. A. (1999). GPS Sensing for Formation Flying Vehicles. Ph.D. Thesis. Department of Aeronautics & Astronautics. Stanford University
- Olynik, M.(2002). Temporal Characteristics of GPS Error Sources and Their Impact on Relative Positioning. MSc. Thesis. UCGE Report #20162, Department of Geomatics Engineering, The University of Calgary.
- Olynik, M., M.E. Cannon, G. Lachapelle, W. Gelatka, and J. Davis (2001), Precise Relative Positioning Using Absolute GPS, Proceedings of Kinematic International Symposium (KIS01), Banff, June 5-8, University of Calgary, pp. 385-391
- Olynik, M., M.G. Petovello, M.E. Cannon and G. Lachapelle (2002), Temporal Variability of GPS Error Sources and Their Effect on Relative Positioning Accuracy, Proceedings of the ION NTM Meeting, San Deigo, January, pp. 877-888.
- Park, C. W. (2001). Precise Relative Navigation Using Augmented CDGPS. Ph.D. Thesis .The Department of Mechanical Engineering. Stanford University
- Parkinson, B.W., J.J. Spilker, Jr., P. Axelrad, P. Enge (1996). Global Positioning System: Theory and Applications, Volumes 1 and 2, American Institute of Aeronautics and Astronautics (AIAA), Progress in Astronautics and Aeronautics Series, Volumes 163 and 164, Washington, DC.
- Positioning, Location, and Navigation Group (2003). FLYKIN+™ Version 1.0 Operating Manual. Department of Geomatics Engineering, The University of Calgary, 24 pages.

- Qiu, J. (2007), RF Interference Impact on GPS L5 Reception Performance. MSc. Thesis, UCGE Report no. 20251, Department of Geomatics Engineering. The University of Calgary,
- Rankin, D., D.D. Kekez, R.E. Zee, and F.M. Pranajaya (2004). The CanX-2 Nanosatellite: Expanding the Science Abiliyies of Nanosatellites. 55th International Astronautical congress 2004-Vancouver, Canada.
- Raquet, J. (1998), Development of a Method for Kinematic GPS Carrier-Phase Ambiguity Resolution Using Multiple Reference Receivers. Ph.D. Thesis, UCGE Report no. 20116, Department of Geomatics Engineering. The University of Calgary.
- Ray, J., M.E. Cannon and P. Fenton (1999), Mitigation of Carrier Phase Multipath Effects Using Multiple Closely-Spaced Antennas, Navigation, Vol. 46, No. 4, pp. 1025-1034.
- Ray, J.K. and M.E. Cannon (1999), Characterization of GPS Carrier Phase Multipath, Proceedings of the ION National Technical Meeting, San Diego, January 25-27, pp. 343-352.
- Ray, J.K. (1998). Mitigation of GPS Code and Carrier Phase Multipath Effects using a Multi-Antenna System, Ph.D. Thesis, UCGE Report no. 20136, Department of Geomatics Engineering. The University of Calgary.
- Rizos, C. (1999), Principles and Practice of GPS Surveying, Satellite Navigation And Position Group, The University of New South Wales. Sydney, Australia.
- Sarda, K.(a), S. Eagleson (a), S. Mauthe (a), T. Tuli (a), R.E. Zee (a), C.C. Grant (a), D.G. Foisy (a), E. Cannon(b), and C.J. Damaren (c) (2006).CanX-4 & CanX-5: Precision Formation Flight Demonstrated by Low Cost Nanosatellites. (a) Space Flight Laboratory, University of Toronto Institute for Aerospace Studies, (b)

- University of Calgary, Geomatics Engineering, (c) University of Toronto Institute for Aerospace Studies, Spacecraft Dynamics and Control.
- Sarda, K., S. Eagleson, E. Caillibot, C. Grant, D. Kekez, F. Pranajaya, and R Zee, (2006), Canadian Advanced Nanospace Experiment 2: Scientific and Technological Innovation on a Three-kilogram Satellite. Proceeding 56th International Astronautica congress Fukuoka, Japan, pp.236 – 245
- Schwarz, K. (1999). Fundamentals of Geodesy. Department of Geomatics Engineering, University of Calgary.
- Schweighart, S. (2001). Development and Analysis of a High Fidelity Linearized J2 Model for satellite Formation Flying. M.Sc. Thesis. Massachusetts Institute of Technology.
- Schweighart, S. A. and R. J. Sedwick (2002). A High Fidelity Linearized J2 Model for Satellite Formation Flight. Journal of Guidance, Control, and Dynamics. Vol. 25, No. 6, November–December. pp. 1073-1080
- Seeber, G. (2003) Satellite Geodesy. 2nd edn., Walter de Gruyeter GmbH & Co. KG, 10785 Berlin.
- Skone, S. (1998). Wide Area Ionosphere Grid Modelling in the Auroral Region. Ph.D. thesis, Department of Geomatics Engineering, The University of Calgary, Calgary, AB.
- Sleewaegen, J. (1997), Multipath Mitigation, Benefits from using the Signal-to-Noise Ratio, Proceedings of ION GPS-97, Kansas City, September 16-19, pp. 531-540.
- Spirent Communications (SW) Ltd (2005). SimGEN Software User Manual. No. DGP00686AAA, 440 pages.

- Talbot, N.C., (1996). Compact Data Transmission Standard for High-Precision GPS. Proceedings of ION GPS-96, Kansas City, September 17-20, pp. 861-871.
- Teunissen, P. (1999). Predicting the Success of Ambiguity Resolution. CGSIC 34th meeting, Nashville, USA.
- Teunissen, P., Kleusberg A. (1998). GPS for Geodesy 4th revised edition. SpringerWienNewYork. ch8 (319-350).
- Teunissen, P.J.G. (1995). The least-squares ambiguity decorrelation adjustment: a method for fast GPS integer ambiguity estimation. *Journal of Geodesy*, 70: 65-82
- Tiberius, C.C.J.M., and P.J. de Jonge (1995). Fast positioning using the LAMBDA-method. Proceedings of the 4th International Symposium on Differential Satellite Navigation Systems DSNS'95, Bergen, Norway, April 24-28, Paper 30, 8 pp.
- Tsoi, R. (2007). Precise GPS Relative Navigation for Future Geodetic Satellite Formation Flying Missions. MSc. Thesis. UCGE Report #20256, Department of Geomatics Engineering, The University of Calgary.
- Verhagen, S. (2004). Integer ambiguity validation: an open problem. *GPS Solutions*.
- Verhagen, S. (2004). The GNSS integer ambiguities: estimation and validation. Delft Institute of Earth Observation and Space Systems, Delft University of Technology
- Wang, J., Lee H., Hewitson S., Rizos C., and Barnes J. Sensitivity Analysis for GNSS Integer Carrier Phase Ambiguity Validation Test. School of Surveying and Spatial Information Systems, The University of New South Wales,
- Wang, J., Stewart M., and Tsakiri M. (2000). A comparative study of the integer ambiguity validation procedures. *Earth Planets Space*, 52, 813–817, 2000.
- Wang, M. (2004). GPS Data Quality Monitoring and Control. Department of Geomatics Engineering University of Calgary, ENGO 625, Research Seminar.

- Weiss, J.P., S. Anderson, C. Fenwick, L. Song, P. Axelrad, P. Belay, and R. Brinkley (2005). Development and Validation of an Aircraft Multipath Model for Land-Based JPALS. Proceedings of the ION 61st Annual Meeting. 27- Cambridge, MA ,29 June 2005, pp. 818-829.
- Welch, G. and G. Bishop (2001). An Introduction to the Kalman Filter. SIGGRAPH 2001, Course 8 Lecture Notes. Department of Computer Science, University of North Carolina at Chapel Hill.
- Xiang, W., J. L. Jorgensen (2005). Formation Flying: A subject being fast unfolding in space, 5th IAA Symposium on Small Satellites for Earth Observation. April 4 - 8, 2005, Berlin, Germany.
- Yun-feng, G., B. He-xi, and L. Jun.-feng (2003). Comparison of Two Methods in Satellite Formation Flying. National Natural Science Foundation of China. pp. 902-908.
- Zee, R. E. (2005). Generic Nanosatellite Mission Requirements Document Supporting CanX-4, CanX-5, BRITE, Space Flight Laboratory, University of Toronto Institute for Aerospace Studies, Toronto, Ontario, Canada.
- Zee, R. E. Research Proposal, Nanosatellite Formation flying and inspection-NSERC Form 101 Part II, Space Flight Laboratory, University of Toronto Institute for Aerospace Studies, Toronto, Ontario, Canada.
- Zhang, Y., and C. Bartone (2004). Real-time Multipath Mitigation with WaveSmooth™ Technique using Wavelets, Proceedings of ION GNSS 2004, September 21-24, Long Beach, CA, pp. 1181-1194.

APPENDIX A

Software Development

This section shows data extraction from the NovAtel format. In addition, it shows the logs used and the data extracted from these logs. Calculations show the save of data bits, which is considered as a very important factor in nanosatellite where memory is an issue. Further details are also shown on data quality checks and what the flags are needed to be checked.

Preliminary and Data Extraction for Satellite Formation Flying

A NovAtel GPS receiver is capable of generating several logs which can be divided into the following three types: synchronous, asynchronous, and polled. The data for synchronous logs is generated on a regular schedule. Asynchronous data is generated at irregular intervals. If asynchronous logs are collected on a regular schedule, they would not output the most current data as soon as it was available. The data in polled logs is generated on demand.

Raw NovAtel RANGE Message

The RANGE message (type 43) contains the channel measurements for the currently tracked satellites. The layout of this is given in NovAtel (2002). The Header is 28 bytes and contains the GPS time of week in milliseconds. The number of observations follows the header and this indicates the number of observations which will follow. If the

receiver is dual frequency (L1 and L2), then the number of observations generally is (but not always) twice the number of satellites tracked. There are 44 bytes per observation followed by a 4 byte cyclic redundancy check (CRC). The Channel Tracking Status contains information about the data quality and type of measurement (e.g. L1 or L2). The various parameters in the Channel Tracking Status are detailed in NovAtel (2002). The size of the raw RANGE message is 28 bytes (Header) + 44 bytes x # obs + 4 bytes CRC. Therefore, when tracking eight satellites on L1, there would be $28 + 44 \times 8 + 4 = 384$ bytes.

Extracted Measurement Record and Quality Checks

The raw data needed for each satellite is the pseudorange, the carrier phase and the Doppler. In addition, the standard deviations of these measurements (except for the Doppler which is not available) can be used in the downstream processing. The time of the measurement is also needed, but this is the same for all observations. A summary of the information is included in Table A-1. For an eight observation example, the total bytes would be $4 + 8 \times 30 = 244$.

Table A-1: Extracted Data from Range Message

Field #	Data Description	Notes	Format	Bytes
1	GPS Time	GPS Time	Long	4
2	Sat PRN	GPS satellite PRN number of range measurement	UShort	2
3	Pseudorange	Pseudorange measurement (m)	Double	8
4	Std Range	Pseudorange measurement standard deviation (m)	Float	4
5	Phase	Carrier phase, in cycles	Double	8
6	Std Phase	Estimated carrier phase standard deviation	Float	4
7	Doppler	Instantaneous carrier Doppler frequency (Hz)	Float	4
8...	Next observation is in fields 8-13, etc. Total bytes is 4 + # obsx30			

Not all raw data should be processed since some measurements may not be of sufficient quality. Several flags are contained in the Channel Tracking Status. The particular flags to check are detailed in Table A-2. Table A-3 gives the total number of bytes as a function of satellites tracked (assuming L1 tracking).

Table A-2: Quality Flags to Check (NovAtel Inc., 2002)

Data Description	Notes	Usage of Data
Phase lock flag	0 = Not locked, 1 = Locked	Use data if the phase lock flag = 1, otherwise no.
Parity known flag	0 = Not known, 1 = Known	If the Parity is “Not Known”, then don’t use Accumulated Doppler Range (ADR) because of large jumps such as (1/2) cycle.
Code locked flag	0 = Not locked, 1 = Locked	Use data if the Code lock flag = 1, otherwise no.
Lock Time	Number of seconds of continuous tracking (no cycle slipping)	Do not use if Lock Time = 0.
Tracking state	0-11 see Table 4 for each value	If it is = 0, do not use the data (Idle). If it is = 4, use data (Phase lock Loop).
Frequency	0 = L1, 1 = L2	Always have L1, unless having dual frequency, then L2 will appear.
C/N ₀	Carrier to noise density ratio $C/N_0 = 10[\log_{10}(S/N_0)]$ (dB-Hz)	$C/N_0 > 40$: Very Strong signal $32 < C/N_0 < 40$: Marginal Signal $C/N_0 < 32$: Probably Losing Lock

Table A-3: Number of Bytes as a Function of Satellites Tracked

Number of Satellites	Total Bytes
1	34
2	64
4	124
6	184
8	244
10	304

NovAtel BESTXYZ Best Available Cartesian Position and Velocity

BESTXYZ contains the receiver's best available position and velocity in Earth-Centered, Earth-Fixed coordinates (See Table A-4). The position and velocity status fields indicate whether or not the corresponding data is valid.

Table A-4: BESTXYZ (Message 241) Structure (NovAtel Inc., 2002)

Field #	Field type	Data Description	Format	Binary Bytes	Binary Offset
1	header	Log header		H	0
2	P-sol status	Solution status, see Table B1, Solution Status on Appendix B.	Enum	4	H
3	pos type	Position type, see Table B2, Position or Velocity Type on Appendix B	Enum	4	H+4
4	P-X	Position X-coordinate (m)	Double	8	H+8
5	P-Y	Position Y-coordinate (m)	Double	8	H+16
6	P-Z	Position Z-coordinate (m)	Double	8	H+24
7	P-X σ	Standard deviation of P-X (m)	Float	4	H+32
8	P-Y σ	Standard deviation of P-Y (m)	Float	4	H+36
9	P-Z σ	Standard deviation of P-Z (m)	Float	4	H+40
10	V-sol status	Solution status, see Table B1, Solution Status on Appendix B.	Enum	4	H+44
11	vel type	Velocity type, see Table B2, Position or Velocity Type on Appendix B	Enum	4	H+48
12	V-X	Velocity vector along X-axis (m/s)	Double	8	H+52
13	V-Y	Velocity vector along Y-axis (m/s)	Double	8	H+60
14	V-Z	Velocity vector along Z-axis (m/s)	Double	8	H+68
15	V-X σ	Standard deviation of V-X (m/s)	Float	4	H+76
16	V-Y σ	Standard deviation of V-Y (m/s)	Float	4	H+80
17	V-Z σ	Standard deviation of V-Z (m/s)	Float	4	H+84
18	stn ID	Base station identification	Char[4]	4	H+88
19	V-latency	A measure of the latency in the velocity time tag in seconds. It should be subtracted from the time to give improved results.	Float	4	H+92
20	diff_age	Differential age	Float	4	H+96
21	sol_age	Solution age in seconds	Float	4	H+100
22	#obs	Number of observations tracked	Uchar	1	H+104
23	#GPSL1	Number of GPS L1 ranges used in computation	Uchar	1	H+105
24	#L1	Number of GPS L1 ranges above the RTK mask angle	Uchar	1	H+106
25	#L2	Number of GPS L2 ranges above the RTK mask angle	Uchar	1	H+107

Note: For field types (Format) see Table B3, Appendix B.

Extracted Position and Velocity Record and Quality Checks

The information extracted from the BESTXYZ record is summarized in Table A-5 whereby the total number of bytes is 72.

Table A-5: Extracted Data From BestXYZ Log reference

Field #	Data Description	Notes	Format	Bytes
1	Position X-coordinate	metre	Double	8
2	Position Y-coordinate	metre	Double	8
3	Position Z-coordinate	metre	Double	8
4	Standard deviation of P-X	x-standard deviation (m)	Float	4
5	Standard deviation of P-Y	y- standard deviation (m)	Float	4
6	Standard deviation of P-Z	Height standard deviation (m)	Float	4
7	Velocity vector along X-axis	m/s	Double	8
8	Velocity vector along Y-axis	m/s	Double	8
9	Velocity vector along Z-axis	m/s	Double	8
10	Standard deviation of V-X	m/s	Float	4
11	Standard deviation of V-Y	m/s	Float	4
12	Standard deviation of V-Z	m/s	Float	4
Total Size				72

Final Data Record

The final message contains time, position and velocity information, as well as the raw data for each satellite tracked. The overall record is shown in Table A-6 and the total number of bytes as a function of the satellites tracked is given in Table A-7. Figure A-1 shows bytes comparison between the extracted and NovAtel format, while Figure A-2 shows the data extraction flowchart, and the steps to follow.

Table A-6: Total Extracted Data to be Transmitted

Field #	Data Description	Notes	Format	Bytes
1	Position X-coordinate	metre	Double	8
2	Position Y-coordinate	metre	Double	8
3	Position Z-coordinate	metre	Double	8
4	Standard deviation of P-X	x-standard deviation (m)	Float	4
5	Standard deviation of P-Y	y- standard deviation (m)	Float	4
6	Standard deviation of P-Z	Height standard deviation (m)	Float	4
7	Velocity vector along X-axis	m/s	Double	8
8	Velocity vector along Y-axis	m/s	Double	8
9	Velocity vector along Z-axis	m/s	Double	8
10	Standard deviation of V-X	m/s	Float	4
11	Standard deviation of V-Y	m/s	Float	4
12	Standard deviation of V-Z	m/s	Float	4
Total Size				72

Field #	Data Description	Notes	Format	Bytes
1	GPS Time	GPS Time	Long	4
2	Sat PRN	GPS satellite PRN number of range measurement	UShort	2
3	Pseudorange	Pseudorange measurement (m)	Double	8
4	Std Range	Pseudorange measurement standard deviation (m)	Float	4
5	Phase	Carrier phase, in cycles	Double	8
6	Std Phase	Estimated carrier phase standard deviation	Float	4
7	Doppler	Instantaneous carrier Doppler frequency (Hz)	Float	4
8...	Next observation is in fields 8-13, etc. Total bytes is 4 + # obsx30			

Table A-7: Number of Bytes as a Function of Satellites Tracked

Number of Satellites	Total Bytes
1	106
2	136
4	196
6	256
8	316
10	376

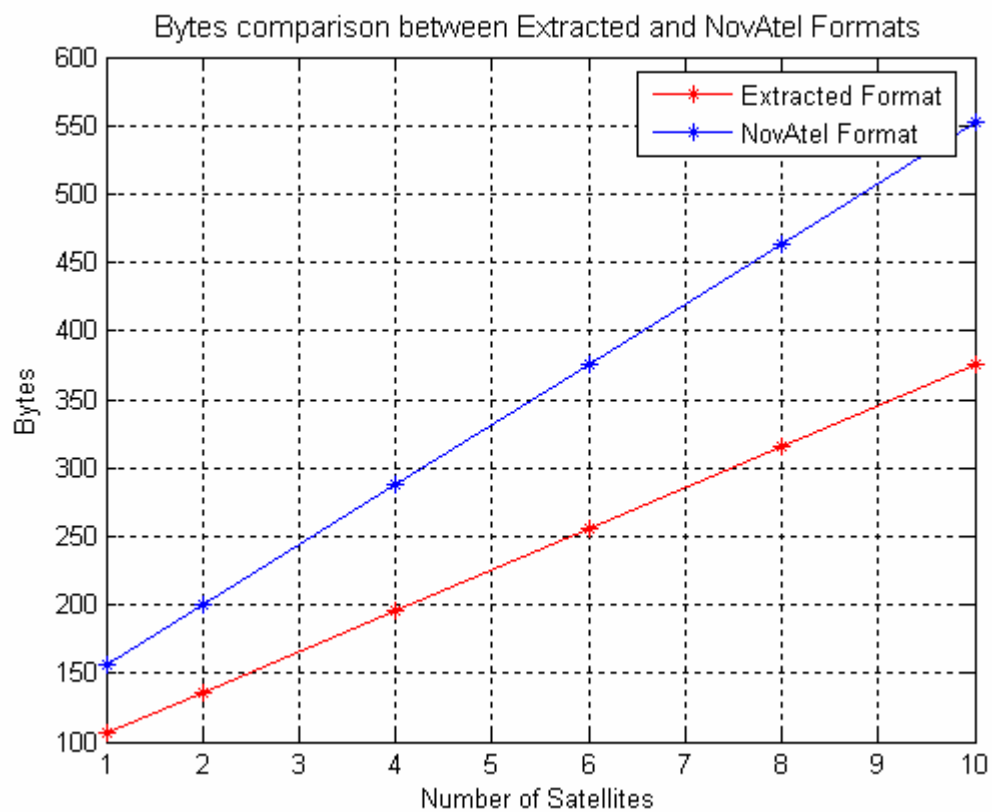


Figure A-1: Bytes Comparison Between New and NovAtel Format

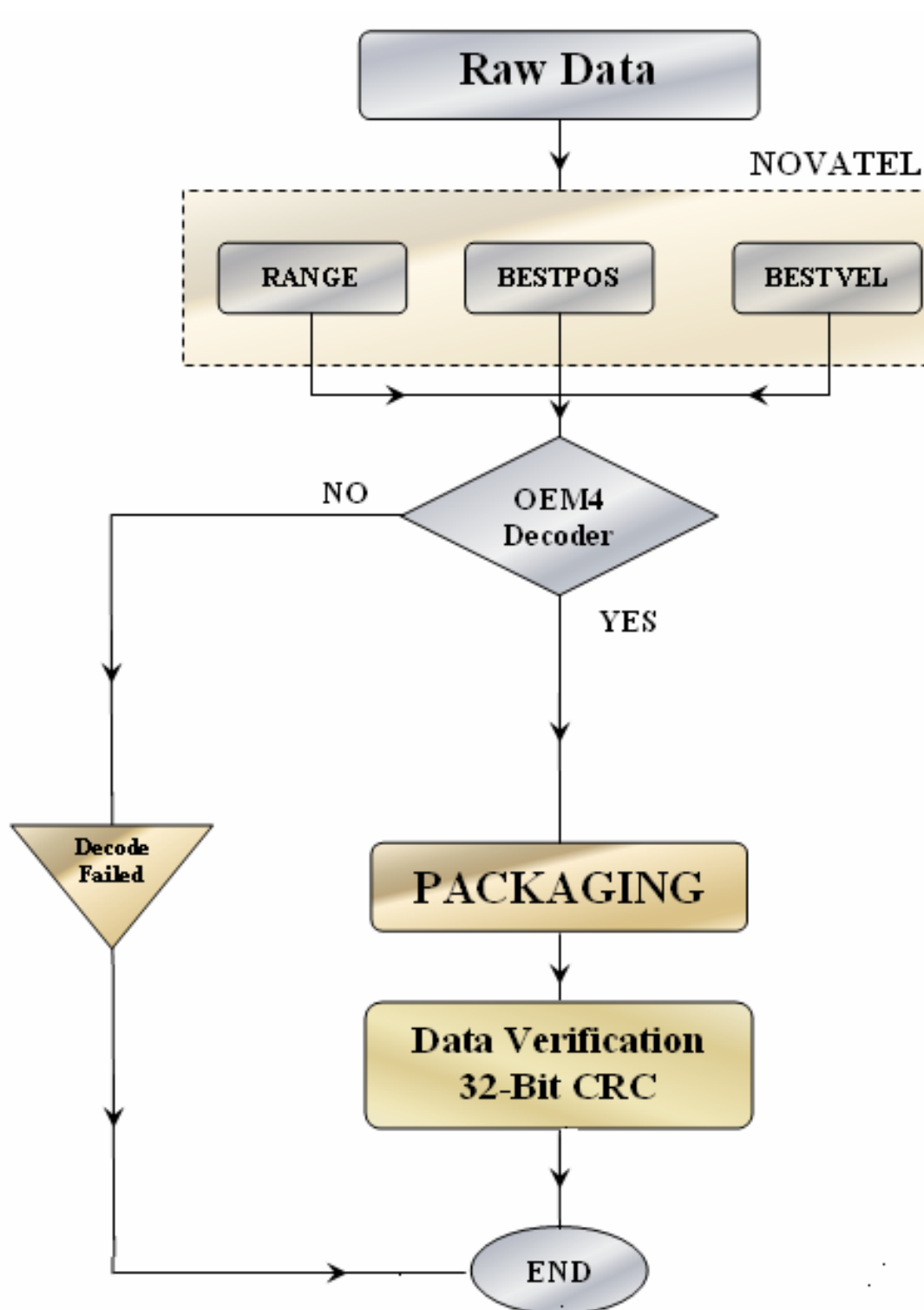


Figure A-2: Data Extraction Flowchart